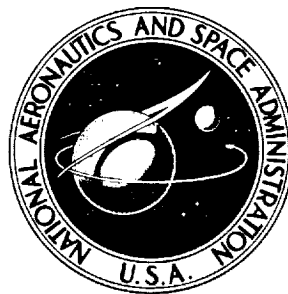


NASA TECHNICAL NOTE



NASA TN D-7511

NASA TN D-7511

**CASE FILE
COPY**

**FLIGHT-DETERMINED STABILITY
AND CONTROL CHARACTERISTICS
OF THE M2-F3 LIFTING BODY VEHICLE**

by Alex G. Sim

*Flight Research Center
Edwards, Calif. 93523*

NATIONAL AERONAUTICS AND SPACE ADMINISTRATION • WASHINGTON, D. C. • DECEMBER 1973

1. Report No. NASA TN D-7511		2. Government Accession No.		3. Recipient's Catalog No.	
4. Title and Subtitle FLIGHT-DETERMINED STABILITY AND CONTROL CHARACTERISTICS OF THE M2-F3 LIFTING BODY VEHICLE				5. Report Date December 1973	
				6. Performing Organization Code	
7. Author(s) Alex G. Sim				8. Performing Organization Report No. H-791	
9. Performing Organization Name and Address NASA Flight Research Center P. O. Box 273 Edwards, California 93523				10. Work Unit No. 756-48-01-00	
				11. Contract or Grant No.	
12. Sponsoring Agency Name and Address National Aeronautics and Space Administration Washington, D. C. 20546				13. Type of Report and Period Covered Technical Note	
				14. Sponsoring Agency Code	
15. Supplementary Notes					
16. Abstract <p style="text-align: center;">Flight data were obtained over a Mach number range from 0.4 to 1.55 and an angle-of-attack range from -2° to 16°. Lateral-directional and longitudinal derivatives, reaction control rocket effectiveness, and longitudinal trim information obtained from flight data and wind-tunnel predictions are compared. The effects of power, configuration change, and speed brake are discussed.</p>					
17. Key Words (Suggested by Author(s)) Aerodynamic stability derivatives M2-F3 lifting body vehicle Reaction control rockets Newton-Raphson method			18. Distribution Statement Unclassified - Unlimited		
19. Security Classif. (of this report) Unclassified		20. Security Classif. (of this page) Unclassified		21. No. of Pages 93	22. Price* Domestic, \$3.75 Foreign, \$6.25

* For sale by the National Technical Information Service, Springfield, Virginia 22151

FLIGHT-DETERMINED STABILITY AND CONTROL CHARACTERISTICS
OF THE M2-F3 LIFTING BODY VEHICLE

Alex G. Sim
Flight Research Center

SUMMARY

A flight evaluation of the stability and control characteristics of the M2-F3 lifting body research vehicle was made at Mach numbers from 0.4 to 1.55 and angles of attack from -2° to 16° . Lateral-directional and longitudinal derivatives, reaction control rocket effectiveness, and longitudinal trim information obtained from flight data and wind-tunnel predictions are compared. Data showing the effects of power, configuration change, and speed brake are included.

The flight data for the directional stability derivative, $C_{n\beta}$, were usually lower than the results from wind-tunnel tests. Near a Mach number of 0.95, the flight-determined aileron effectiveness derivative, $C_{l\delta_a}$, was lower than the wind-tunnel prediction; otherwise, it was higher than predicted.

Although there was considerable scatter in the longitudinal data, the flight values of the static stability derivative, $C_{m\alpha}$, were near the wind-tunnel predictions at Mach numbers of 0.5, 0.7, 0.8, and 1.3. However, at a Mach number of 1.1, the flight values were higher than the wind-tunnel results.

Reaction control rocket lateral control effectiveness was adequate for maneuvering as well as for stability augmentation, whereas longitudinal control effectiveness was adequate only for stability augmentation.

The longitudinal trim flight data indicated generally that more lower flap deflection was needed to trim at a given angle of attack than was estimated from wind-tunnel data. Speed-brake deflection induced a nose-down pitching moment, and power effects generally resulted in a nose-up pitching moment. An unsteady power-off trim phenomenon in the transonic Mach number range from 0.88 to 0.95 was indicated by the tendency of the vehicle to trim at more than one lower flap deflection for the same angle of attack.

INTRODUCTION

Lifting bodies are a class of vehicle designed to enter the earth's atmosphere from orbital speeds and make a horizontal landing. The M-2 shape was one of the first lifting body shapes to evolve. After a lightweight plywood version of the M-2 vehicle (the M2-F1) was flown successfully, a heavier, aluminum vehicle (the M2-F2) was built to investigate "in-the-atmosphere" vehicle characteristics at subsonic and transonic speeds. On the sixteenth M2-F2 flight, lateral-directional handling-qualities problems were experienced, followed by a gear-up landing which extensively damaged the vehicle and terminated the flight program. Stability and control derivatives of the M2-F2 vehicle are given in reference 1, and the lateral-directional handling qualities are analyzed in reference 2.

The M2-F2 vehicle was rebuilt and modified by the addition of a third vertical stabilizer. Extensive wind-tunnel tests and dynamic analysis indicated that this modification would improve the lateral-directional handling qualities. The modified M2-F2 vehicle was redesignated the M2-F3. A photograph and three-view drawing of the vehicle are shown in figures 1 and 2, respectively.

During the M2-F3 flight-test program, conducted jointly by the National Aeronautics and Space Administration and the U.S. Air Force, stability and control data were obtained at Mach numbers from 0.4 to 1.55 and angles of attack from -2° to 16° . These data were used to update the flight simulator for flight planning and pilot training, revise the analysis of handling qualities, verify wind-tunnel predictions, and document dynamic characteristics. Longitudinal trim information was also obtained from flight data.

In one of the control system studies made with the M2-F3 vehicle, reaction control rockets were used to control roll or pitch in the atmosphere.

This report presents the stability and control data obtained during the M2-F3 flight program and compares the results with wind-tunnel predictions.

SYMBOLS

Derivatives are presented as standard NASA coefficients of forces and moments. A right-hand sign convention (shown in fig. 3) is used to determine the direction of all forces, moments, angular displacements, and velocity.

Physical quantities are given in the International System of Units (SI) and parenthetically in U.S. Customary Units. All measurements were taken in U.S. Customary Units. Conversion factors are included in reference 3.

A stability matrix, $P \times P$

a_n normal acceleration, g

a_x	longitudinal acceleration, g
a_y	lateral acceleration, g
B	control matrix, $P \times Q$
b	reference body span, m (ft)
C	transformation matrix, $P \times P$
\bar{c}	reference longitudinal length, m (ft)
F	force, N (lb)
G	partition of matrix relating the state vector to the observation vector, $(R - P) \times P$
g	acceleration due to gravity, 9.8 m/sec^2 (32.2 ft/sec^2)
H	partition of matrix relating the control vector to the observation vector, $(R - P) \times Q$
h	altitude, m (ft)
I	identity matrix
I_X	rolling moment of inertia, kg-m^2 (slug-ft ²)
I_{XZ}	product of inertia, kg-m^2 (slug-ft ²)
I_Y	pitching moment of inertia, kg-m^2 (slug-ft ²)
I_Z	yawing moment of inertia, kg-m^2 (slug-ft ²)
M	Mach number
\bar{M}	moment, m-N (ft-lb)
m	mass, kg (slugs)
O	null matrix
P	number of state variables
p	rolling rate, rad/sec or deg/sec
Q	number of control variables
q	pitching rate, rad/sec or deg/sec

\bar{q}	dynamic pressure, N/m^2 (lb/ft^2)
R	number of observation variables
r	yawing rate, rad/sec or deg/sec
S	reference planform area, m^2 (ft^2)
s	Laplace transform variable, rad/sec
u	velocity along X-axis, m/sec (ft/sec)
\underline{u}	control vector, $Q \times 1$
V	velocity, m/sec (ft/sec)
w	velocity along Z-axis, m/sec (ft/sec)
X	X-axis
\underline{x}	state vector, $P \times 1$
Y	Y-axis
\underline{y}	observation vector, $R \times 1$
Z	Z-axis
α	angle of attack, deg
β	angle of sideslip, deg
γ	flightpath angle, deg
Δ	increment
δ_a	aileron deflection, $\delta_{u_{left}} - \delta_{u_{right}}$, deg
δ_l	lower-flap deflection, deg
δ_r	rudder deflection, $\delta_{r_{left}} + \delta_{r_{right}}$, deg
δ_{sb}	average speed-brake deflection, $\frac{1}{2} \left[\left(\delta_{r_{left}} - \delta_{r_{right}} \right) - \left \delta_r \right \right]$, deg
δ_u	average upper-flap position, $\frac{1}{2} \left(\delta_{u_{left}} + \delta_{u_{right}} \right)$, deg

δ_0	constant control deflection, rad or deg
δ_1	reaction control rocket chamber pressure, N/m^2 (psia)
$\epsilon = \frac{1}{2} \arctan \left(\frac{2I_{XZ}}{I_Z - I_X} \right)$	
ζ	damping ratio
θ	pitching attitude, deg
τ	time constant, sec
φ	angle of bank, deg
ω_n	undamped natural frequency, rad/sec
C_L	lift coefficient, $\frac{\text{Lift}}{\bar{q}S}$
C_l	rolling-moment coefficient, $\frac{\bar{M}_X}{\bar{q}Sb}$
C_m	pitching-moment coefficient, $\frac{\bar{M}_Y}{\bar{q}Sc}$
C_n	yawing-moment coefficient, $\frac{\bar{M}_Z}{\bar{q}Sb}$
C_X	axial-force coefficient, $\frac{F_X}{\bar{q}S}$
C_Y	side-force coefficient, $\frac{F_Y}{\bar{q}S}$
C_Z	normal-force coefficient, $\frac{F_Z}{\bar{q}S}$

Nondimensional derivatives, where $i = m, X, Z$ and $j = 1, n, Y$:

$$C_{i_\alpha} = \frac{\partial C_i}{\partial \alpha}$$

$$C_{j_\beta} = \frac{\partial C_j}{\partial \beta}$$

$$C_{i_q} = \frac{\partial C_i}{\partial \frac{q\bar{c}}{2V}}$$

$$C_{j_p} = \frac{\partial C_j}{\partial \frac{pb}{2V}}$$

$$C_{i_M} = \frac{\partial C_i}{\partial M}$$

$$C_{j_r} = \frac{\partial C_j}{\partial \frac{rb}{2V}}$$

$$C_{i_{\delta_1}} = \frac{\partial C_i}{\partial \delta_1}$$

$$C_{j_{\delta_a}} = \frac{\partial C_j}{\partial \delta_a}$$

$$C_{i_{\delta_1}} = \frac{\partial C_i}{\partial \delta_1}$$

$$C_{j_{\delta_r}} = \frac{\partial C_j}{\partial r}$$

$$C_{L_\alpha} = \frac{\partial C_L}{\partial \alpha}$$

$$C_{j_{\delta_1}} = \frac{\partial C_j}{\partial \delta_1}$$

$$C_{L_{\delta_1}} = \frac{\partial C_L}{\partial \delta_1}$$

Dimensional derivatives:

$$M_q = \frac{\bar{q}S\bar{c}^{-2}}{2VI_Y} C_{m_q}$$

$$M_{\delta_1, \delta_1} = \frac{\bar{q}S\bar{c}}{I_Y} C_{m_{\delta_1, \delta_1}}$$

$$Z_q = -\frac{\bar{q}S\bar{c}}{2mV^2} C_{Z_q} + 1$$

$$Z_{\delta_1, \delta_1} = \frac{\bar{q}S}{mV} C_{Z_{\delta_1, \delta_1}}$$

$$X_q = -V\alpha$$

$$X_{\delta_1, \delta_1} = -\frac{\bar{q}S}{m} C_{X_{\delta_1, \delta_1}}$$

$$X_\theta = -g \cos \theta$$

$$Z_\theta = -\frac{g}{V} \sin \theta$$

$$M_\alpha = \frac{\bar{q}S\bar{c}}{I_Y} \left[C_{m_\alpha} + 2 \tan(\alpha) \left(\frac{M}{2} C_{m_M} \right) \right] \cos \alpha$$

$$Z_\alpha = \frac{\bar{q}S}{mV} \left[C_{Z_\alpha} + 2 \tan(\alpha) \left(C_Z + \frac{M}{2} C_{Z_M} \right) \right] \cos \alpha$$

$$X_\alpha = -\frac{\bar{q}S}{m} \left[C_{X_\alpha} + 2 \tan(\alpha) \left(C_X + \frac{M}{2} C_{X_M} \right) \right] \cos \alpha$$

$$M_u = \frac{\bar{q}S\bar{c}}{VI_Y} \left[C_{m_M} \frac{M}{2} - \frac{1}{2} \tan(\alpha) C_{m_\alpha} \right] \cos \alpha$$

$$Z_u = \frac{\bar{q}S}{mV^2} \left[C_Z + C_{Z_M} \frac{M}{2} - \frac{1}{2} \tan(\alpha) C_{Z_\alpha} \right] 2 \cos \alpha$$

$$X_u = -\frac{\bar{q}S}{mV} \left[C_X + C_{X_M} \frac{M}{2} - \frac{1}{2} \tan(\alpha) C_{X_\alpha} \right] 2 \cos \alpha$$

$$L_\beta = \frac{\bar{q}Sb}{I_X} C_{l_\beta}$$

$$L_{\delta_a, \delta_r, \delta_1} = \frac{\bar{q}Sb}{I_X} C_{l_{\delta_a, \delta_r, \delta_1}}$$

$$N_\beta = \frac{\bar{q}Sb}{I_Z} C_{n_\beta}$$

$$N_{\delta_a, \delta_r, \delta_1} = \frac{\bar{q}Sb}{I_Z} C_{n_{\delta_a, \delta_r, \delta_1}}$$

$$Y_\beta = \frac{\bar{q}S}{mV} C_{Y_\beta}$$

$$Y_{\delta_a, \delta_r, \delta_1} = \frac{\bar{q}S}{mV} C_{Y_{\delta_a, \delta_r, \delta_1}}$$

$$L_p = \frac{\bar{q}Sb^2}{2VI_X} C_{l_p}$$

$$L_r = \frac{\bar{q}Sb^2}{2VI_X} C_{l_r}$$

$$N_p = \frac{\bar{q}Sb^2}{2VI_Z} C_{n_p}$$

$$N_r = \frac{\bar{q}Sb^2}{2VI_Z} C_{n_r}$$

$$Y_p = \sin \alpha$$

Subscripts:

i	i^{th} component
j	j^{th} component
X	X-axis component
Y	Y-axis component
Z	Z-axis component

A dot over a symbol signifies a derivative with respect to time.

M2-F3 VEHICLE

The M2-F3 vehicle is basically a 13° blunt, half cone with a boat-tailed afterbody and three vertical fins. Powered flight was achieved by using any combination of the four chambers of the XLR11 rocket engine. Physical characteristics of the vehicle are given in table 1. Typical variations of the moments of inertia and center of gravity with gross weight are presented in table 2.

Midway through the flight program, operational considerations dictated that the jettison tubes be moved from the base area to just aft of the outboard vertical fins. The repositioned tubes (fig. 4) are referred to as the outboard fin jettison tubes.

M2-F3 FLIGHT CONTROL SYSTEM

The primary manual control system of the M2-F3 vehicle was an irreversible, dual, hydraulic system. Pitch control was accomplished by moving the center stick longitudinally, which positioned the lower flap. Roll control was achieved by moving the center stick laterally, which differentially positioned the upper flaps. Yaw control was obtained through the rudder pedals, which deflected one of the two rudder surfaces on the outboard side of the two outer vertical fins. Outboard bias of both rudders was used as a speed brake. Coarse longitudinal trim (configuration change) was achieved by biasing the upper flaps. These control surface locations are shown in figure 3.

Two vehicle configurations--subsonic and transonic--were used to provide adequate stability at transonic speeds as well as low drag (increased lift-to-drag ratio) for approach and landing. Average upper-flap positions of -11.8° and -20° were used as the subsonic and transonic configurations, respectively. Control surface deflection limits and maximum rates used in the latter part of the flight program are given in table 3.

The primary stability augmentation system was a three-axis rate feedback system. The feedback gains were adjustable in flight. Additional augmentation was provided by a rate command augmentation system or reaction control rockets.

The command augmentation system was mechanized in pitch and roll and included an angle-of-attack hold. The rate command gains were adjustable in flight. When the command augmentation system was engaged, the pilot maneuvered the vehicle by means of a side stick on the right side of the cockpit.

The four 400-newton- (90-pound-) thrust reaction control rockets were normally fired in pairs to control roll or pitch. At first the rockets were pulsed manually, with a simple switch for roll control. Later they were mechanized with either a roll or a pitch rate feedback and manually controlled through the side stick. The two rocket geometries used are illustrated in figure 5. Roll control was achieved by using an outboard-opposite-inboard rocket combination. Wind-tunnel information indicated that Geometry 1 would minimize the aerodynamic interference contribution to yawing while providing proverse yaw from the static geometry during a roll maneuver. On the basis of flight-test results, however, it was decided that better handling qualities in roll would result if the total yawing moment were eliminated. Thus Geometry 2 was used in succeeding flights.

INSTRUMENTATION

Data were obtained by means of a 9-bit pulse code modulation telemetry system and were analyzed by using a ground-based computer.

Angle of attack, angle of sideslip, dynamic pressure, and static pressure were measured by an instrumented NACA nose boom (ref. 4). Angular positions and rates were measured by rate gyros, and linear accelerations by conventional accelerometers. Control surface positions were determined by control position transmitters.

Corrections were made to the angle-of-attack and angle-of-sideslip data for boom position, alignment, angular rate, and bending, as well as for upwash (ref. 4). Velocity, altitude, and Mach number were calculated on the basis of corrected dynamic and static pressures. Angular rates and linear accelerations were not corrected for instrument location because this error was within the accuracy of the data acquisition system. The parameters used and the resolution and accuracy of the instrumentation are presented in table 4.

FLIGHT TESTS

Procedures

Frequent weight and balance measurements were made to verify the location of the vehicle center of gravity. Moments of inertia were determined experimentally before the first M2-F3 flight by means of an inertia swing (ref. 5). The inertia estimate was updated analytically whenever the mass distribution changed.

Like other lifting bodies, the M2-F3 vehicle was air-launched from a modified B-52 airplane at an altitude of approximately 14,000 meters (45,000 feet) and a Mach number of 0.67. (Air launches of the M2-F2 lifting body are analyzed in reference 6.) After launch, the pilot flew a preplanned flight profile. The unpowered, or glide, flights lasted less than 4 minutes and were usually made below a Mach number of 0.7. For powered flights, the engine was lit immediately after launch, angle of attack was increased to gain altitude, and the vehicle was pushed over to increase Mach number. The powered portion of the flight, which usually lasted from 90 seconds to 180 seconds, was made in the transonic configuration (upper flap at -20°). A change to the subsonic configuration (upper flap at -11.8°) was made when the Mach number decreased to about 0.7. The altitude at this time was about 9150 meters (30,000 feet). Most of the stability and control data were obtained after engine burnout.

In general, maneuvers from which data were obtained were performed at altitudes above approximately 6100 meters (20,000 feet) to provide the pilot with enough time to set up for the final approach and landing. The trajectories flown precluded steady flight conditions. To maintain satisfactory handling qualities, at least one augmentation system was generally used throughout the flight profile, particularly above a Mach number of 0.75. However, damper gains were often reduced or turned to zero for data maneuvers.

Maneuvers

Because of the limited time available for obtaining flight data and the rapidly changing flight conditions, there was only one opportunity to perform each maneuver. Thus maneuvers were practiced on a simulator before each flight. Postflight analysis of these maneuvers showed that a doublet or pulse, followed by 2 seconds to 5 seconds in which the pilot made no input, was most effective in providing derivative data when augmentation damper gains were zero or below 0.5 deg/deg/sec. An example of this type of maneuver, which has been used often to obtain data from which derivatives can be extracted, is shown in figure 6. When moderate-to-high damper gains were used, a pilot-induced continuous control input produced better results. An example of this type of maneuver is shown in figure 7. In the latter part of the flight program, the angle-of-attack-hold of the command augmentation system aided the pilot in holding a constant angle of attack during lateral-directional maneuvers.

The effectiveness of the reaction control rockets was evaluated by manually pulsing the rockets.

Power-off longitudinal trim information was obtained from planned pushover-pullup maneuvers as well as during other portions of the flight. No planned maneuvers were used to obtain power-on trim data.

METHOD OF ANALYSIS

Derivative Determination

A digital computer program was used to identify either lateral-directional or longitudinal sets of derivatives from flight data. This computer program, which uses

a modification of the Newton-Raphson method, is referred to as the Newton-Raphson program. The program, its theory, and its application are discussed in detail in references 8 to 10. The sets of equations (model) used to identify the derivatives for this report are given in appendix A.

The Newton-Raphson program is an iterative technique which usually takes from three to six iterations to converge to a final set of derivatives. Basically, the program simultaneously changes all derivatives to minimize the error between computed and measured time histories. This error is based on the integral of the sum of the differences squared of each of an ensemble of flight and computed time histories. The output time histories are assumed to contain noise, but the (control) input time histories are defined as noise free.

In the lateral-directional mode, the input time histories normally used were the recorded aileron and rudder deflections. Occasionally, reaction control rocket chamber pressure was used. The output time histories used were roll rate, yaw rate, sideslip angle, bank angle, and lateral acceleration. Rolling and yawing angular acceleration were used when available. In the longitudinal mode, the input time histories used were lower flap deflection and sometimes reaction control rocket chamber pressure. The output time histories used were angle of attack, pitch angle, pitch rate, and normal acceleration. Pitching angular acceleration was sometimes used.

A frequently used option, called "a priori," allowed the starting set of derivatives to be weighed, which tended to hold derivatives near their starting value if no information about them was contained in the maneuver. Early in the flight program, wind-tunnel predictions were used as starting values. However, as different trends in the data developed, previously obtained flight-determined derivatives were used. At first and then after every few flights, maneuvers were analyzed without using the a priori option to insure that the a priori weighing values were not too high.

Effect of stability augmentation.—When augmentation systems are engaged, a linear dependence can develop between stability and control derivatives; therefore, the a priori option was used in this study. Furthermore, increasing the damper gains removes progressively more of the vehicle's transient response, so that the control system characteristics gradually dominate the output time response. These effects of the automatic control system may improve handling qualities; however, at the same time, they make identifying the basic open-loop vehicle extremely difficult. Unfortunately, stability augmentation was generally used above a Mach number of 0.75. If it is desirable to fly through an area where a vehicle has poor open-loop characteristics, then it will usually be the area of greatest interest, but unfortunately also the one requiring the highest damper gains to insure satisfactory handling qualities. With the high damper gains, the resulting lack of transient response necessitated continuous pilot control inputs, because, it was reasoned, more information would be contained in forced motion than in no motion at all. Control derivatives extracted were used only if the maneuver contained a pilot input for that control (i.e., rudder derivatives obtained from aileron maneuver data were not considered valid).

Longitudinal derivative considerations.—Both longitudinal and lateral-directional derivatives were extracted from data obtained when an augmentation system was

engaged. The longitudinal mode, because of additional problems, was the more troublesome of the two. An indication of some of the problems experienced in this mode is evident in the nonlinearity of wind-tunnel pitching-moment curves at transonic speeds. An example is shown in figure 8 for a Mach number of 0.95. The nonlinearities in these pitching-moment curves cause the longitudinal static stability and the lower flap control effectiveness to be sensitive to small changes in angle of attack and longitudinal trim. The curves also change significantly with upper flap bias; however, in flight the bias was kept between $\pm \frac{1}{3}^\circ$ of the wind-tunnel reference values. All flight-determined longitudinal derivatives were corrected to the wind-tunnel reference center of gravity of 0.496 of chord (body length).

Longitudinal Trim

Longitudinal trim information was obtained during periods in the flights when the pitching angular acceleration was less than $\pm 3 \text{ deg/sec}^2$, the pitching rate was less than $\pm 9 \text{ deg/sec}$, and the rate of lower flap movement was subjectively small. Trim data that met the first two requirements were identified by using a simple digital computer program. Lower flap movement was scanned by hand. Data were categorized by engine chamber, speed-brake setting, and configuration. All trim data were corrected to the longitudinal wind-tunnel reference center of gravity (0.496 of chord). For comparison with wind-tunnel data, the lower flap position data were adjusted analytically to compensate for the flight upper flap bias being slightly different from the selected references of -11.8° (subsonic configuration) and -20° (transonic configuration).

Dynamic Characteristics

The open-loop dynamic characteristics were determined by fairing flight data for nine flight conditions. Data were calculated by using a three-degree-of-freedom digital computer program which solved for the characteristic roots and transfer function numerators. When flight data were not available, wind-tunnel data were used. The open-loop characteristics of the vehicle are tabulated in appendix B.

WIND-TUNNEL DATA

Wind-tunnel tests of the M2-F3 vehicle were made at the Ames Research Center. Although results of the tests have not yet been published, a limited amount of data for a vehicle with a center fin configuration similar to that of the M2-F3 vehicle is included in reference 11.

For this study, damping derivatives were estimated from trends of theoretical and flight results for earlier vehicle configurations (refs. 1 and 2). All other derivatives and trim data referred to as wind-tunnel data are based on the unpublished M2-F3 data. The wind-tunnel lateral-directional derivatives were obtained from data for the available boattail angles (upper flap and lower flap settings) at wind-tunnel-predicted longitudinal trim conditions. Thus the boattail angles obtained from the

wind-tunnel tests are not necessarily the same as those used in flight.

PRESENTATION OF DATA

The flight conditions, in terms of Mach number and angle of attack, at which derivatives were obtained are presented in figure 9(a) for the lateral-directional derivatives and in figure 9(b) for the longitudinal derivatives. The lateral-directional derivatives are presented as a function of angle of attack for wind-tunnel Mach numbers of 0.5, 0.7, 0.8, 0.9, 0.95, 1.1, and 1.3 in figures 10 to 16. The corresponding longitudinal derivatives for Mach numbers near 0.5, 0.7, 0.8, 1.1, and 1.3 are presented in figures 17(a) to 17(e). For Mach numbers from 0.86 to 1.08, longitudinal derivatives are presented in figures 18(a) to 18(c) as a function of Mach number for angles of attack of 3.6° , 5.1° , 7.2° , 10.5° , and 12.4° , except for the pitch-damping derivative, C_{m_q} , which was estimated only as a function of Mach number. Flight derivatives were also determined for Mach numbers and angles of attack beyond those shown in the figures. The values of all the derivatives obtained are presented in table 5.

Control-effectiveness data for the reaction control rockets are presented in the form of changes in moment coefficients due to the pulsing of one or two rockets. Data obtained during rolling maneuvers are presented in figures 19 and 20. Data obtained in pitching maneuvers are shown in figures 21(a) and 21(b).

Longitudinal trim data for the subsonic configuration are presented as a function of angle of attack for Mach numbers of 0.5 and 0.7 in figures 22(a) and 22(b). Data for the transonic configuration are presented in figures 23 and 24 for Mach numbers of 0.5, 0.7, 0.8, 1.1, and 1.3. Trim data are presented as a function of Mach number, over the Mach range from 0.88 to 1.04, in figures 25(a) to 25(c).

DISCUSSION

Lateral-Directional Derivatives

Figures 10 to 16 show that the effective dihedral derivative, C_{l_β} , and the yawing-moment coefficient due to aileron deflection, $C_{n_{\delta_a}}$, are generally in agreement with the wind-tunnel predictions, whereas the directional stability derivative, C_{n_β} , is usually lower than predicted, especially at subsonic speeds and high angles of attack. At transonic Mach numbers the agreement between wind-tunnel and flight values of C_{n_β} is better. The side force derivative, C_{Y_β} , and the roll-damping derivative, C_{l_p} , are also generally lower than predicted from wind-tunnel tests.

The rolling-moment coefficients due to rudder deflection and yawing rate, $C_{l_{\delta_r}}$ and C_{l_r} , the yawing-moment coefficient due to rolling rate, C_{n_p} , and the side force coefficients due to aileron and rudder deflection, $C_{Y_{\delta_a}}$ and $C_{Y_{\delta_r}}$, are difficult to identify as indicated by the amount of scatter in the flight data. However, the data do indicate specific trends, and the derivatives are well defined at subsonic Mach numbers. The yaw-damping derivative, C_{n_r} , is usually well defined, although the values are slightly different from the preflight estimates.

Except for the comparison at a Mach number of 0.95 (fig. 14(b)), flight values of the aileron effectiveness derivative, $C_{l_{\delta_a}}$, were higher than the wind-tunnel results.

However, near Mach 0.95 at low angles of attack, changes in $C_{l_{\delta_a}}$ were found to significantly affect the handling qualities. In the flight program this Mach region was extremely troublesome. More than once, vehicle disturbances occurred that were followed by an oscillation sustained by damper augmentation. It was determined that a large reduction in $C_{l_{\delta_a}}$ coupled with certain combinations of roll and yaw gains could produce an unstable closed-loop vehicle. Lower values of $C_{l_{\delta_a}}$

were determined from flight data; however, only one data point (fig. 14(b))-- at a Mach number of 0.936 and an angle of attack of 5.06° --yielded high quality results. This point, as well as others of less than acceptable quality, showed that the flight vehicle followed the wind-tunnel curve based on longitudinally untrimmed data at the flight upper flap bias setting. This is supported by the data in figure 25(a) which show that the vehicle was seldom in longitudinal trim when these data were obtained. Without the angle-of-attack-hold of the command augmentation system, it was difficult for the pilot to hold a steady angle of attack in this region either with the power on or off. This difficulty, coupled with the problem of not knowing the true Mach number in flight at Mach numbers near 0.95, made it difficult to perform maneuvers at these flight conditions.

As noted previously, midway through the flight envelope expansion, the vehicle geometry was changed slightly just aft of the rudders (fig. 4). Figures 10 to 16 show that although rudder control effectiveness may have been changed as a result of this geometry change, the effect on vehicle dynamics was negligible.

Longitudinal Derivatives

The flight data from which the longitudinal derivatives were obtained generally had an unusually large amount of scatter. The scatter was attributed to the nonlinear trends of the longitudinal characteristics with angle of attack (fig. 8), the large trim changes with Mach number (fig. 25), the inability to maintain constant flight conditions with a boost-glide vehicle of this type, and the high stability augmentation

gains needed to provide acceptable handling qualities. However, despite the scatter, some trends are evident.

The flight values of the longitudinal static stability derivative, C_{m_α} , were near the wind-tunnel values at Mach numbers of 0.5, 0.7, 0.8, and 1.3 (figs. 17(a), 17(b), 17(c), and 17(e)). At Mach 1.1, the flight values were higher than the wind-tunnel values (fig. 17(d)). In the transonic speed region, the trend of the flight-determined C_{m_α} is as nonlinear as that of the wind-tunnel data (fig. 18(a)).

Transonic nonlinearities are also evident in the variations of the lower flap effectiveness derivative, $C_{m_{\delta_1}}$ (fig. 18(b)), and the pitch-damping derivative, C_{m_q} (fig. 18(c)), with Mach number and are somewhat supported by the fluctuations of the trim curves in figure 25(a). At subsonic speeds the flight-determined values of $C_{m_{\delta_1}}$ correlate well with the wind-tunnel values. At other Mach numbers, $C_{m_{\delta_1}}$ was not well defined.

The flight values of C_{m_q} , although not well defined, are of about the same magnitude as the preflight estimates. Except in the transonic speed region, C_{m_q} generally decreases with increasing angle of attack.

Effectiveness of the Reaction Control Rockets

The effectiveness of the reaction control rockets was determined from flight data as part of a study of the usefulness of the rockets for terminal area maneuvering and stability augmentation.

Figure 19 compares flight and wind-tunnel results for rocket Geometry 1 when a combination of an outboard and an opposite inboard rocket was used. The flight roll control effectiveness data agree reasonably well with the predictions, but the accompanying incremental yawing-moment coefficient data are higher. The resulting lateral control effectiveness was adequate for maneuvering as well as for stability augmentation. Agreement between flight results and wind-tunnel predictions was reasonably good.

Figures 20(a) and 20(b) show the results of operating either an outboard or an inboard reaction control rocket. These data have considerable scatter because of the small vehicle motions produced by just one rocket. The resulting motions in pitch were too small to analyze.

The pitch control effectiveness using either both inboard or both outboard rockets is shown in figures 21(a) and 21(b). The resulting control effectiveness was adequate to provide stability augmentation over most of the flight envelope but was not of enough magnitude to maneuver the vehicle adequately.

Longitudinal Trim

The flight trim data indicate, in general, that more lower flap deflection was needed to obtain a given angle of attack than predicted by data from power-off wind-tunnel tests (figs. 22 to 24). This difference increases with increasing angle of attack. No attempt was made to predict power-on trim from wind-tunnel data. As shown in figures 22(a) and 22(b), opening the speed brake induced a nose-down trend. This trend was predicted by wind-tunnel data but is not shown. Figure 22(b) shows that with a speed-brake setting of 27° , an instability occurs at low angles of attack, as indicated by the positive slope of the trim curve (which implies a positive or unstable C_{m_α}). As a result of this instability, speed-brake deflections were limited to 20° . The general effect of power is shown in figures 24 and 25 to be a nose-up trim increment, even though the thrust line was above the vehicle center of gravity.

Figures 25(a) to 25(c) define the in-flight vehicle trim characteristics for various power levels. In figure 25(a) the solid lines indicate the trim curves that were normally obtained from flight data. However, about 20 percent of the time, the curves shown by the dashed lines were obtained. These curves show that the vehicle can be trimmed at more than one lower flap deflection for the same angle of attack, thus indicating that an unsteady power-off trim phenomenon occurs in the transonic Mach number range from 0.88 to 0.95 at higher angles of attack. In this same Mach number range at lower angles of attack, no trim data were obtained even though many flights were made through this region.

CONCLUDING REMARKS

A flight investigation of the stability and control characteristics of the M2-F3 lifting body vehicle was made at Mach numbers from 0.4 to 1.55. The flight data were compared with predictions based on wind-tunnel results.

Noticeable differences were observed between some flight and wind-tunnel lateral-directional results. The flight-determined values of the directional stability derivative, C_{n_β} , were usually lower than the values predicted from wind-tunnel tests, especially at subsonic speeds and high angles of attack. Near Mach 0.95 and at low angles of attack, the flight values of the aileron effectiveness derivative, $C_{l_{\delta a}}$, followed data based on longitudinally untrimmed wind-tunnel data, which were lower than those for trimmed conditions.

Although the longitudinal data had considerable scatter, flight values of the static stability derivative, C_{m_α} , were in fair agreement with wind-tunnel predictions at Mach numbers of 0.5, 0.7, 0.8, and 1.3. At a Mach number of 1.1, the flight values were higher than the wind-tunnel results.

The effectiveness of the reaction control rockets was determined from flight data. Lateral control effectiveness was adequate for maneuvering as well as for stability augmentation; whereas longitudinal control effectiveness was adequate only for stability augmentation. The agreement was reasonably good between the flight results and the wind-tunnel predictions for lateral-directional control effectiveness using the combination of an outboard and an opposite inboard rocket.

The longitudinal trim flight data indicated, in general, that more lower flap deflection was needed to trim at a specified angle of attack than estimated from wind-tunnel data. Speed-brake deflection induced a nose-down pitching moment, whereas power effects generally resulted in a nose-up pitching moment. An unsteady power-off trim phenomenon in the Mach number range from 0.88 to 0.95 was indicated by the tendency of the vehicle to trim at more than one lower flap deflection for the same angle of attack.

Flight Research Center,
National Aeronautics and Space Administration,
Edwards, Calif., October 17, 1973.

APPENDIX A

EQUATIONS OF MOTION MECHANIZED IN THE NEWTON-RAPHSON DIGITAL COMPUTER PROGRAM

The following state equations were used in the basic model for this study:

$$C\dot{\underline{x}} = A\underline{x} + B\underline{u}$$

$$\underline{y} = \begin{bmatrix} I \\ G \end{bmatrix} \underline{x} + \begin{bmatrix} O \\ H \end{bmatrix} \underline{u}$$

where \underline{x} , $\dot{\underline{x}}$, \underline{u} , and \underline{y} are time varying.

For the lateral-directional mechanization,

$$\underline{x} = \begin{bmatrix} p \\ r \\ \beta \\ \varphi \end{bmatrix} \quad \underline{u} = \begin{bmatrix} \delta_a \\ \delta_r \\ \delta_1 \\ 1 \end{bmatrix} \quad \underline{y} = \begin{bmatrix} p \\ r \\ \beta \\ \varphi \\ \dot{p} \\ \dot{r} \\ a_y \end{bmatrix}$$

$$A = \begin{bmatrix} L_p & L_r & L_\beta & 0 \\ N_p & N_r & N_\beta & 0 \\ Y_p & -\cos(\alpha)* & Y_\beta & g/V \cos(\varphi)* \\ 1* & \tan(\theta)* & 0 & 0 \end{bmatrix}$$

*Normally held fixed.

APPENDIX A - Continued

$$B = \begin{bmatrix} L_{\delta_a} & L_{\delta_r} & L_{\delta_1}^* & L_{\delta_0} \\ N_{\delta_a} & N_{\delta_r} & N_{\delta_1}^* & N_{\delta_0} \\ Y_{\delta_a} & Y_{\delta_r} & Y_{\delta_1}^* & Y_{\delta_0} \\ 0 & 0 & 0 & 0 \end{bmatrix}$$

$$C = \begin{bmatrix} 1 & -\frac{I_{XZ}}{I_X} & 0 & 0 \\ -\frac{I_{XZ}}{I_Z} & 1 & 0 & 0 \\ 0 & 0 & 1 & 0 \\ 0 & 0 & 0 & 1 \end{bmatrix}$$

$$G = \begin{bmatrix} L_p & L_r & L_\beta & 0 \\ N_p & N_r & N_\beta & 0 \\ 0 & 0 & Y_\beta & 0 \end{bmatrix}$$

$$H = \begin{bmatrix} L_{\delta_a} & L_{\delta_r} & L_{\delta_1} & L_{\delta_0} \\ N_{\delta_a} & N_{\delta_r} & N_{\delta_1} & N_{\delta_0} \\ Y_{\delta_a} & Y_{\delta_r} & Y_{\delta_1} & Y_{\delta_0} \end{bmatrix}$$

*Normally held fixed.

APPENDIX A - Continued

For the longitudinal mechanization:

$$\underline{x} = \begin{bmatrix} q \\ \alpha \\ V \\ \theta \end{bmatrix} \quad \underline{u} = \begin{bmatrix} \delta_1 \\ \delta_1 \\ \delta_0 \\ 1 \end{bmatrix} \quad \underline{y} = \begin{bmatrix} q \\ \alpha \\ V \\ \theta \\ q \\ a_n \end{bmatrix}$$

$$A = \begin{bmatrix} M_q & M_\alpha & M_u^* & 0 \\ Z_q^* & Z_\alpha & Z_u^* & Z_\theta^* \\ X_q^* & X_\alpha^* & X_v^* & X_\theta^* \\ 1^* & 0 & 0 & 0 \end{bmatrix}$$

$$B = \begin{bmatrix} M_{\delta_1} & M_{\delta_1}^* & M_{\delta_0} & 0 \\ Z_{\delta_1} & Z_{\delta_1}^* & Z_{\delta_0} & g/V \\ X_{\delta_1}^* & X_{\delta_1}^* & X_{\delta_0}^* & 0 \\ 0 & 0 & 0 & 0 \end{bmatrix}$$

*Normally held fixed.

APPENDIX A - Concluded

$$C = I$$

$$G = \begin{bmatrix} M_q & M_\alpha & M_u \\ Z_q & Z_\alpha & Z_u \\ X_q & X_\alpha & X_u \end{bmatrix}$$

$$H = \begin{bmatrix} M_{\delta_1} & M_{\delta_1} & M_{\delta_0} & 0 \\ Z_{\delta_1} & Z_{\delta_1} & Z_{\delta_0} & 0 \\ X_{\delta_1} & X_{\delta_1} & X_{\delta_0} & 0 \end{bmatrix}$$

APPENDIX B

OPEN-LOOP DYNAMIC CHARACTERISTICS

The open-loop dynamic characteristics of the M2-F3 vehicle, including flight conditions and mass parameters, are presented in the following tables.

FLIGHT CONDITIONS AND MASS PARAMETERS

	Flight condition								
	1	2	3	4	5	6	7	8	9
h, m (ft)	1520 (5000)	13,700 (45,000)	6710 (22,000)	14,600 (48,000)	10,700 (35,000)	15,200 (50,000)	16,800 (55,000)	18,300 (60,000)	19,800 (65,000)
M	0.50	0.67	0.70	0.80	0.90	0.90	0.95	1.10	1.30
V, m/sec (ft/sec)	167 (549)	198 (649)	219 (720)	236 (774)	267 (876)	265 (871)	280 (920)	324 (1060)	383 (1260)
Gross weight, kg (lb)	3171 (7000)	4757 (10,500)	3171 (7000)	4304 (9500)	3171 (7000)	3851 (8500)	3624 (8000)	3398 (7500)	3171 (7000)
Center of gravity, fraction of c	0.492	0.503	0.492	0.504	0.492	0.502	0.499	0.496	0.492
I _X , kg-m ² (slug-ft ²)	2175 (1605)	2266 (1672)	2175 (1605)	2220 (1638)	2175 (1605)	2203 (1625)	2196 (1620)	2175 (1605)	2175 (1605)
I _Y , kg-m ² (slug-ft ²)	11,790 (8700)	12,310 (9080)	11,790 (8700)	12,170 (8980)	11,790 (8700)	12,040 (8880)	11,970 (8830)	11,870 (8760)	11,790 (8700)
I _Z , kg-m ² (slug-ft ²)	11,640 (8590)	12,100 (8930)	11,640 (8590)	11,960 (8820)	11,640 (8590)	11,819 (8720)	11,738 (8660)	11,640 (8590)	11,640 (8590)
I _{XZ} , kg-m ² (slug-ft ²)	-836 (-617)	-865 (-638)	-836 (-617)	-862 (-636)	-836 (-617)	-857 (-632)	-855 (-631)	-847 (-625)	-836 (-617)
ε, deg	5.01	4.99	5.01	5.02	5.01	5.05	5.08	5.07	5.01
q̄, hN/m ² (lb/ft ²)	147 (307)	46.6 (97.5)	147 (307)	57.4 (120)	136 (283)	66.6 (139)	58.4 (122)	61.3 (128)	67.5 (141)
α, deg	6.0	10.0	3.0	13.0	3.0	10.0	5.0	5.0	5.0
γ, deg	-18.0	-10.0	-23.0	2.0	-23.0	10.0	15.0	15.0	15.0

APPENDIX B - Continued

δ_a TRANSFER FUNCTION FACTORS¹

[Body-axis system]

		Flight condition								
		1	2	3	4	5	6	7	8	9
		Denominator								
$\xi, (1/\tau)$.617	.779	.487	.690	(-.276)	.829	.929	-.369	.359
$\omega_n, (1/\tau)$.366	.154	.282	.154	(-1.95)	.356	.755	.364	.291
ξ		.111	.0289	.108	.0355	.910	.112	-.462	.251	.0735
ω_n		5.63	3.80	4.97	4.63	1.98	2.63	.928	1.59	1.77
		Numerator								
β/δ_a										
Gain		-.09711	.008295	-.00539	-.60969	-.00136	-.00232	-.00171	-.000474	.246
$1/\tau$		-.230	.2285	-.133	-.699	-.241	-.232	-.130	-.299	
$\xi, (1/\tau)$.432	.765	-.0496	.816	(1.58)	.890	.489	-.541	.354
$\omega_n, (1/\tau)$.675	.274	.770	.329	(645.)	.409	.546	.510	.331
p/δ_a										
Gain		14.9	4.33	14.8	4.56	12.3	5.81	5.34	4.29	4.37
$1/\tau$.0121	0.	.0152	-.0110	.0116	-.0124	-.0123	-.0101	-.00854
$\xi, (1/\tau)$.138	.0525	.107	.0626	.384	.215	(-.957)	.177	.191
$\omega_n, (1/\tau)$		4.34	2.77	4.44	3.61	1.34	1.26	(1.41)	1.03	.847
r/δ_a										
Gain		-.0871	.0798	-.0478	.356	1.52	.479	.249	.233	.136
$1/\tau$.555	.287	.840	.179	1.13	.202	.356	.395	.302
$\xi, (1/\tau)$		(12.6)	.0701	.661	.0372	.378	.116	(-1.37)	.425	.305
$\omega_n, (1/\tau)$		(-25.2)	8.56	17.4	6.19	.646	1.80	(2.04)	1.14	1.34
ϕ/δ_a										
Gain		14.9	4.33	14.8	4.65	11.7	5.99	5.47	4.37	4.42
$1/\tau$.139	.0525	.106	.0655	.373	.208	(-.969)	.181	.190
$\omega_n, (1/\tau)$		4.29	2.77	4.40	3.68	1.35	1.28	(1.42)	1.04	.854
a_y/δ_a										
Gain		-3.90	.191	-3.88	-.751	-1.19	-2.02	-1.57	-.505	-21.9
$1/\tau$.456	(11.2)	.0695	.751	(-2.42)	.873	.520	-.530	.354
$\omega_n, (1/\tau)$.588	(-10.2)	.592	.277	(1.60)	.394	.594	.495	.331
$\xi, (1/\tau)$.0468	.774	.0733	.0385	(10.8)	-.0116	-.0240	.0984	
$\omega_n, (1/\tau)$		9.59	.291	7.23	8.09	(-10.9)	4.92	3.07	4.97	

¹Factored polynomials are in the form $(s + 1/\tau)$ or $(s^2 + 2\xi\omega_n + \omega_n^2)$.

APPENDIX B - Continued

δ_r TRANSFER FUNCTION FACTORS¹

[Body-axis system]

Flight condition									
	1	2	3	4	5	6	7	8	9
Denominator									
$\zeta, (1/\tau)$.617	.779	.487	.690	(-.276)	.829	.929	-.369	.359
$\omega_n, (1/\tau)$.366	.154	.282	.158	(-1.95)	.356	.755	.364	.293
ζ	.111	.0269	.108	.3355	.910	.0112	-.462	.251	.0735
ω_n	5.63	3.80	4.97	4.63	1.98	2.63	.928	1.59	1.77
Numerator									
β/δ_r - Gain	.0237	.00295	.00359	4.08	.0177	.00662	.00487	2.62	.00142
$1/\tau$.00963	.00439	.0386	.0505	462.	.0465	.0130	.00767	.0198
$1/\tau, (\xi)$.392	.155	.287	.0867	(.910)	.133	.0951	.116	.120
$1/\tau, (\omega_n)$	346.	915.	1704.		(.167)	729.	591.		1442.
p/δ_r - Gain	13.1	4.17	12.6	6.42	17.3	7.40	4.40	3.67	3.49
$1/\tau$.0122	.00110	.0153	-.0110	.0126	-.0128	-.0120	-.0104	-.00879
$1/\tau$	-6.50	-3.59	-5.00	-3.77	-6.22	-5.52	-4.91	-5.68	-4.73
$1/\tau$	4.54	3.71	5.25	3.92	6.66	5.68	5.00	5.21	4.87
r/δ_r - Gain	-6.83	-2.00	-5.46	-2.70	-7.28	-3.60	-2.50	-2.31	-1.75
$1/\tau$.544	.283	.739	.178	.634	.200	.369	.321	.274
ζ	.00199	-.0292	-.0815	-.00577	-.0504	.00180	-.00552	-.0384	-.0227
ω_n	2.94	2.25	1.86	2.85	2.32	3.37	1.97	1.93	2.01
φ/δ_r - Gain	14.6	4.17	14.6	5.70	19.9	6.09	3.49	2.83	2.85
$1/\tau$	-6.07	-3.68	-4.57	-4.14	-5.72	-6.30	-5.63	-5.90	-5.33
$1/\tau$	6.17	3.71	4.86	4.28	6.16	6.43	5.58	6.00	5.45
θ_y/δ_r - Gain	13.0	1.91	2.58	-199.	15.5	5.77	4.48	-205.	1.78
$1/\tau$	-.132	-.0525	.1190	.0505	.00507	-.0682	-.0549	.00767	-.00190
$1/\tau$.595	.178	.311	.0867	.363	.181	.157	.116	.139
$1/\tau$	-7.15	-5.62	-17.7		-8.85	-6.66	-5.37		-9.82
$1/\tau$	8.21	5.89	19.5		9.69	7.12	6.75		10.1

¹Factored polynomials are in the form $(s + 1/\tau)$ or $(s^2 + 2\zeta\omega_n + \omega_n^2)$.

APPENDIX B - Concluded

δ_1 TRANSFER FUNCTION FACTORS¹
[Body-axis system]

Flight condition									
	1	2	3	4	5	6	7	A	9
Denominator									
ξ	.372	.258	.406	.268	.498	.167	.460	.472	.495
ω_n	.122	.0512	.0863	.0455	.0960	.0314	.0644	.0200	.0264
$\xi \cdot (1/\tau)$.27	.133	.237	.208	.143	.173	.0649	.1925	.0770
$\omega_n \cdot (1/\tau)$	2.69	1.42	2.67	1.33	3.27	1.34	1.87	2.39	2.51
Numerator									
u/δ_1 - Gain	-17.9	-6.69	-25.1	-12.4	-32.4	-13.0	-10.9	-9.43	-8.01
$1/\tau$	-38.9	4.26	-15.5	.174	-19.3	.138	.6843	.104	-64.1
$\xi \cdot (\omega_n)$.07	(.24)	.697	(.194)	.658	(.205)	(.467)	(.200)	.915
$\omega_n \cdot (1/\tau)$.523	(-61.1)	.545	(-82.4)	.418	(-65.5)	(-37.7)	(-62.5)	.157
w/δ_1 - Gain	-55.9	-5.60	-64.1	-17.8	-66.2	-31.6	-20.5	-19.7	-21.0
$1/\tau$	1.01	4.13	1.30	2.43	1.84	1.58	2.25	3.04	280.
ξ	.375	.221	.436	.231	.596	.213	.273	.462	.532
ω_n	.111	.0445	.3783	.0432	.0710	.0399	.0367	.0233	.0227
θ/δ_1 - Gain	-12.3	-3.63	-10.7	-5.73	-13.9	-5.71	-5.04	-5.66	-4.69
$1/\tau$.516	.0229	.3560	.0189	.0788	.0205	.0245	.0292	.0343
$1/\tau$.485	.104	.357	.134	.253	.141	.135	.1942	.0423
h/δ_1 - Gain	69.1	5.60	68.9	14.0	73.3	24.7	15.6	15.7	17.0
$1/\tau$.397	-0.0638	.0541	-0.0517	.0708	-0.0183	.03121	.0139	.0185
$1/\tau$	6.66	6.22	-5.94	6.02	6.25	4.94	5.07	5.77	5.32
$1/\tau$	6.7	-6.58	6.19	-6.11	-6.27	-5.01	-5.33	-5.86	-5.32
a_n/δ_1 - Gain	65.9	5.60	64.1	17.8	66.2	31.6	20.5	19.7	21.0
$1/\tau$	6.87	6.	-6.51	.0116	.0172	.0143	.0163	-0.137	-0.112
$1/\tau$	-6.93	-0.0638	6.63	-0.0199	-0.0563	-0.0196	-0.195	-0.233	-0.245
$1/\tau, (\xi)$	(.818)	5.22	(.961)	-5.43	6.82	4.55	4.62	5.30	-4.81
$1/\tau, (\omega_n)$	(.3255)	-6.58	(.3292)	5.46	-7.00	4.61	-4.77	-5.31	4.86

¹Factored polynomials are in the form $(s + 1/\tau)$ or $(s^2 + 2\xi\omega_n + \omega_n^2)$.

REFERENCES

1. Kempel, Robert W.; and Thompson, Ronald C.: Flight-Determined Aerodynamic Stability and Control Derivatives of the M2-F2 Lifting Body Vehicle at Subsonic Speeds. NASA TM X-2413, 1971.
2. Kempel, Robert W.: Analysis of a Coupled Roll-Spiral-Mode, Pilot-Induced Oscillation Experienced With the M2-F2 Lifting Body. NASA TN D-6496, 1971.
3. Mechtly, E. A.: The International System of Units - Physical Constants and Conversion Factors (Revised). NASA SP-7012, 1969.
4. Pyle, Jon S.; and Swanson, Robert H.: Lift and Drag Characteristics of the M2-F2 Lifting Body During Subsonic Gliding Flight. NASA TM X-1431, 1967.
5. Boucher, Robert W.; Rich, Drexel A.; Crane, Harold L.; and Matheny, Cloyce E.: A Method for Measuring the Product of Inertia and the Inclination of the Principal Longitudinal Axis of Inertia of an Airplane. NACA TN 3084, 1954.
6. Kock, Berwin M.; and Painter, Weneth D.: Investigation of the Controllability of the M2-F2 Lifting-Body Launch From the B-52 Carrier Airplane. NASA TM X-1713, 1968.
7. Kempel, Robert W.; Strutz, Larry W.; and Kirsten, Paul W.: Stability and Control Derivatives of the Lifting Body Vehicles. Flight Test Results Pertaining to the Space Shuttlecraft. NASA TM X-2101, 1970, pp. 11-27.
8. Iliff, Kenneth W.; and Taylor, Lawrence W., Jr.: Determination of Stability Derivatives From Flight Data Using a Newton-Raphson Minimization Technique. NASA TN D-6579, 1972.
9. Taylor, Lawrence W., Jr.; and Iliff, Kenneth W.: Systems Identification Using a Modified Newton-Raphson Method - A Fortran Program. NASA TN D-6734, 1972.
10. Wolowicz, Chester H.; Iliff, Kenneth W.; and Gilyard, Glenn B.: Flight Test Experience in Aircraft Parameter Identification. AGARD CP-119, Nov. 1972, pp. 23-1 - 23-13.
11. Keener, Earl R.; and Brownson, Jack J.: Wind-Tunnel Investigation of the Aerodynamic Characteristics of the M2-F2 Lifting-Body Entry Configuration at Transonic and Supersonic Mach Numbers. NASA TM X-2511, 1972.

TABLE 1.- PHYSICAL CHARACTERISTICS OF M2-F3 VEHICLE

Body -	
Planform area, m ² (ft ²):	
Actual	14.49 (156.0)
Reference (S)	14.86 (160.0)
Longitudinal length, m (ft):	
Reference (c)	6.77 (22.2)
Span, m (ft):	
Actual	2.93 (9.63)
Reference (b)	3.03 (9.95)
Leading-edge sweep, deg	77
Lower flap -	
Area, m ² (ft ²)	1.42 (15.25)
Span, m (ft)	1.65 (5.42)
Chord, m (ft)	0.86 (2.81)
Design hinge moment, m-N (in-lb)	7570 (67,000)
Upper flaps, two -	
Area, each, m ² (ft ²)	0.85 (9.20)
Span, each, m (ft)	1.26 (4.21)
Chord, m (ft)	0.68 (2.23)
Design hinge moment, each, m-N (in-lb)	3390 (30,000)
Vertical stabilizers, two -	
Area, each, m ² (ft ²)	1.50 (16.10)
Height, trailing edge, m (ft)	1.16 (3.79)
Chord, m (ft):	
Root	2.24 (7.36)
Tip	0.79 (2.58)
Leading-edge sweep, deg	62.3
Center fin -	
Area, m ² (ft ²)	1.12 (12.02)
Height, trailing edge, m (ft)	1.26 (4.13)
Chord, m (ft):	
Root, at horizontal reference plane	1.59 (5.21)
Tip	0.30 (1.00)
Leading-edge sweep, deg	58
Rudders, two -	
Area, each, m ² (ft ²)	0.49 (5.27)
Span, each, m (ft)	1.28 (4.20)
Chord, m (ft)	0.38 (1.25)
Design hinge moment, each, m-N (in-lb)	2600 (23,000)
Center of gravity, reference -	
Decimal fraction of chord	0.496

TABLE 2.— TYPICAL VARIATION OF MOMENTS OF INERTIA AND
 CENTER OF GRAVITY WITH GROSS WEIGHT

[Body axis]

Gross weight, kg (lb)	I_X' , kg-m ² (slug-ft ²)	I_Y' , kg-m ² (slug-ft ²)	I_Z' , kg-m ² (slug-ft ²)	I_{XZ}' , kg-m ² (slug-ft ²)	Center of gravity, per \bar{c}
4763 (10,500)	2266 (1672)	12,307 (9080)	12,104 (8930)	-865 (-638)	0.503
4309 (9500)	2220 (1638)	12,172 (8980)	11,955 (8820)	-862 (-636)	0.504
3856 (8500)	2203 (1625)	12,036 (8880)	11,819 (8720)	-857 (-632)	0.502
3402 (7500)	2175 (1605)	11,873 (8760)	11,643 (8590)	-847 (-625)	0.496
3180 (7000)	2175 (1605)	11,792 (8700)	11,643 (8590)	-836 (-617)	0.491

TABLE 3.- FINAL CONTROL SURFACE CHARACTERISTICS

	δ_a	δ_r	δ_l	δ_u	δ_{sb}
Pilot control surface authority	$\pm 20^\circ$	$\pm 4.5^\circ$	10° to 48.5°	-11.8° to -20°	20°
Automatic control system surface authority	$\pm 10^\circ$	$\pm 2^\circ$	$\pm 7.5^\circ$	- - - -	- - - -
Automatic control system maximum surface rate	30 deg/sec	22 deg/sec	25 deg/sec	- - - -	2.9 deg/sec
Automatic trim (command augmentation system only) maximum rate	- - - -	- - - -	4.8 deg/sec	- - - -	- - - -

TABLE 4.- PARAMETER RESOLUTION AND ACCURACY

Parameter	Resolution	Accuracy
\bar{q} , hN/m ² (lb/ft ²)	0.670 (1.40)	1.57 (3.29)
δ_a , deg	0.111	0.675
δ_r , deg	0.097	0.380
δ_1 , hN/m ² (lb/ft ²)	1.08	- - - -
δ_1 , deg	0.0851	0.462
δ_u , deg	0.111	0.675
δ_{sb} , deg	0.0594	0.462
p, deg/sec	0.157	0.830
r, deg/sec	0.050	0.550
β , deg	0.040	0.220
φ , deg	0.380	2.48
\dot{p} , deg/sec ²	0.829	- - - -
\dot{r} , deg/sec ²	0.380	- - - -
a_y , g	0.00539	0.0164
q, deg/sec	0.168	0.550
α , deg	0.0607	0.43
θ , deg	0.187	1.24
\dot{q} , deg/sec ²	0.349	- - - -
a_n , g	0.0174	0.0328
a_x , g	0.00870	0.082

TABLE 5 - Concluded

(b) Longitudinal derivatives

M	α , deg	$C_{m\alpha}$, deg ⁻¹	$C_{m\delta_1}$, deg ⁻¹	C_{mq} , rad ⁻¹	$C_{L\alpha}$, deg ⁻¹	$C_{L\delta_1}$, deg ⁻¹
.582	2.09	-.000729	-.002120	-.5700	.02400	-.002120
.597	4.23	-.000611	-.001640	-.4840	.02080	.002131
.522	4.34	-.000853	-.001697	-.1616	.02400	.002166
.484	4.50	-.000830	-.001970	-.3690		
.561	4.84	-.001050	-.001955	-.4260	.02060	.002870
.466	5.10	-.000819	-.002053	-.4050	.02184	-.002083
.514	6.66	-.000993	-.001707	-.4150	.02520	.002340
.522	7.15	-.001035	-.001657	-.4200	.02453	.000736
.587	8.17	-.000821	-.001638	-.3390	.02340	.004590
.544	8.28	-.001102	-.001645	-.0657	.02522	.001168
.478	9.00	-.000989	-.001764	-.1400	.02160	.004440
.461	9.76	-.001169	-.002007	-.2119	.02250	.003775
.484	10.29	-.001040	-.001698	-.2189	.02260	.003300
.515	15.20	-.000723	-.001484	-.1200	.02900	.023170
.590	-.40	-.000764	-.001490	-.5480	.02220	.000430
.694	3.14	-.000793	-.001733	-.6233	.02440	.000005
.736	5.28	-.001208	-.001413	-.7670	.02370	
.645	6.72	-.000667	-.002040	-.2660	.02672	-.000025
.674	6.72	-.000986	-.002230	-.4570	.02330	.001490
.711	7.89	-.000889	-.001665	-.7570	.02260	.003889
.749	9.84	-.000874	-.001562	.1970	.02240	.003369
.724	12.50	-.000968	-.001724	-.4810	.02380	.001110
.677	15.31	-.000510	-.001769	.2520	.03800	-.008100
.806	2.72	-.001307	-.001250	-.9720	.02270	.003090
.800	7.00	-.001125	-.002160	-1.2300	.02440	.000143
.849	7.92	-.001176	-.002339	-.5860	.02530	.000273
.832	8.81	-.001448	-.002486	-.6840	.02450	.002780
.785	9.99	-.000782	-.001854	.1040	.02230	.001698
.764	12.80	-.000644	-.002120	-.6070	.02510	.001330
.906	3.61	-.001611	-.002037	-.7106	.02459	-.001610
.885	10.40	-.000729	-.001800	-.2095	.02205	.003140
.916	10.70	-.000258	-.001690	-.9630	.01900	.004320
.935	12.44	-.000387	-.002175	.3940	.02126	.008450
.996	3.77	-.002252	-.001573	-.1959	.01685	.008190
1.002	6.73	-.002245	-.001090	-.2446	.02095	.003830
.972	7.75	-.001840	-.001784	.5180	.02520	-.002280
1.136	-.79	-.023860	-.001180	-1.0100	.01858	.003119
1.017	5.15	-.001890	-.001990	-.6600	.02250	.001190
1.129	5.94	-.002170	-.001633	-.4100	.01820	.002350
1.104	8.12	-.002390	-.002210	-.3650	.01870	.002210
1.340	.23	-.001778	-.001480	-.7500	.02070	.000298
1.210	.91	-.001726	-.001440	-.7051	.01906	.001538

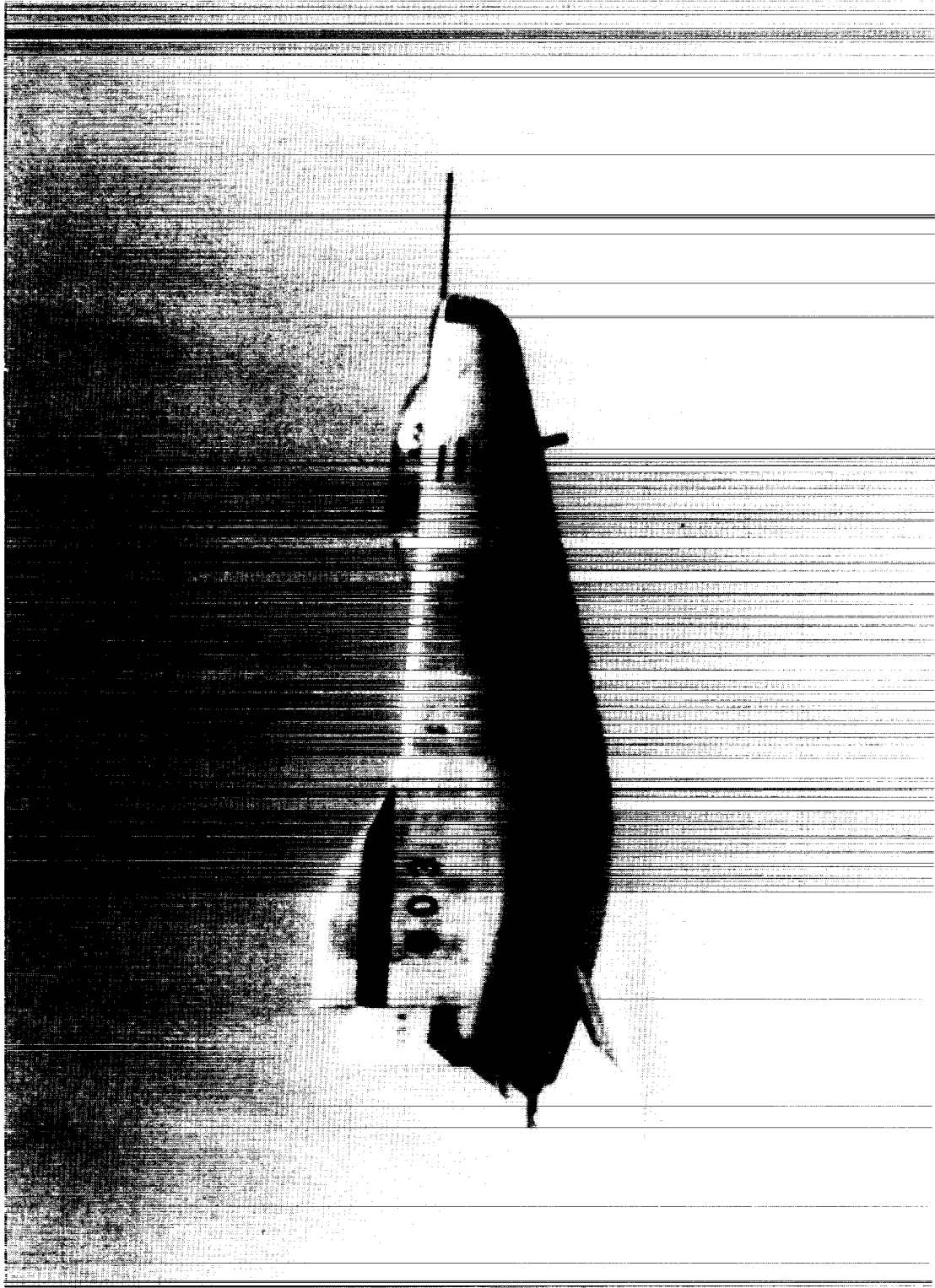


Figure 1. M2-F3 vehicle in flight.

E-23575

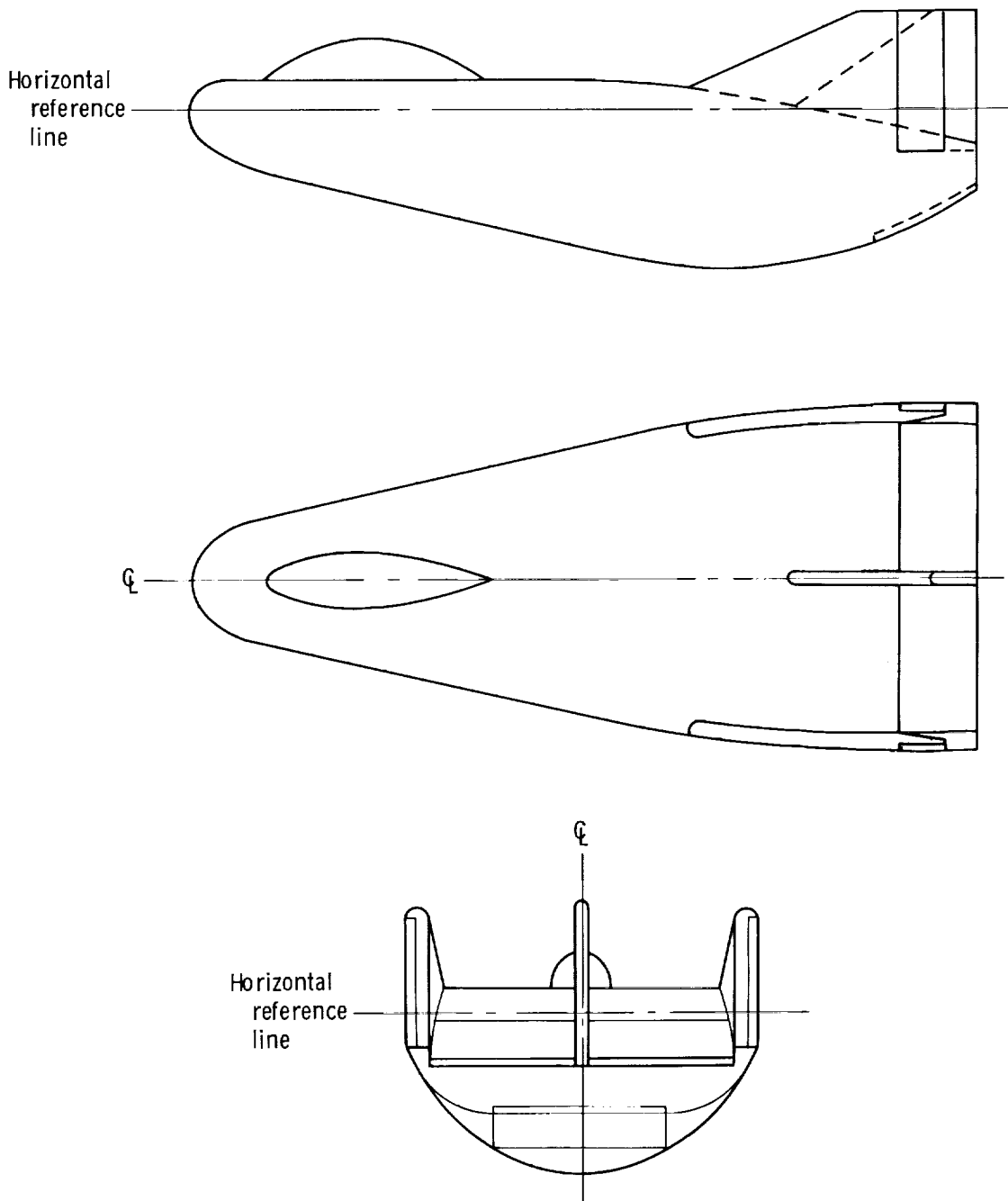


Figure 2. Three-view drawing of the M2-F3 vehicle.

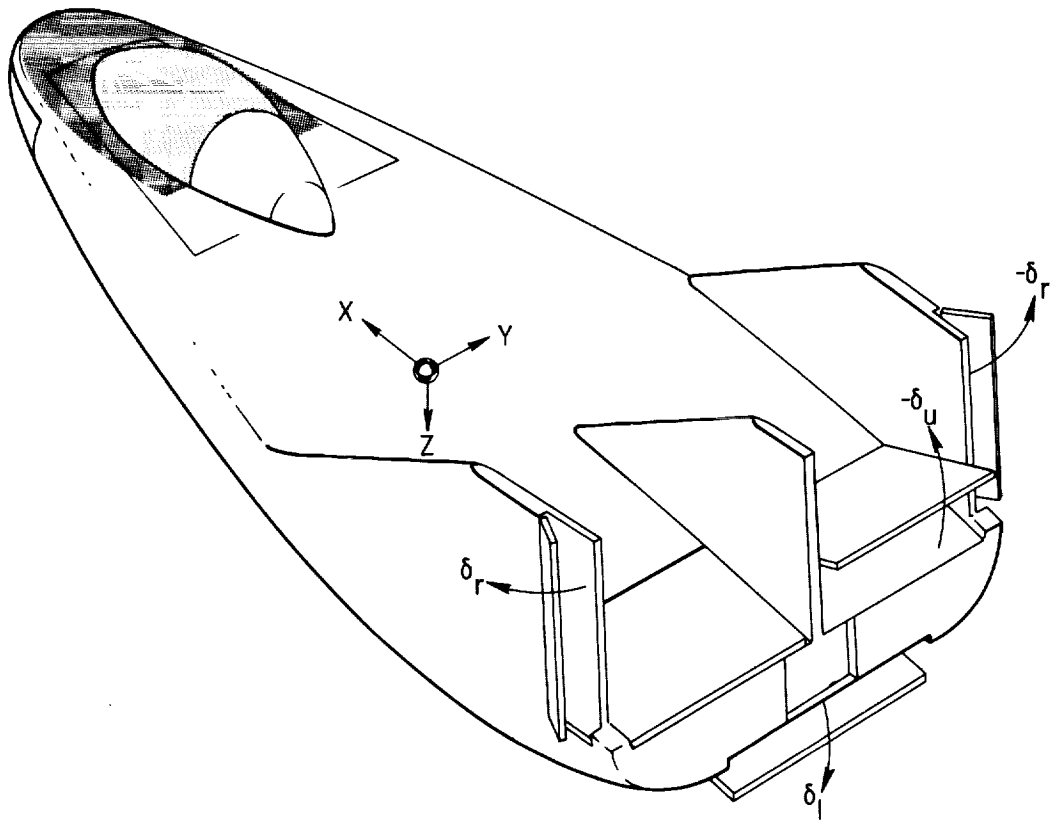


Figure 3. Sign convention and control surface location.

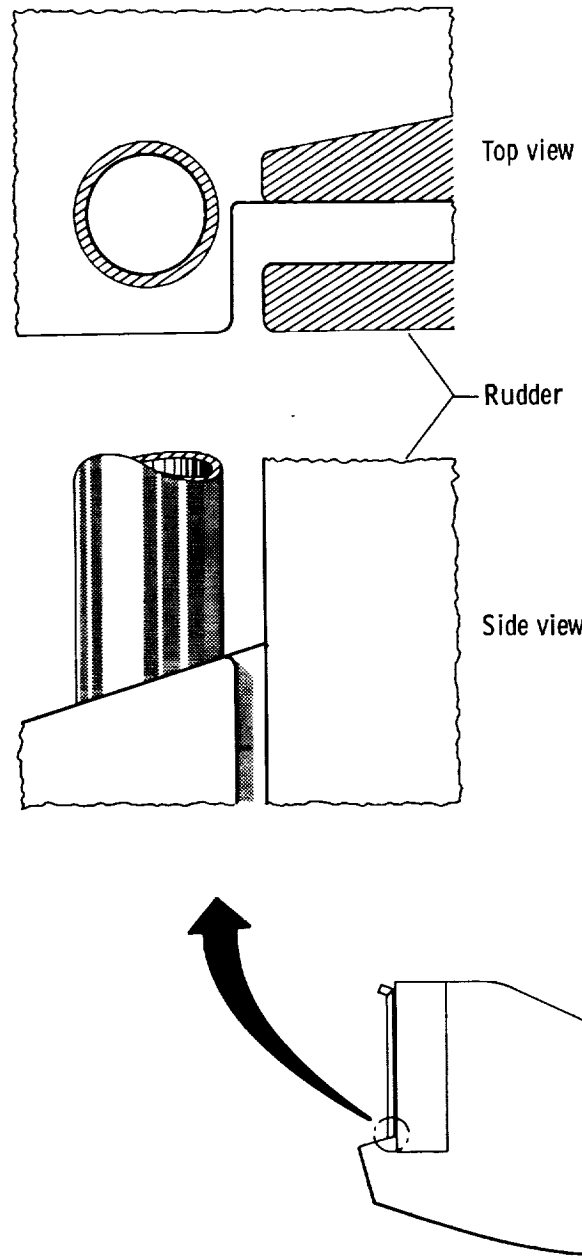
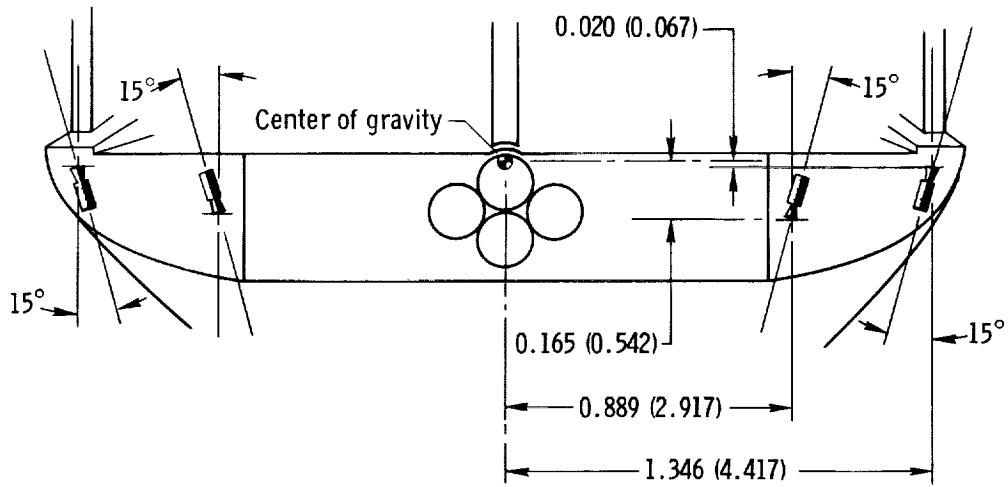
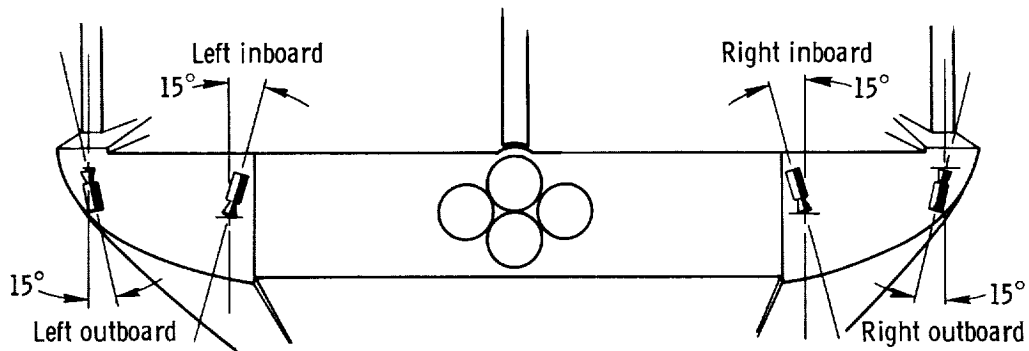


Figure 4. Right-hand jettison tube location on outboard vertical fin.



(a) Geometry 1. (Dimensions in meters (feet) unless otherwise indicated.)



(b) Geometry 2.

Figure 5. Reaction control rocket geometries.

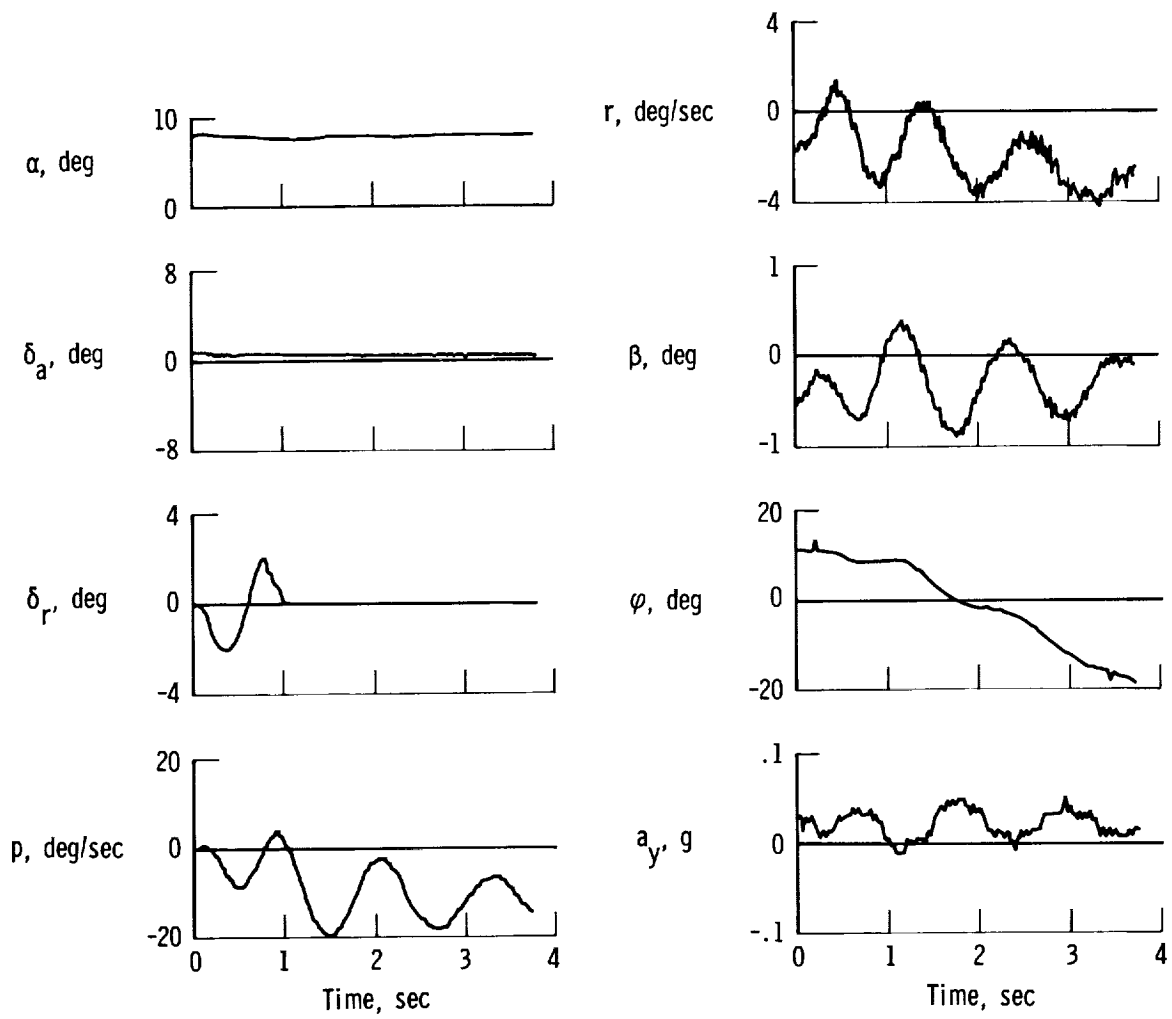


Figure 6. Typical doublet control input maneuver.

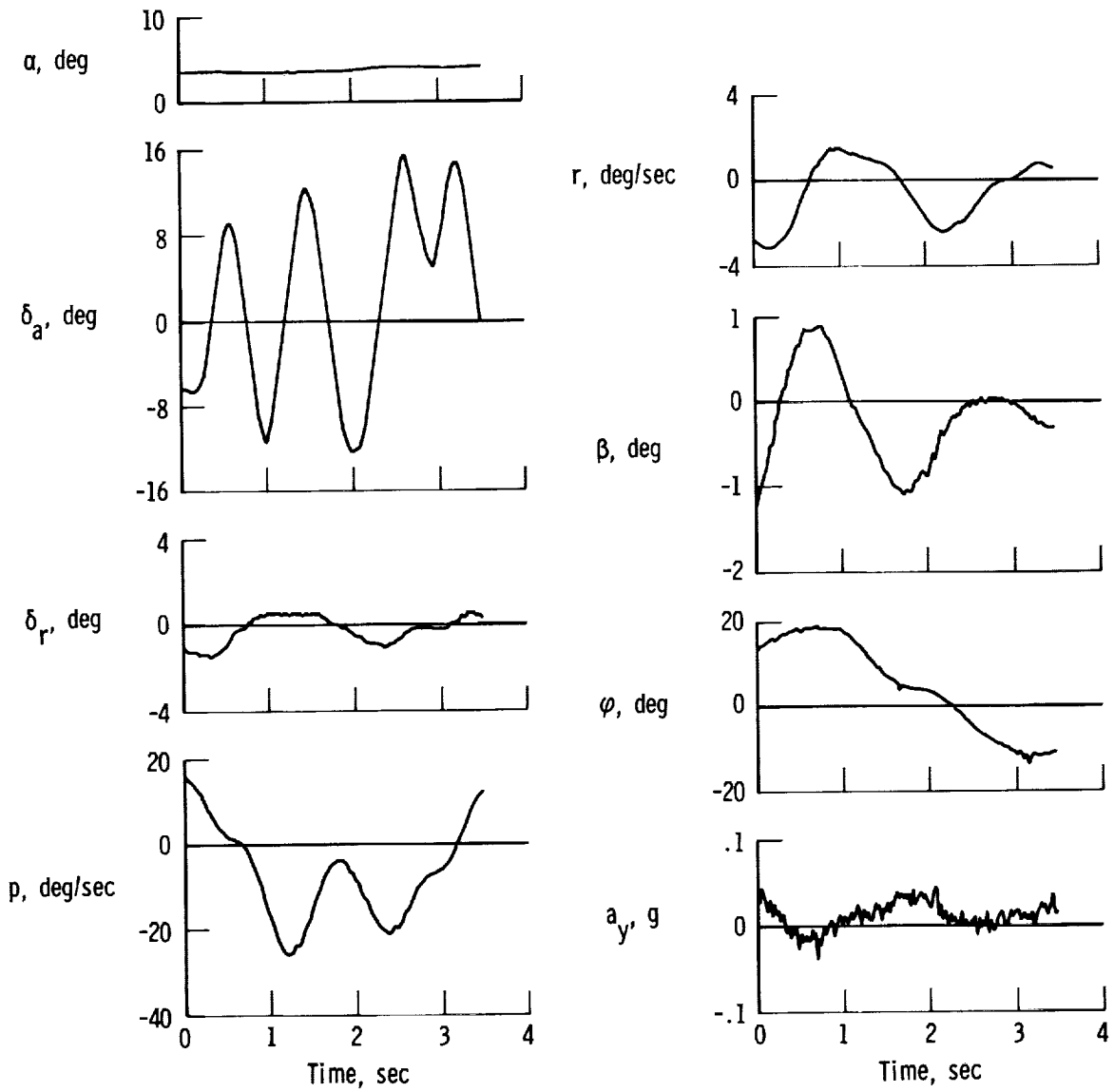


Figure 7. Typical pilot-induced oscillatory aileron control input maneuver.

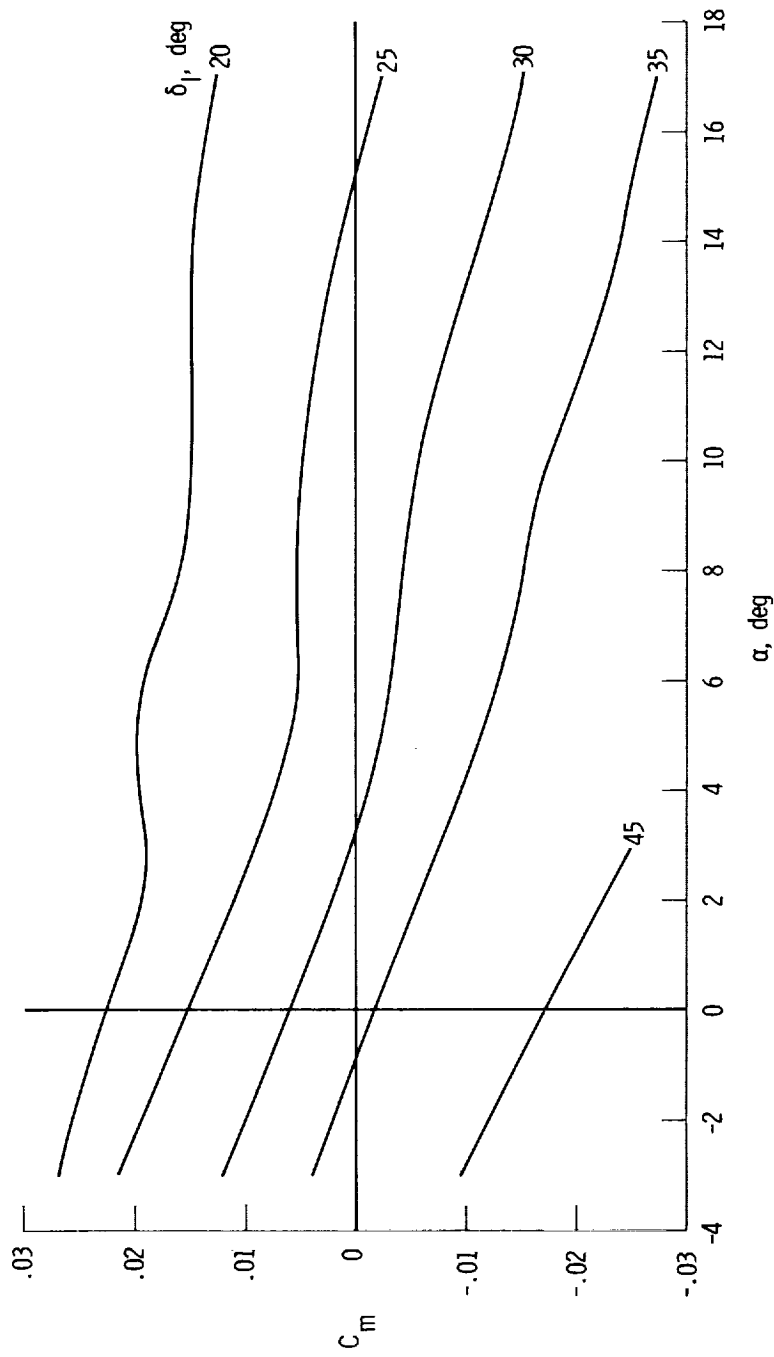
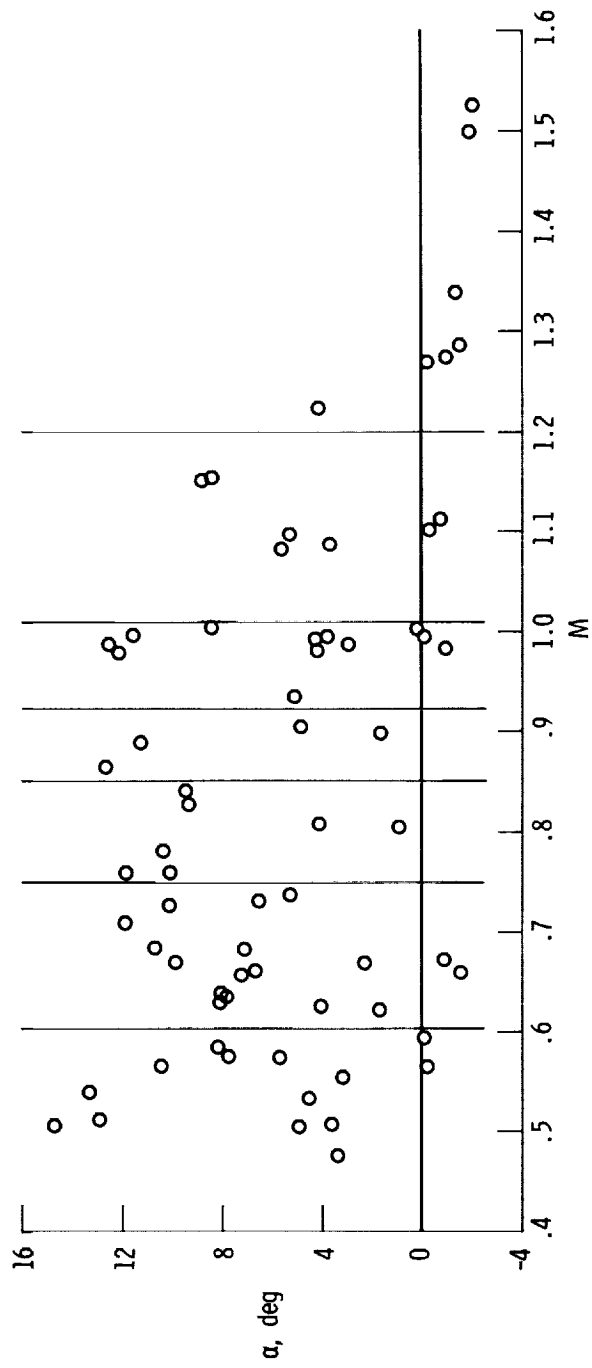
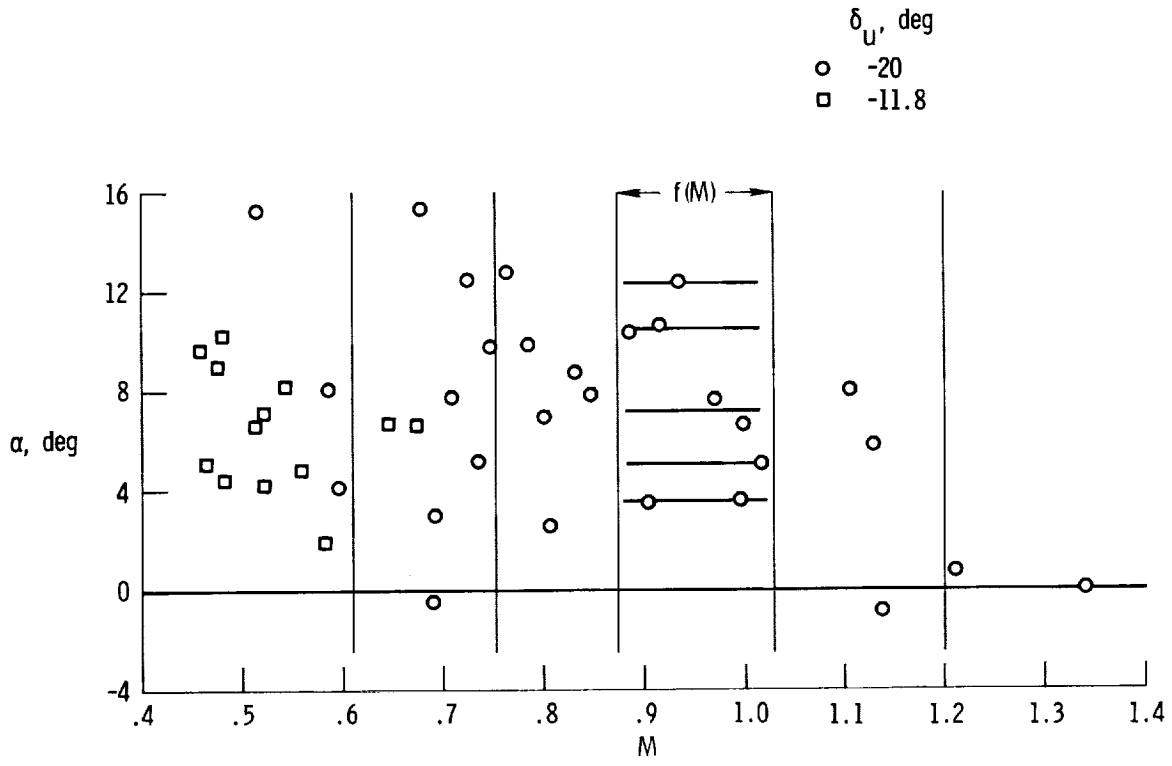


Figure 8. Pitching-moment curve from wind-tunnel data. $M = 0.95$; $\delta_u = -20^\circ$; center of gravity = $0.496\bar{c}$.



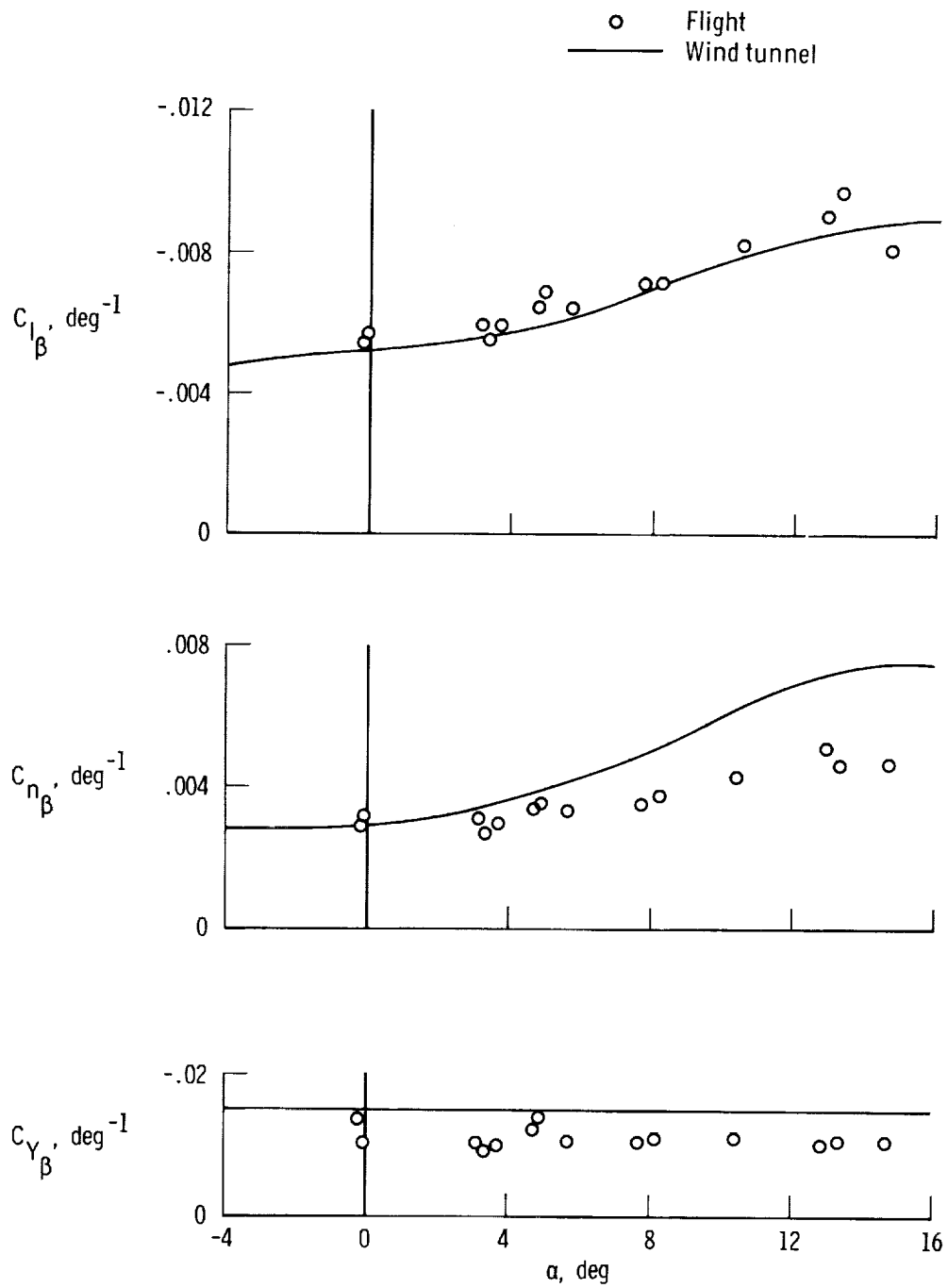
(a) Lateral-directional derivatives.

Figure 9. Flight conditions at which lateral-directional and longitudinal sets of derivatives were obtained. Vertical lines indicate separation of data for comparison with wind-tunnel predictions.



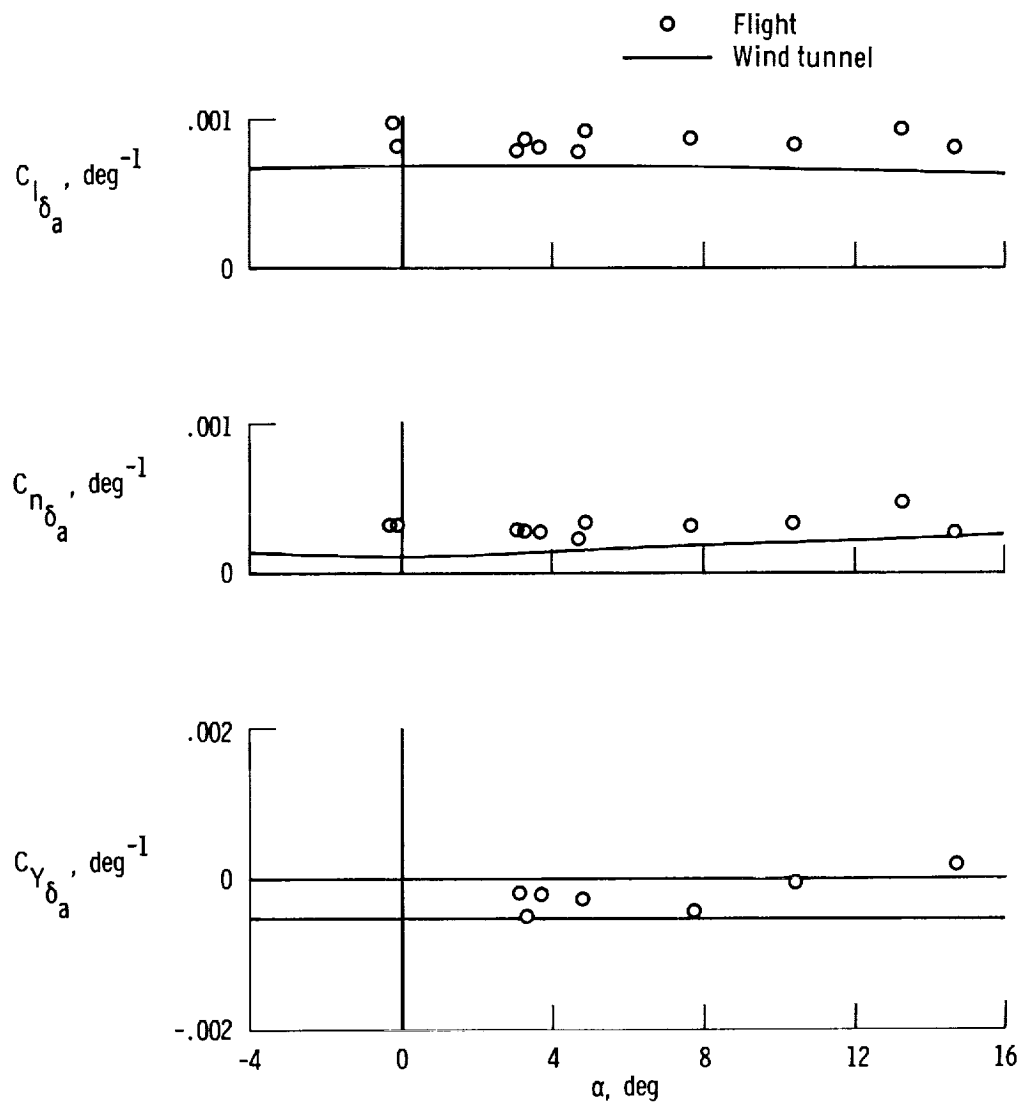
(b) Longitudinal derivatives.

Figure 9. Concluded.



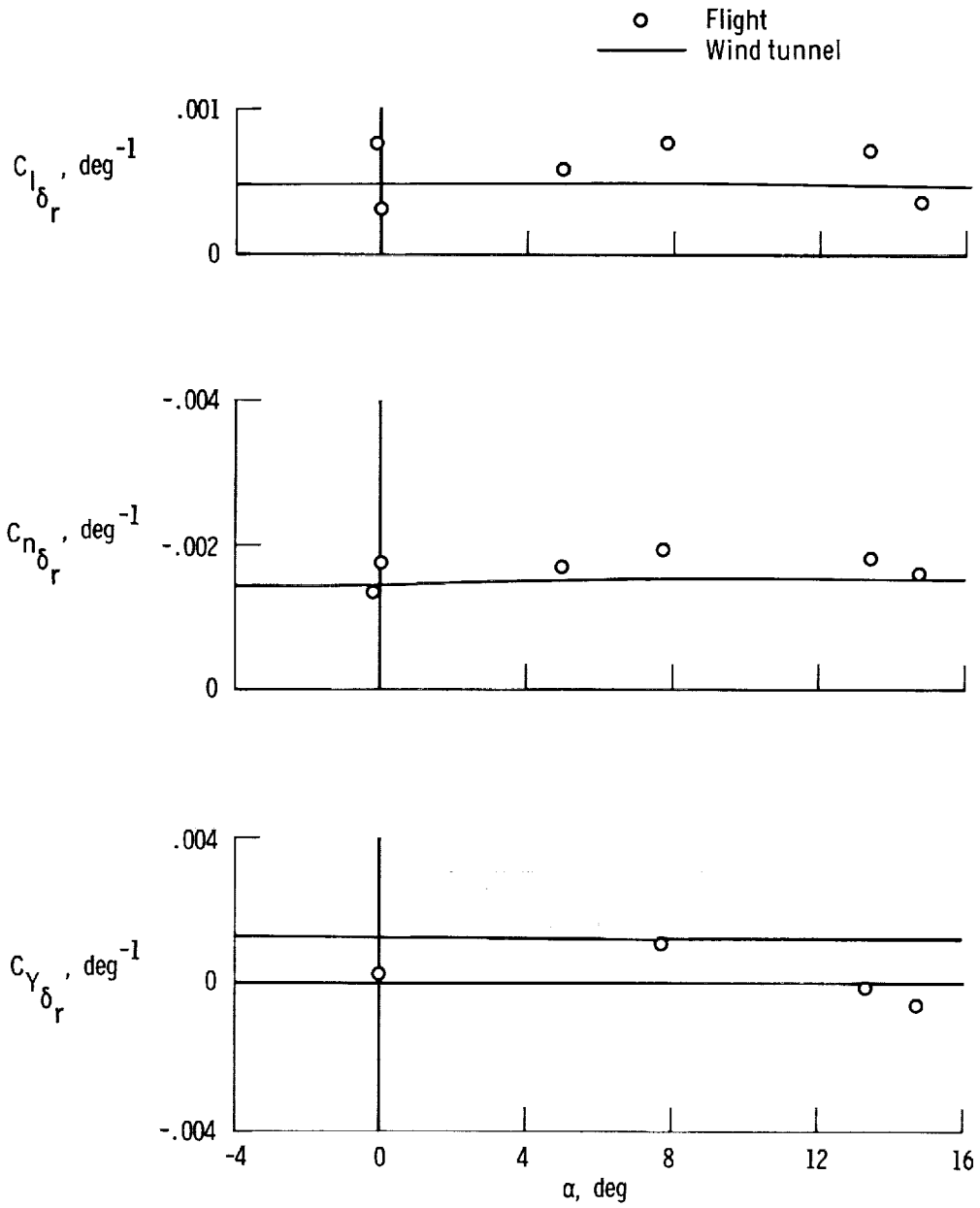
(a) C_{l_β} , C_{n_β} , C_{Y_β} .

Figure 10. Comparison of lateral-directional derivatives obtained from flight data with wind-tunnel predictions for a Mach number of 0.5.



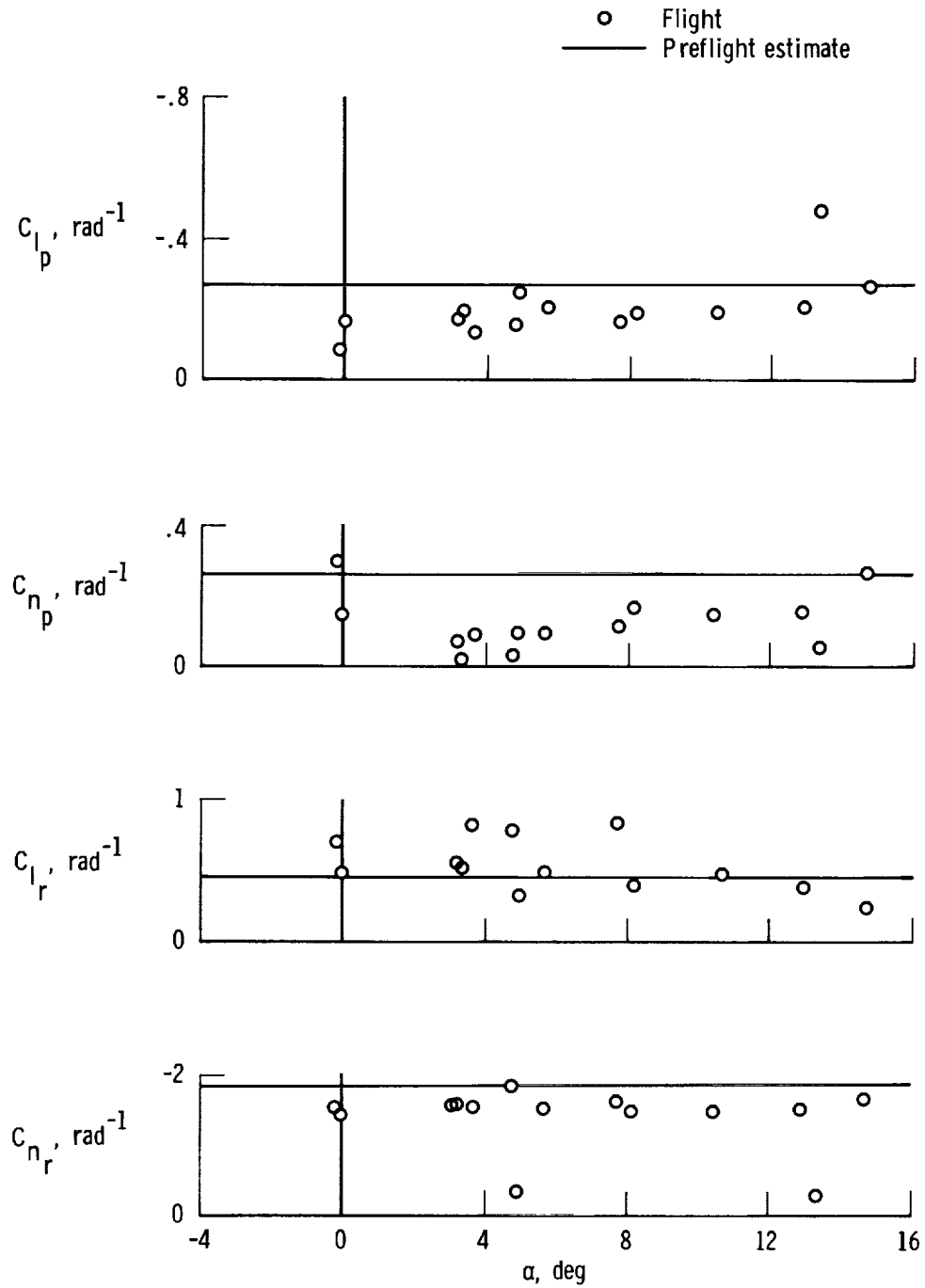
(b) $C_{l_{\delta_a}}$, $C_{n_{\delta_a}}$, $C_{Y_{\delta_a}}$.

Figure 10. Continued.



(c) $C_{l_{\delta_r}}$, $C_{n_{\delta_r}}$, $C_{Y_{\delta_r}}$.

Figure 10. Continued.



(d) C_{l_p} , C_{n_p} , C_{l_r} , C_{n_r} .

Figure 10. Concluded.

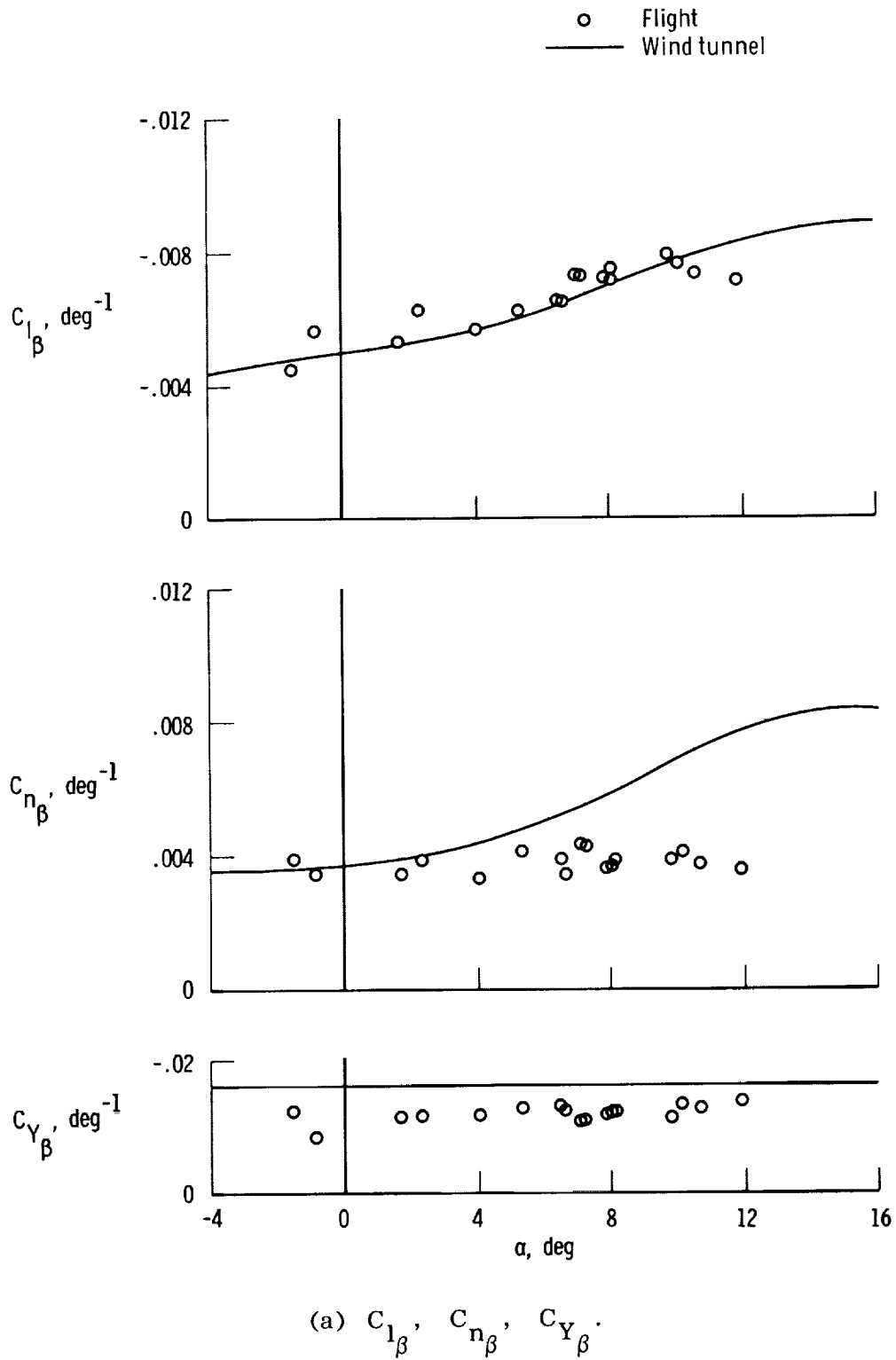
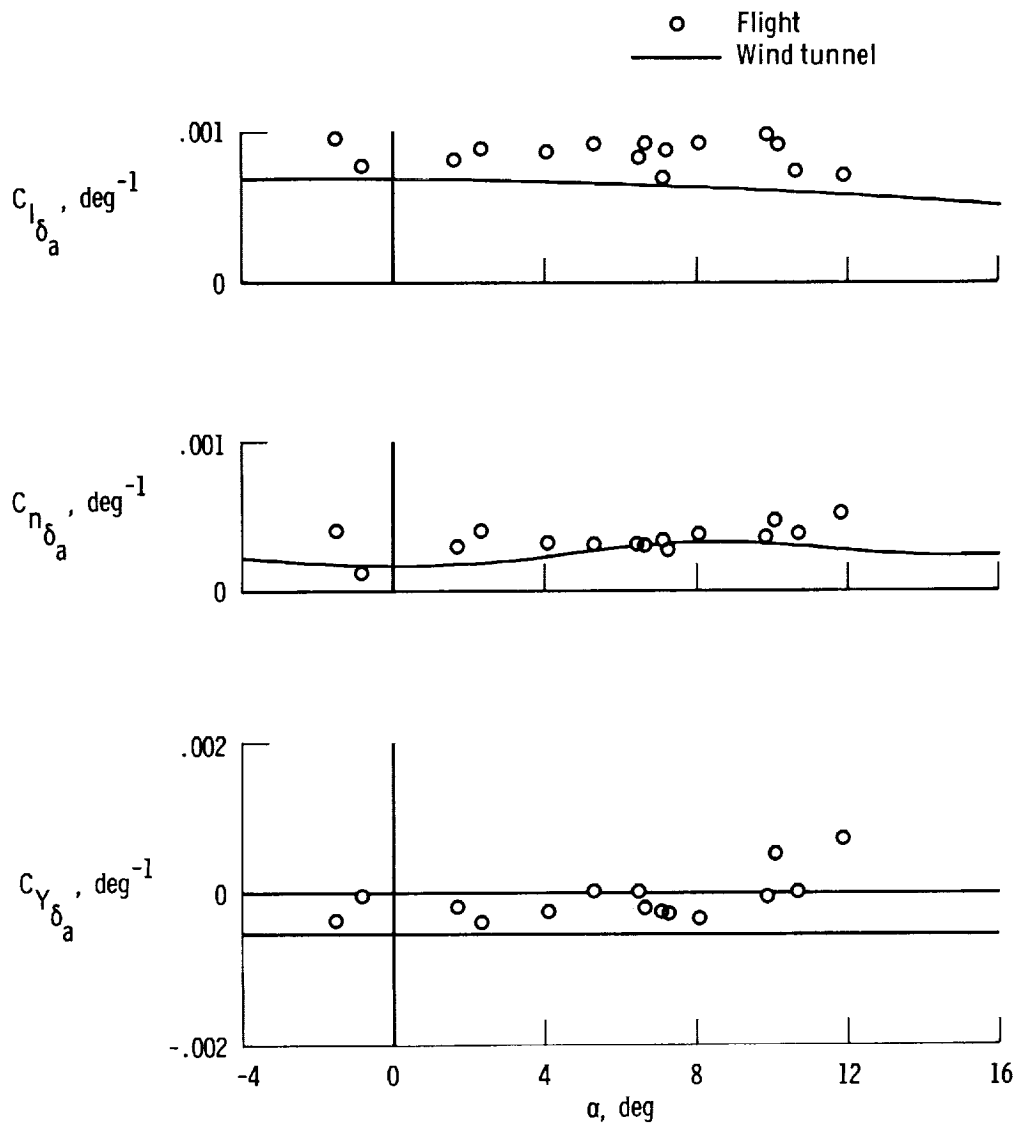
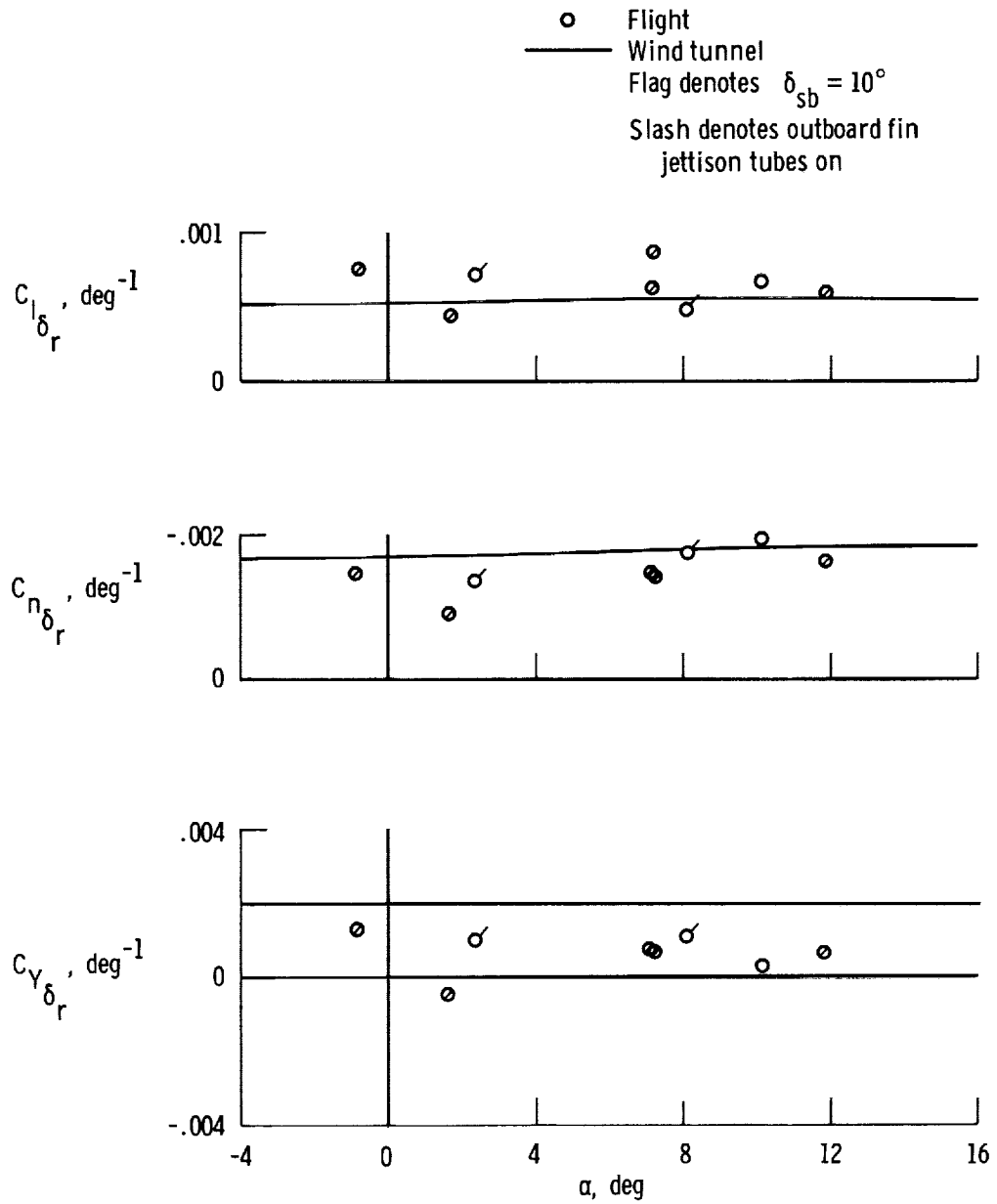


Figure 11. Comparison of lateral-directional derivatives obtained from flight data with wind-tunnel predictions for a Mach number of 0.7.



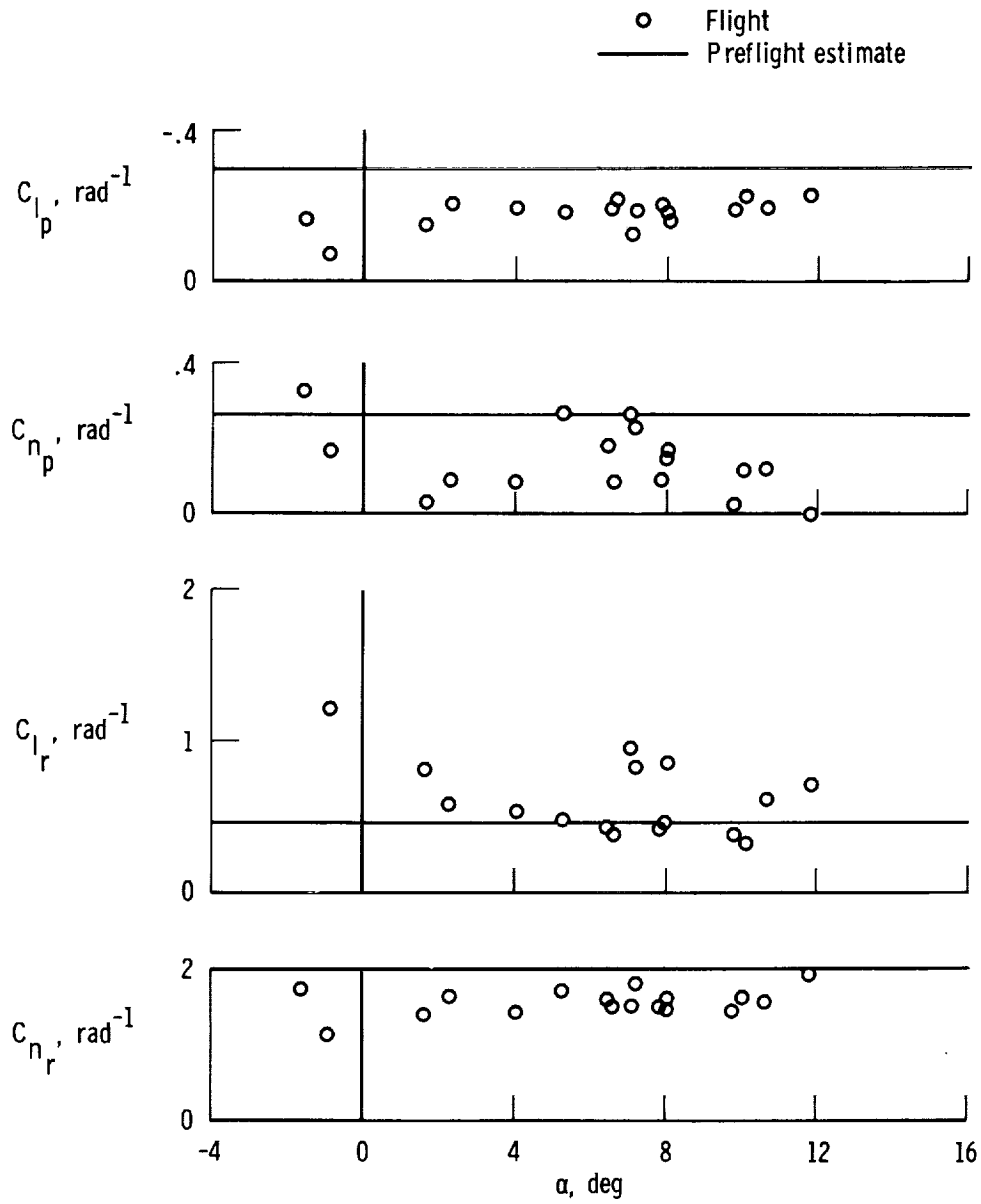
(b) $C_{l_{\delta a}}, C_{n_{\delta a}}, C_{Y_{\delta a}}$.

Figure 11. Continued.



(c) $C_{l\delta_r}$, $C_{n\delta_r}$, $C_{Y\delta_r}$.

Figure 11. Continued.



(d) C_{l_p} , C_{n_p} , C_{l_r} , C_{n_r} .

Figure 11. Concluded.

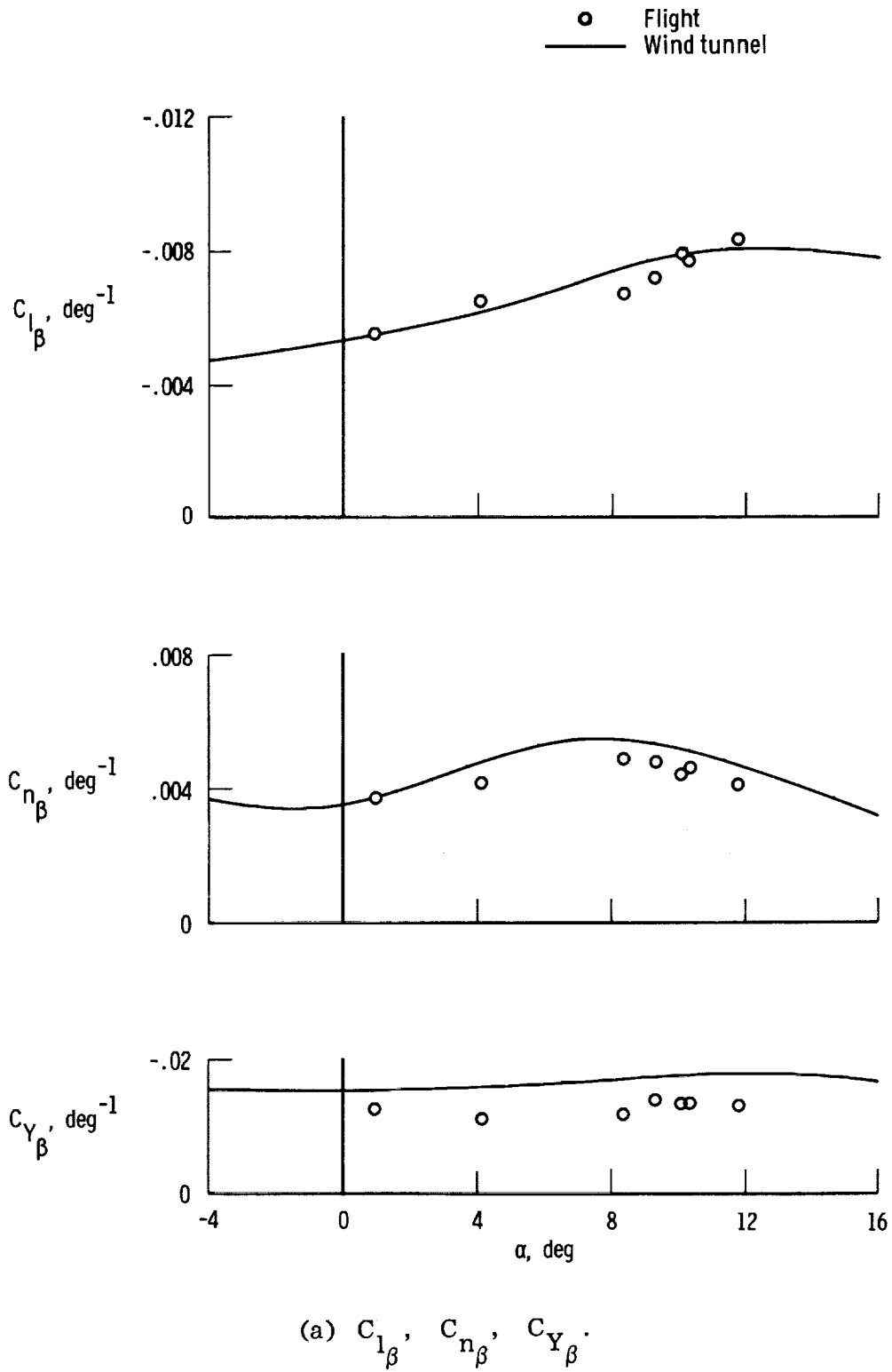
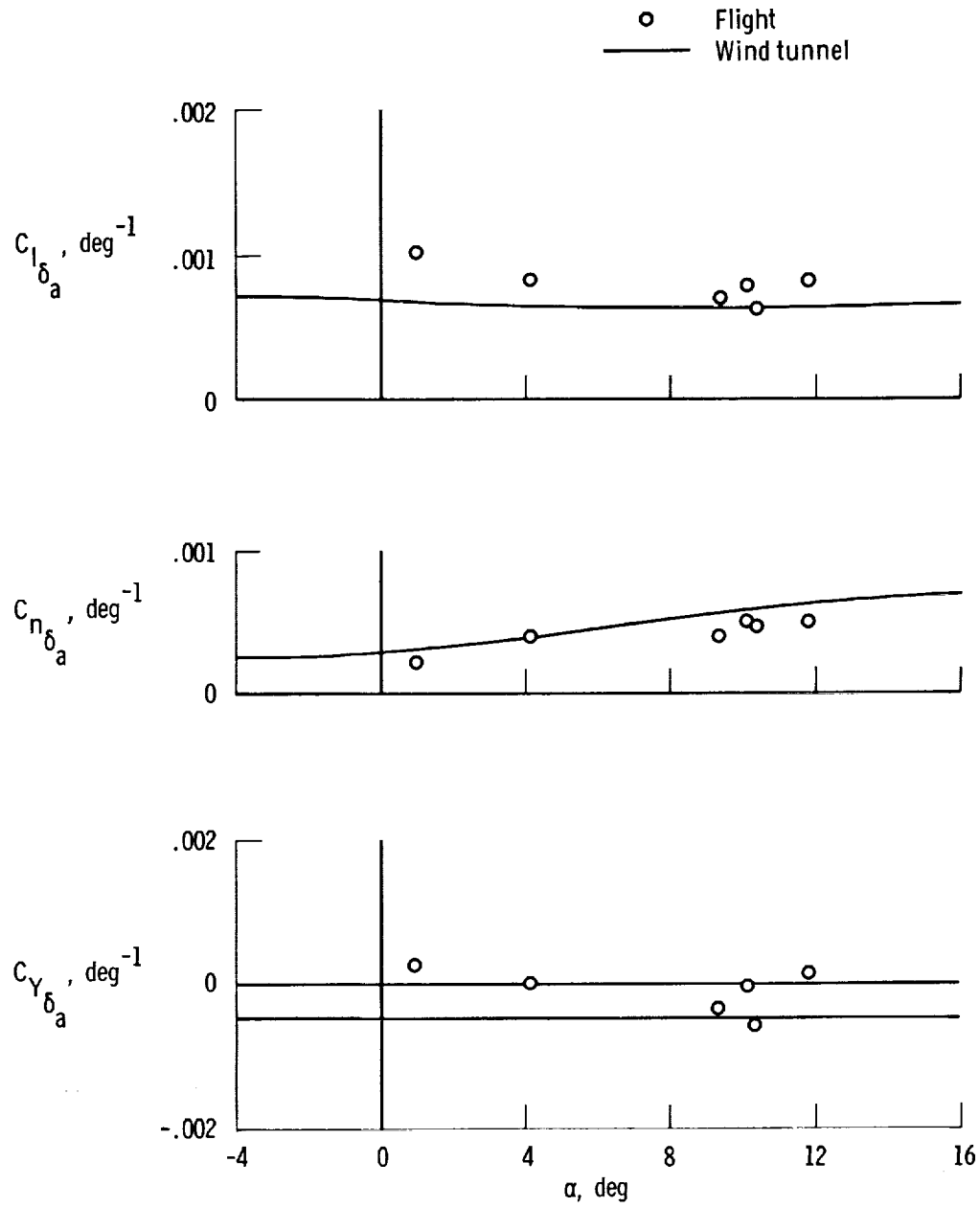
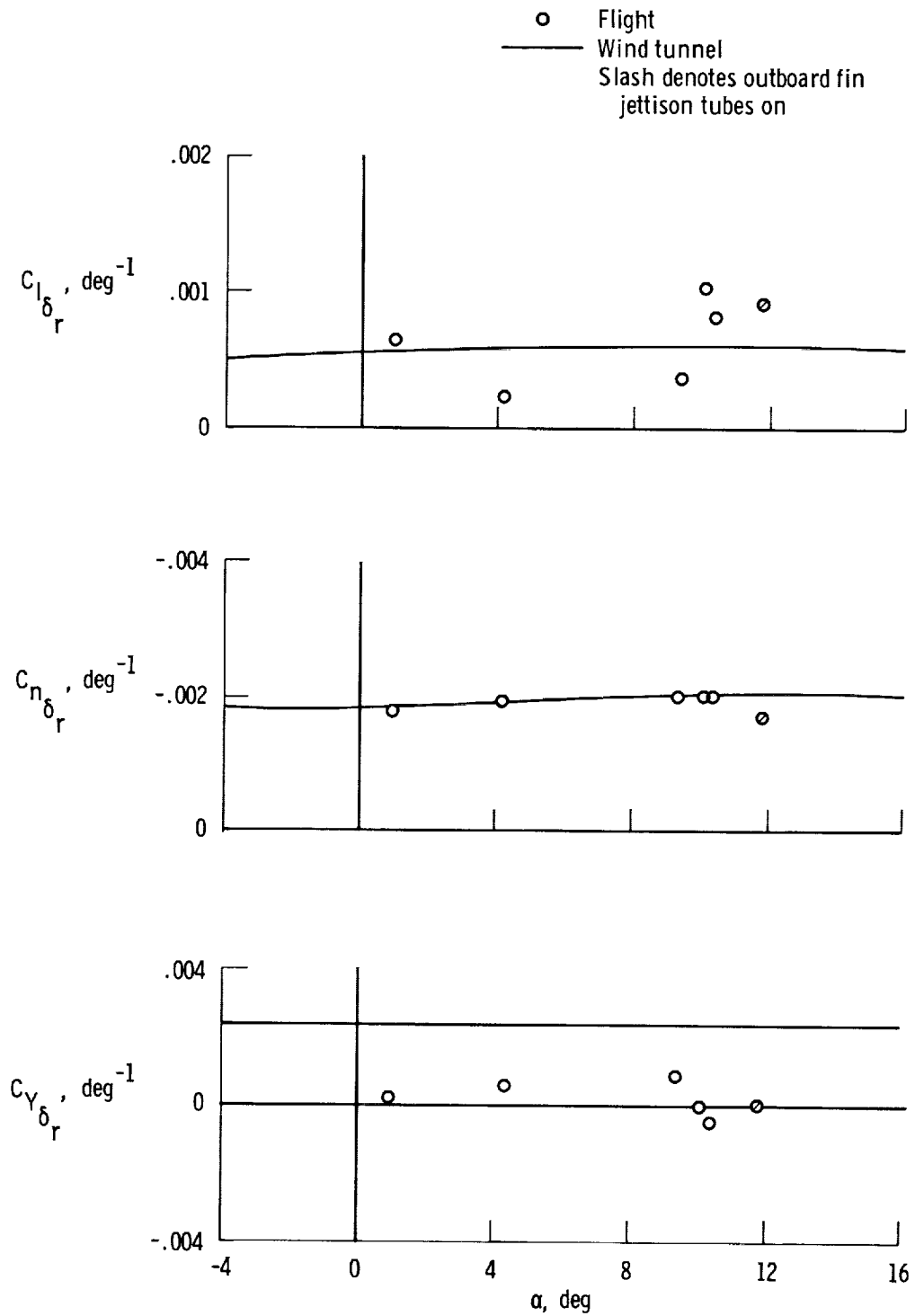


Figure 12. Comparison of lateral-directional derivatives obtained from flight data with wind-tunnel predictions for a Mach number of 0.8.



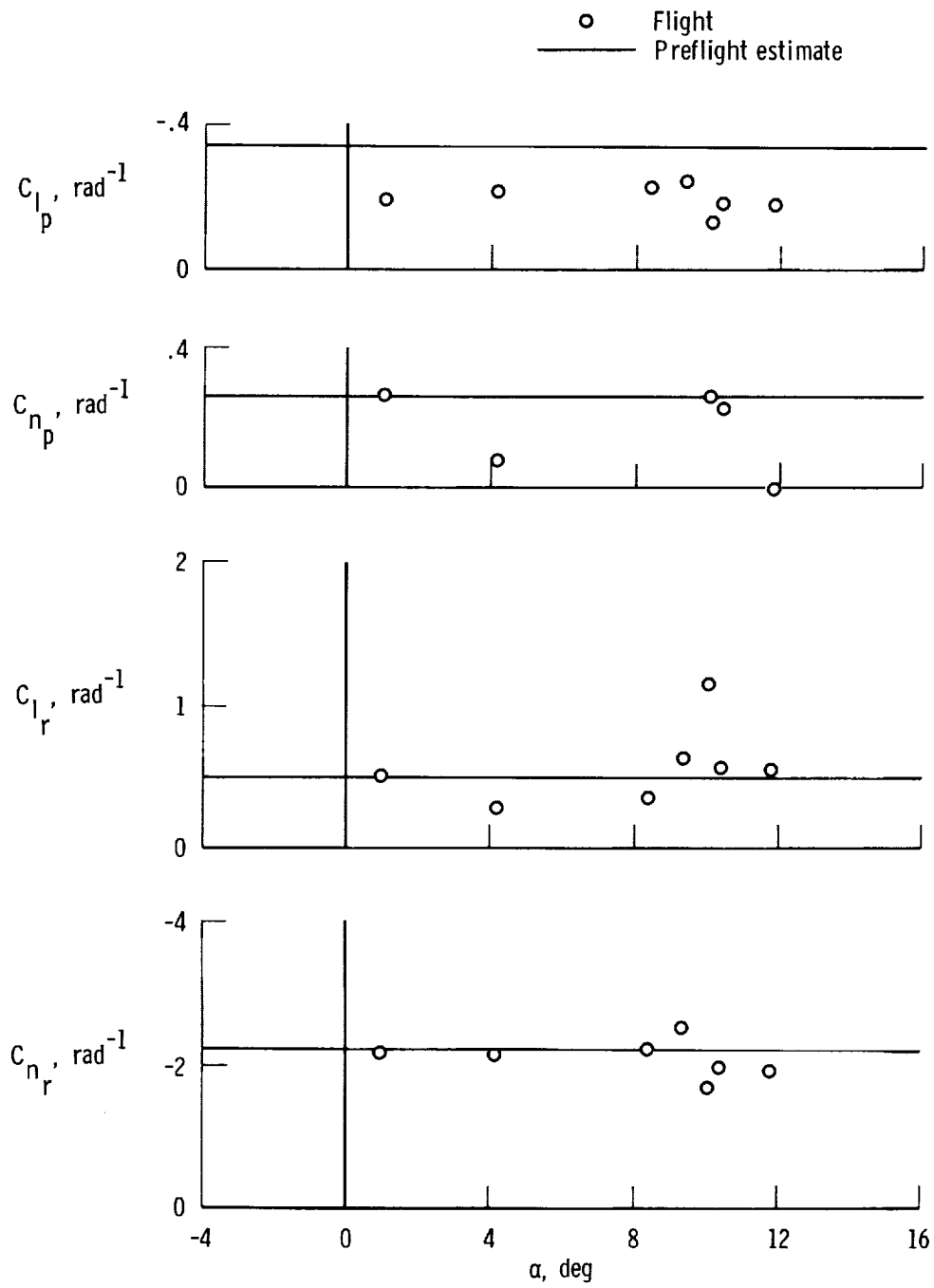
(b) $C_{l_{\delta_a}}$, $C_{n_{\delta_a}}$, $C_{Y_{\delta_a}}$.

Figure 12. Continued.



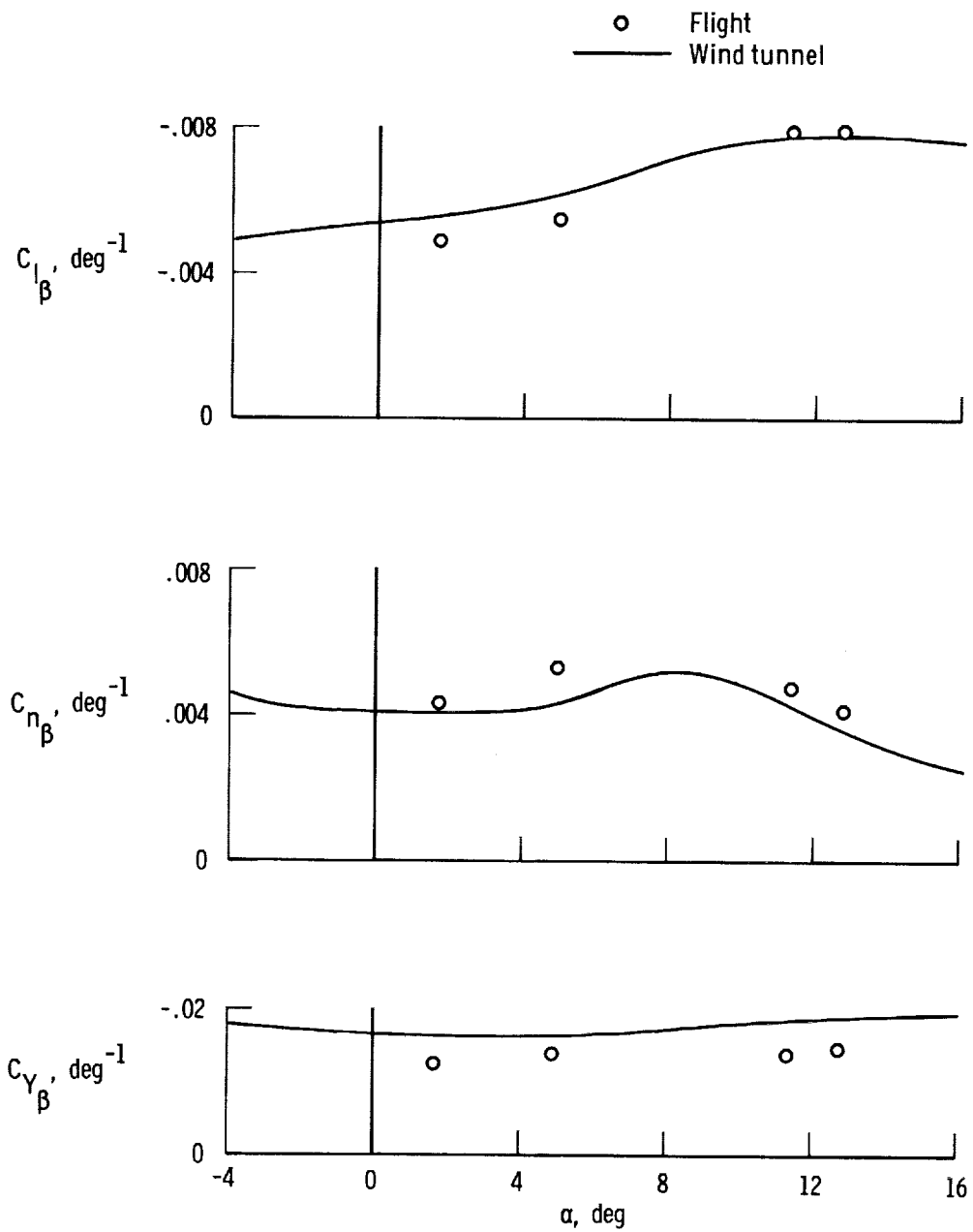
(c) $C_{l_{\delta_r}}$, $C_{n_{\delta_r}}$, $C_{Y_{\delta_r}}$.

Figure 12. Continued.



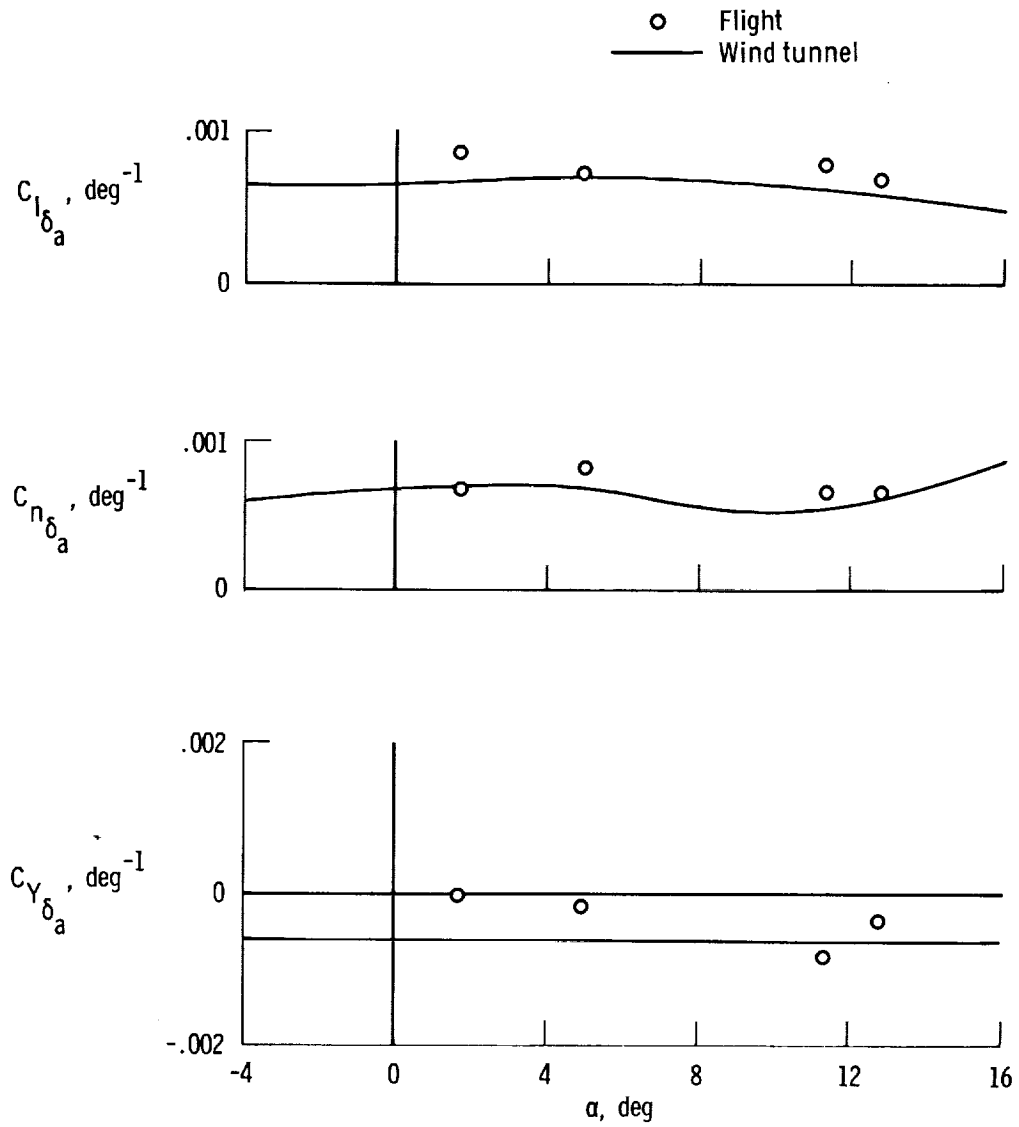
(d) C_{l_p} , C_{n_p} , C_{l_r} , C_{n_r} .

Figure 12. Concluded.



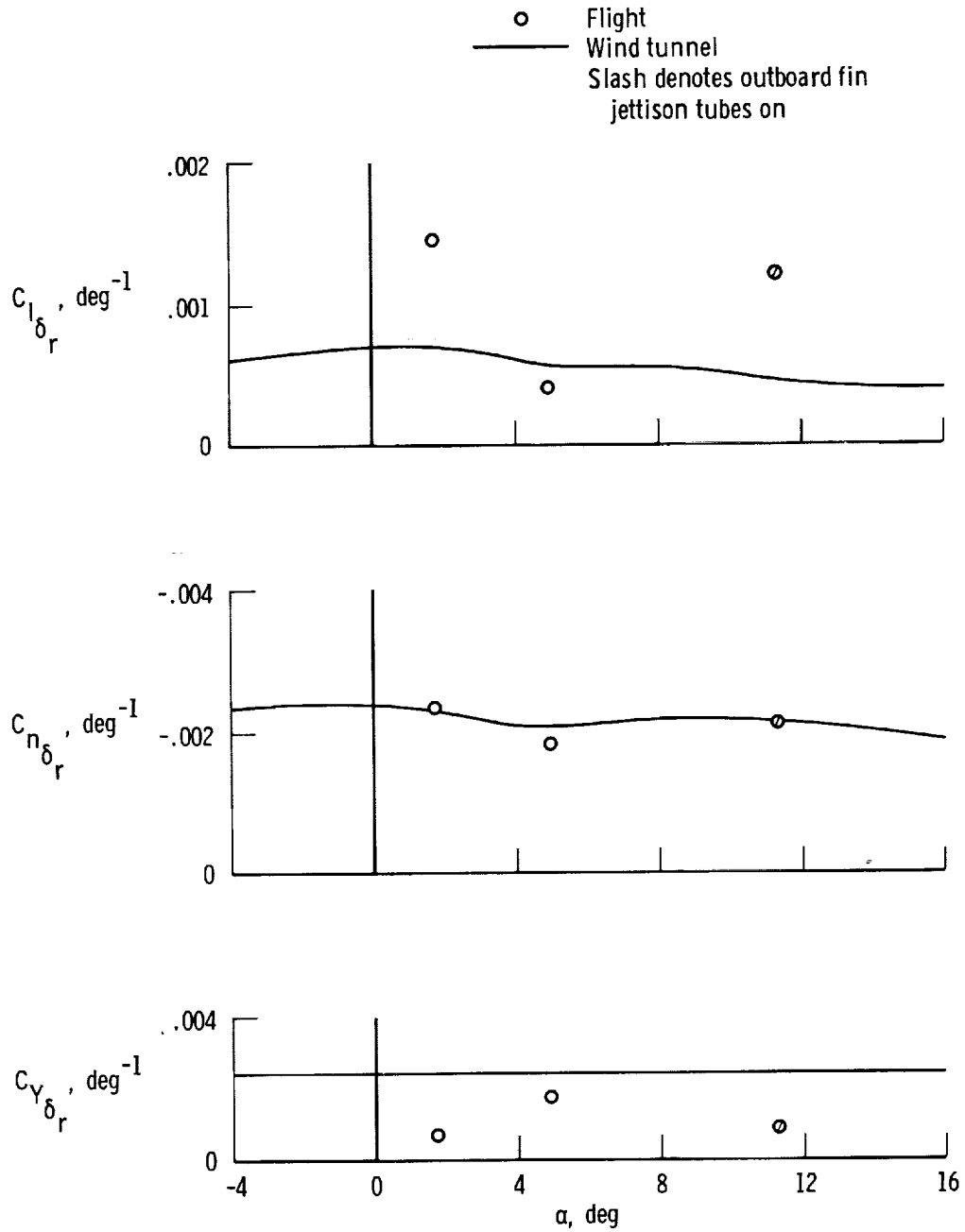
(a) $C_{l_{\beta}}$, $C_{n_{\beta}}$, $C_{Y_{\beta}}$.

Figure 13. Comparison of lateral-directional derivatives obtained from flight data with wind-tunnel predictions for a Mach number of 0.9.



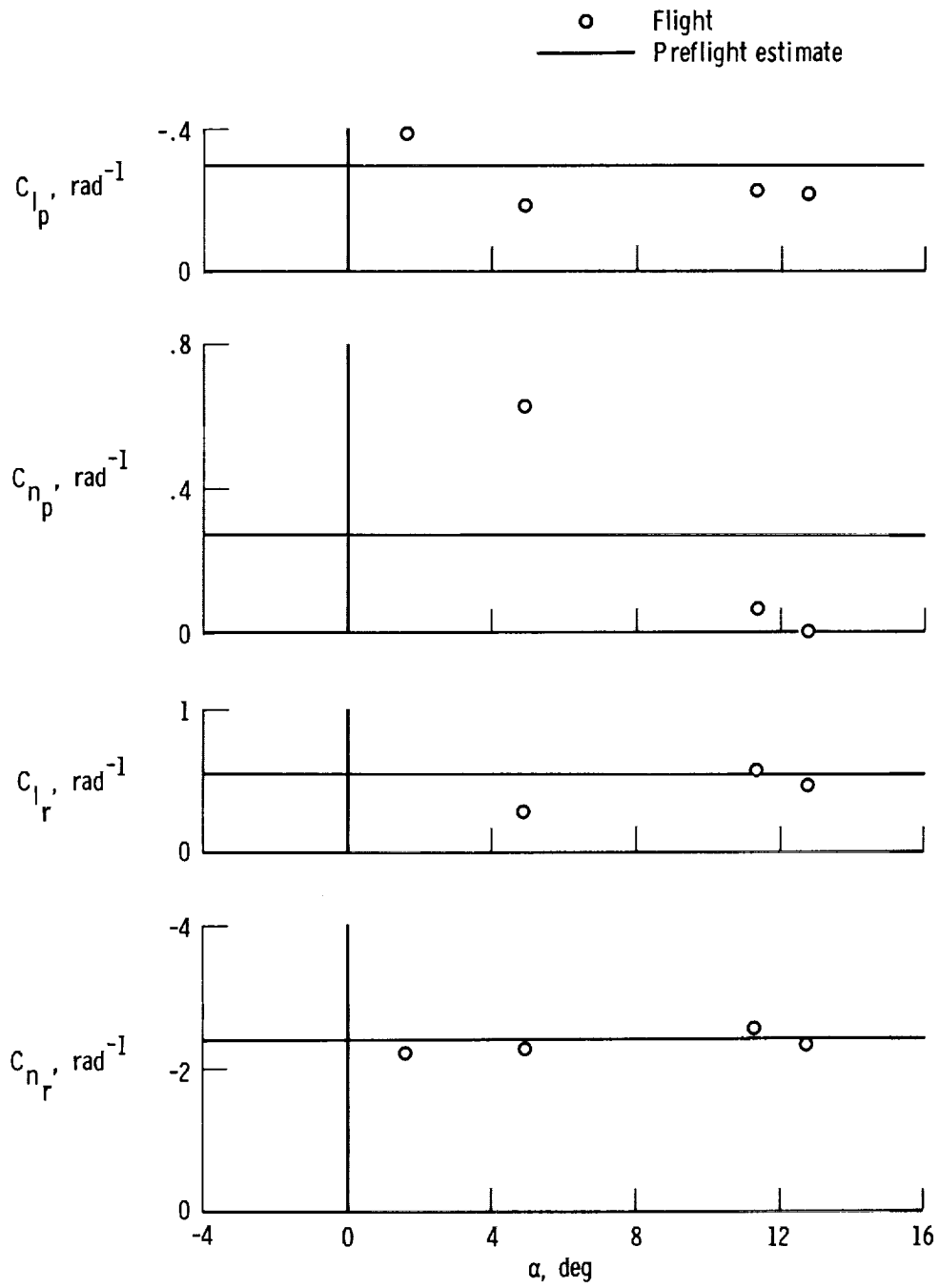
(b) $C_{l_{\delta_a}}, C_{n_{\delta_a}}, C_{Y_{\delta_a}}$.

Figure 13. Continued.



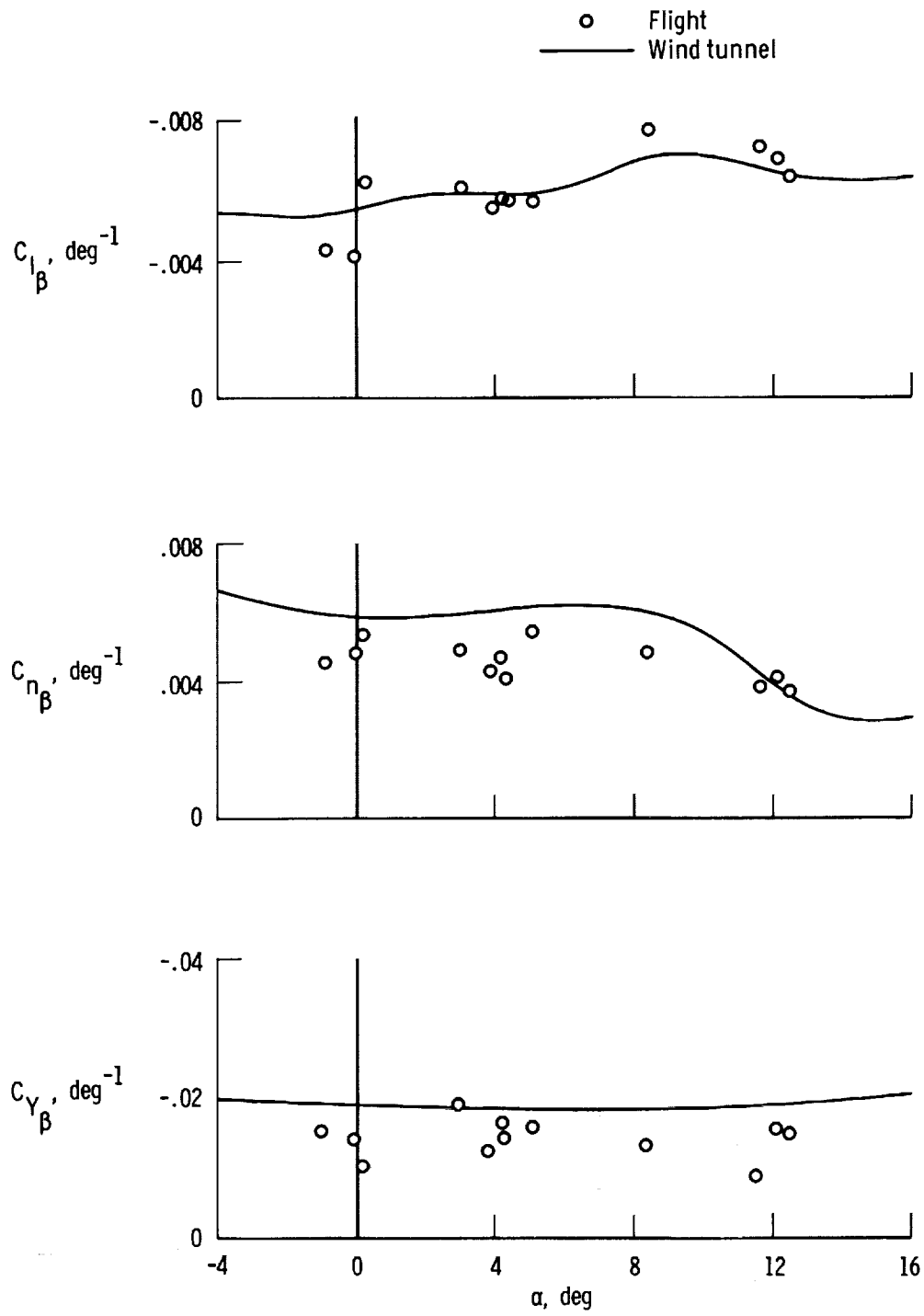
(c) $C_{l_{\delta_r}}$, $C_{n_{\delta_r}}$, $C_{Y_{\delta_r}}$.

Figure 13. Continued.



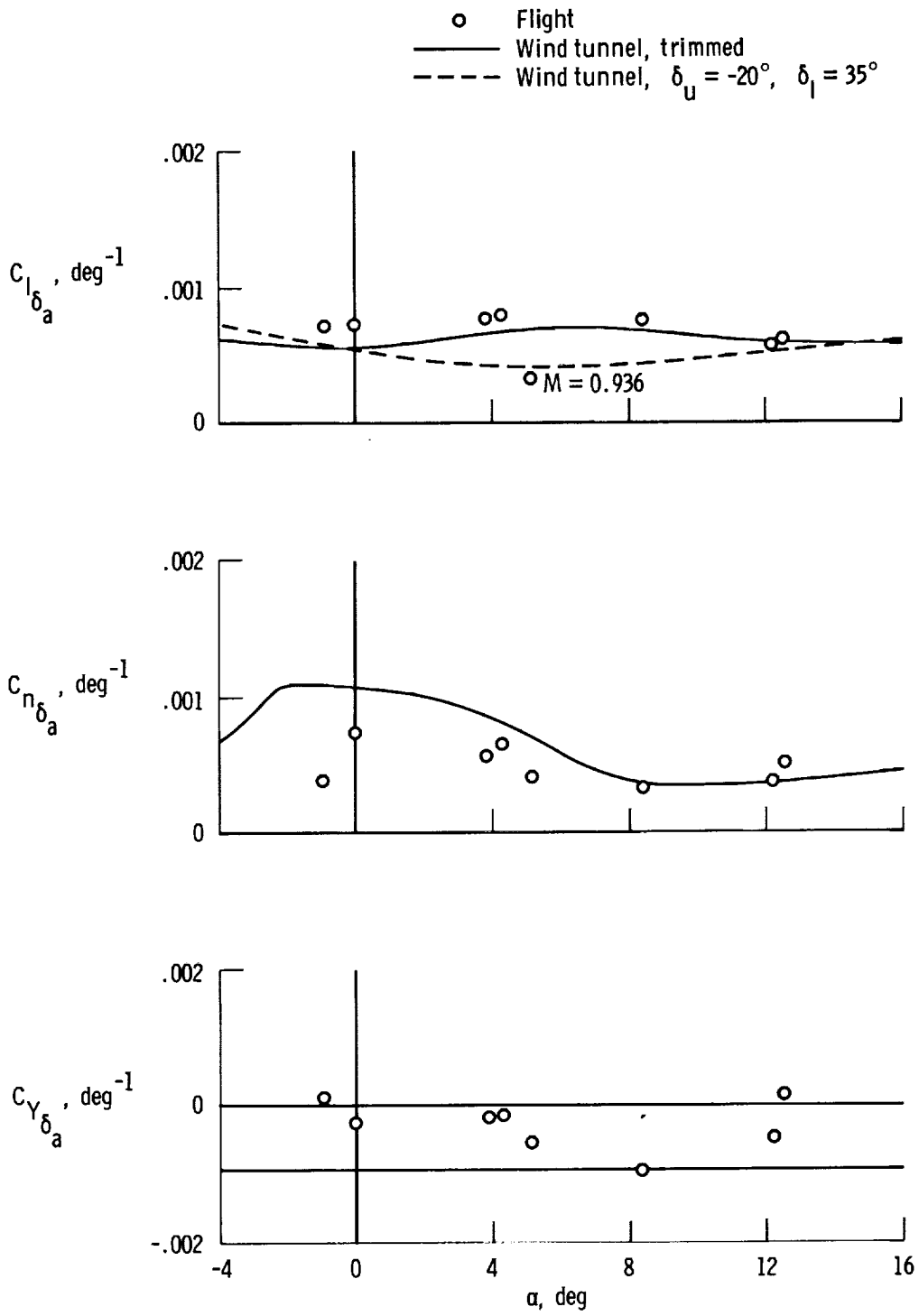
(d) C_{l_p} , C_{n_p} , C_{l_r} , C_{n_r} .

Figure 13. Concluded.



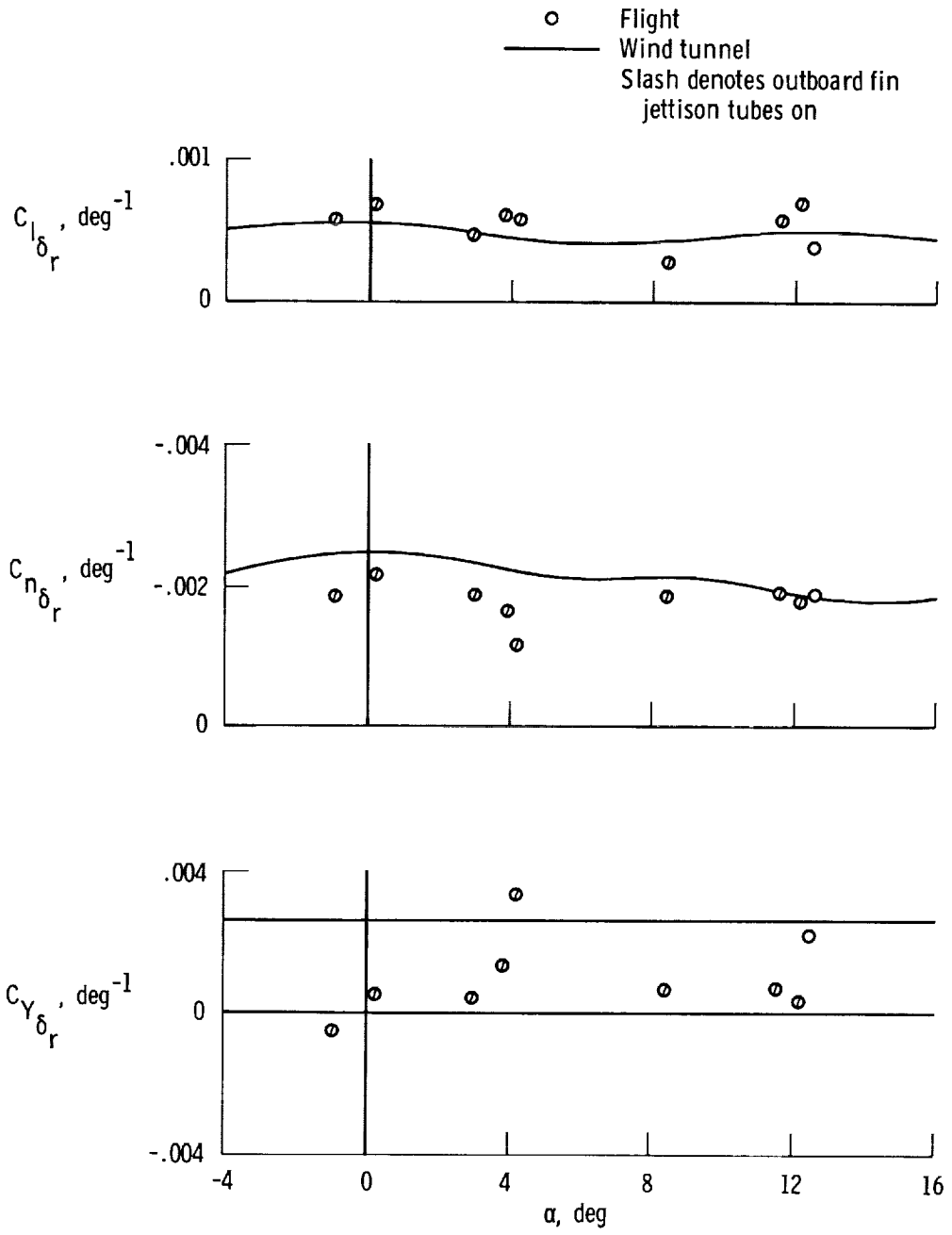
(a) $C_{l\beta}, C_{n\beta}, C_{Y\beta}$.

Figure 14. Comparison of lateral-directional derivatives obtained from flight data with wind-tunnel predictions for a Mach number of 0.95.



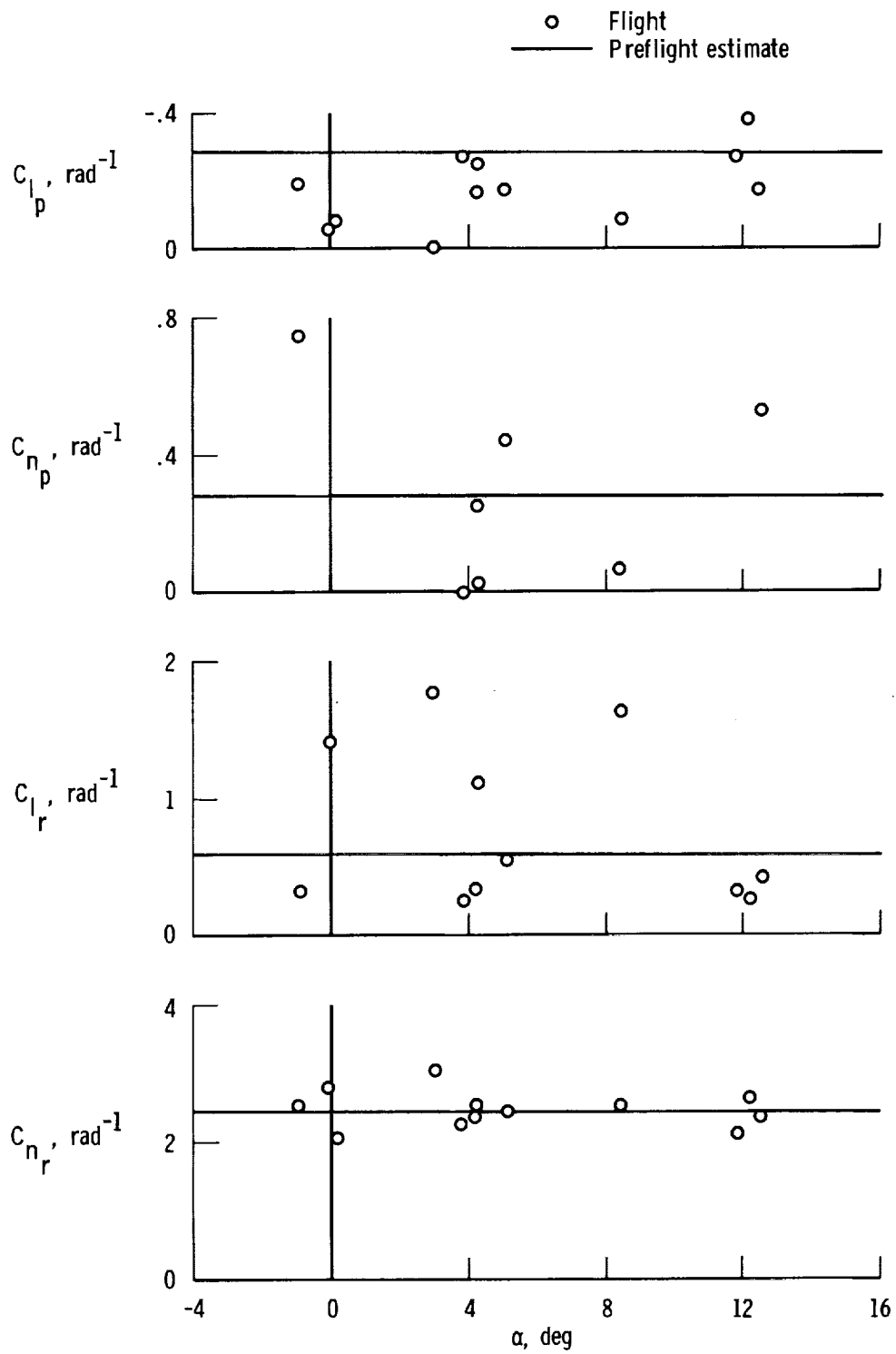
(b) $C_{l_{\delta_a}}$, $C_{n_{\delta_a}}$, $C_{Y_{\delta_a}}$.

Figure 14. Continued.



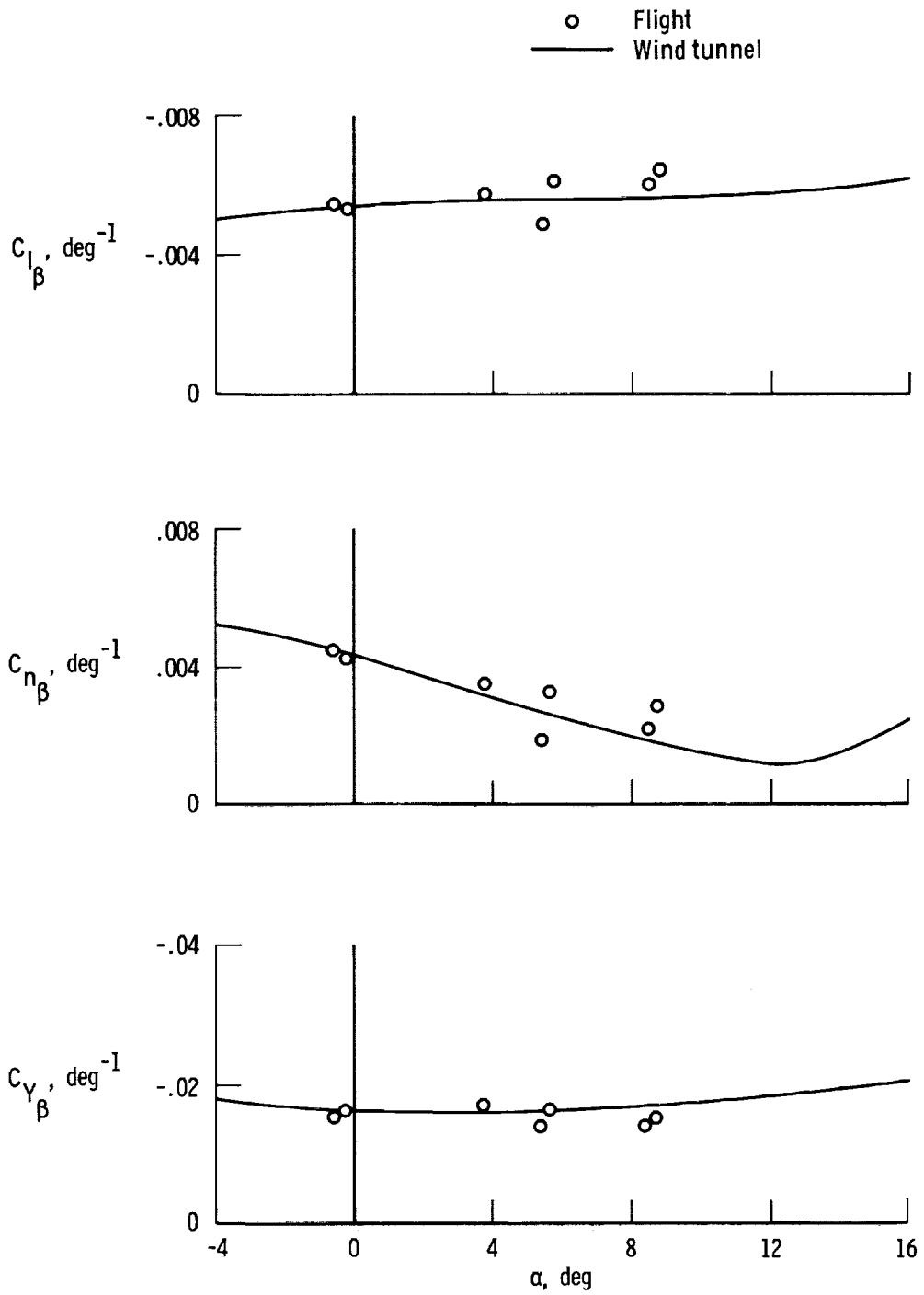
(c) $C_{l_{\delta_r}}$, $C_{n_{\delta_r}}$, $C_{Y_{\delta_r}}$.

Figure 14. Continued.



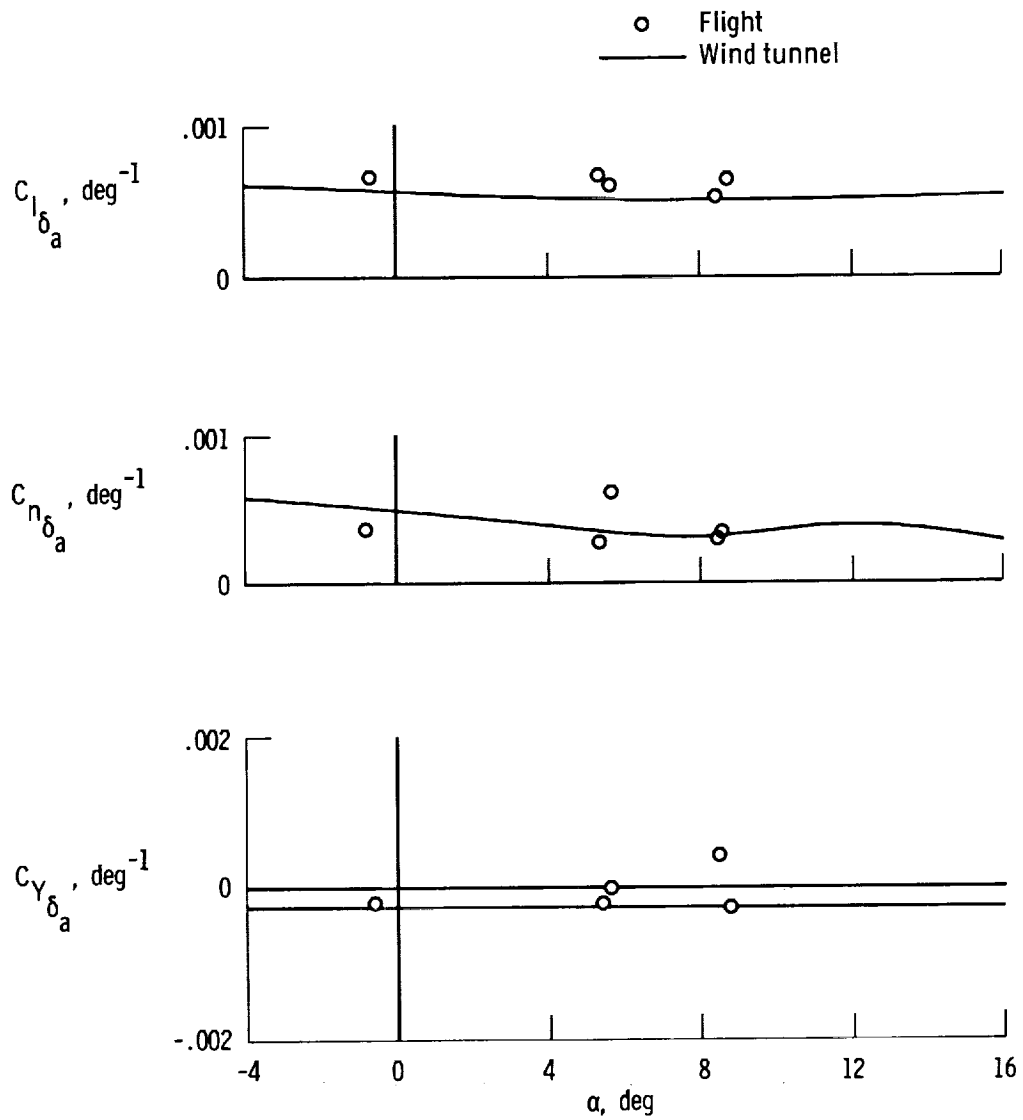
(d) C_{l_p} , C_{n_p} , C_{l_r} , C_{n_r} .

Figure 14. Concluded.



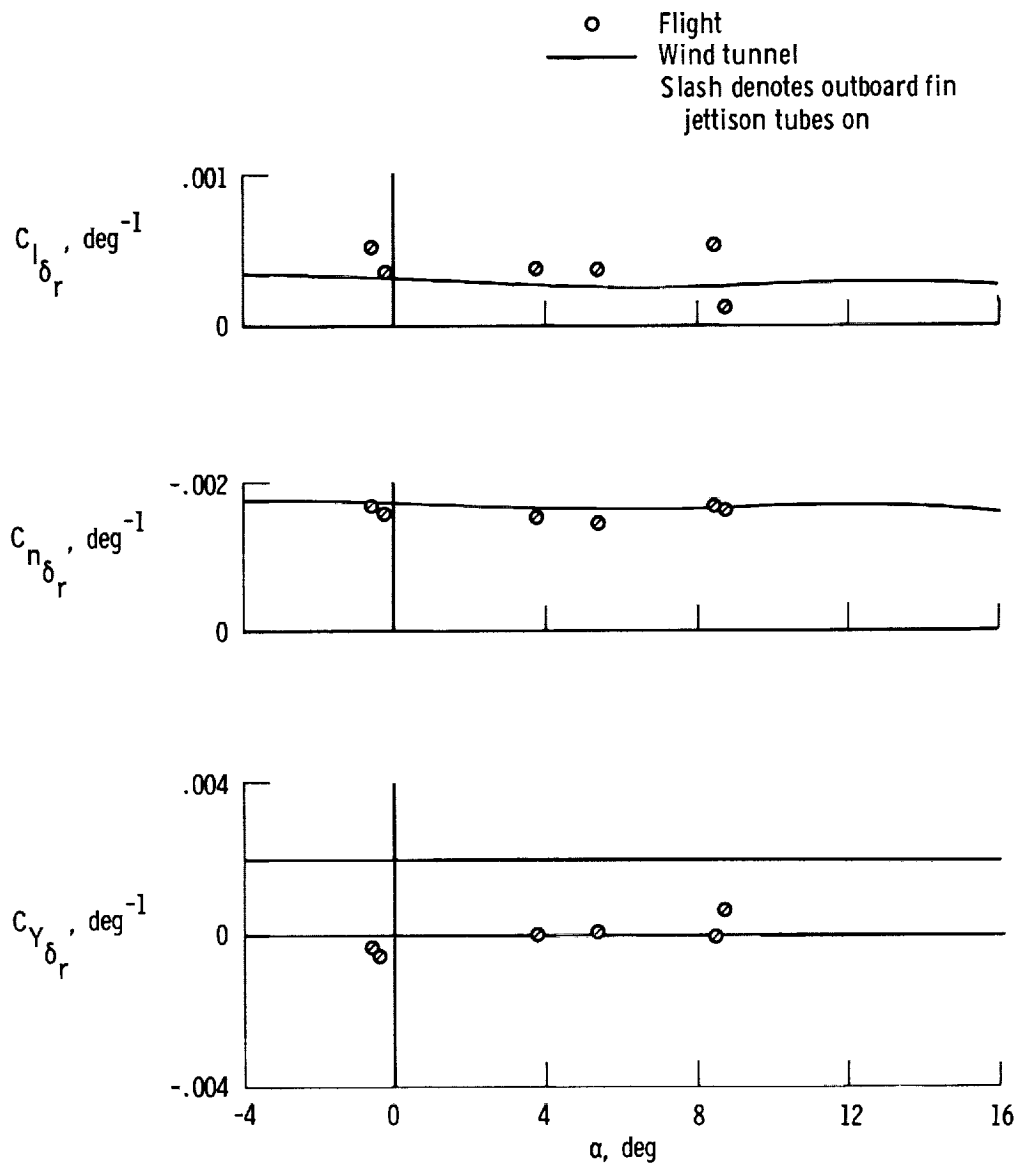
(a) C_{l_β} , C_{n_β} , C_{Y_β} .

Figure 15. Comparison of lateral-directional derivatives obtained from flight data with wind-tunnel predictions for a Mach number of 1.1.



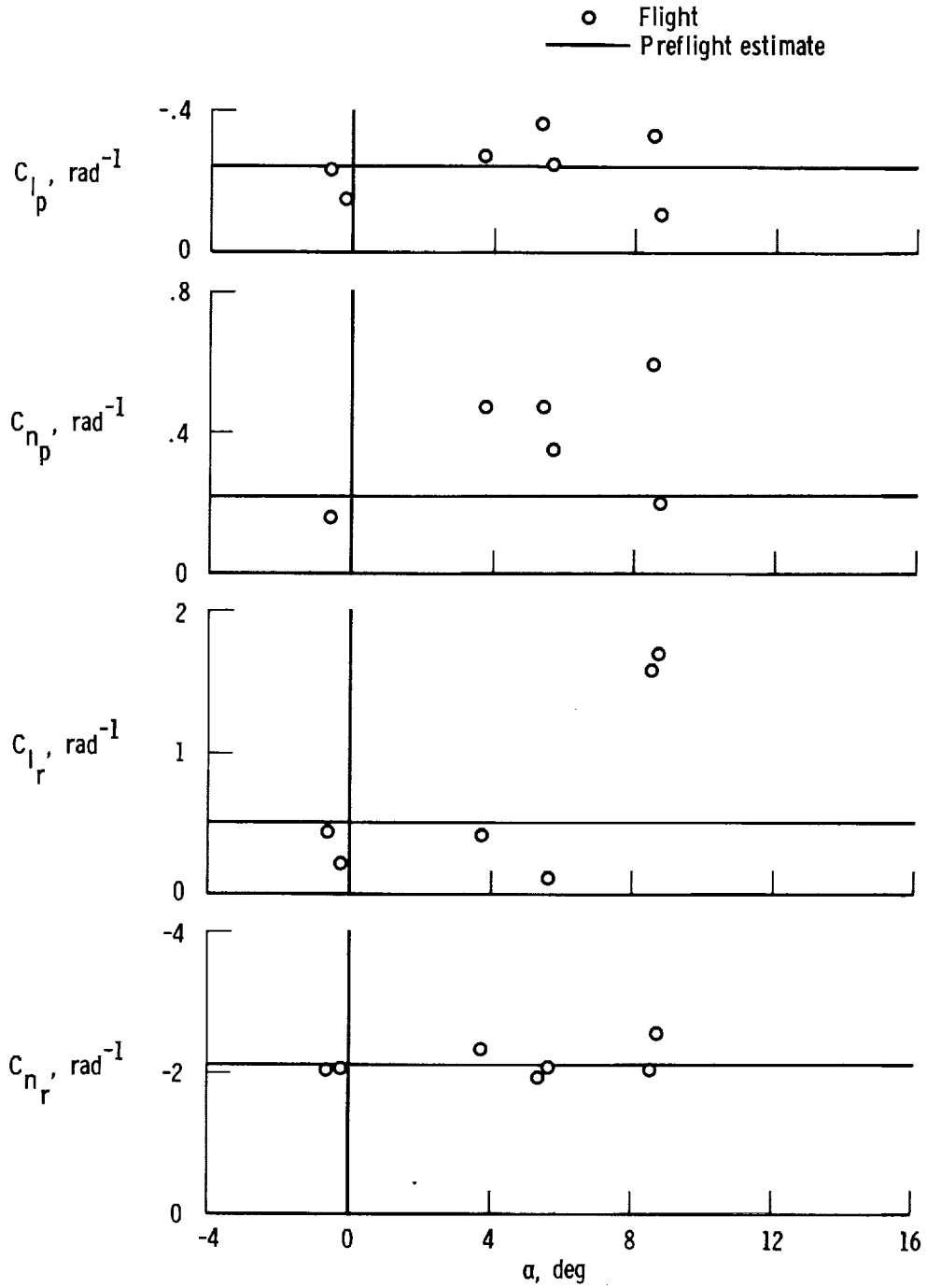
(b) $C_{l_{\delta_a}}, C_{n_{\delta_a}}, C_{Y_{\delta_a}}$.

Figure 15. Continued.



(c) $C_{l_{\delta_r}}$, $C_{n_{\delta_r}}$, $C_{Y_{\delta_r}}$.

Figure 15. Continued.



(d) C_{l_p} , C_{n_p} , C_{l_r} , C_{n_r} .

Figure 15. Concluded.

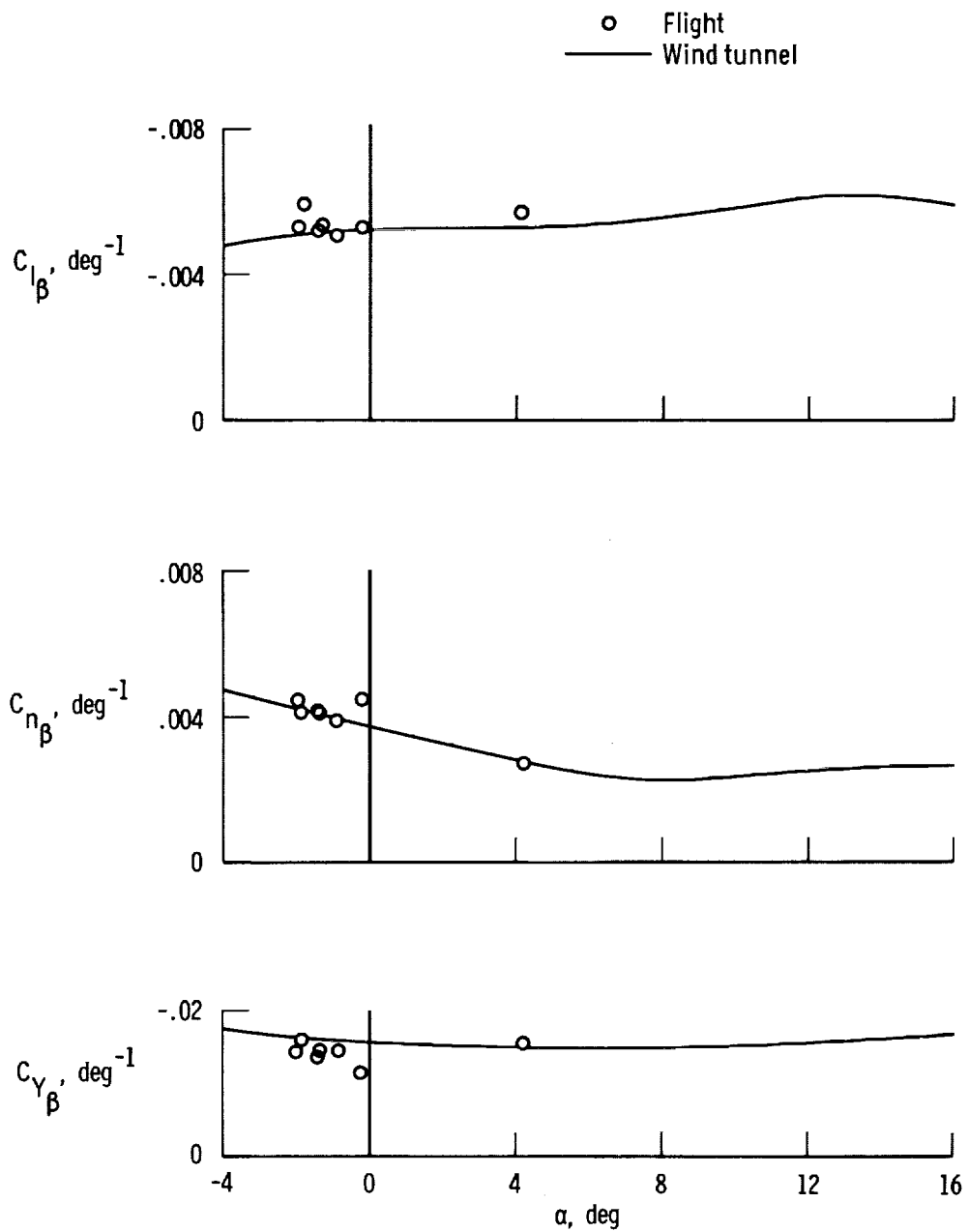
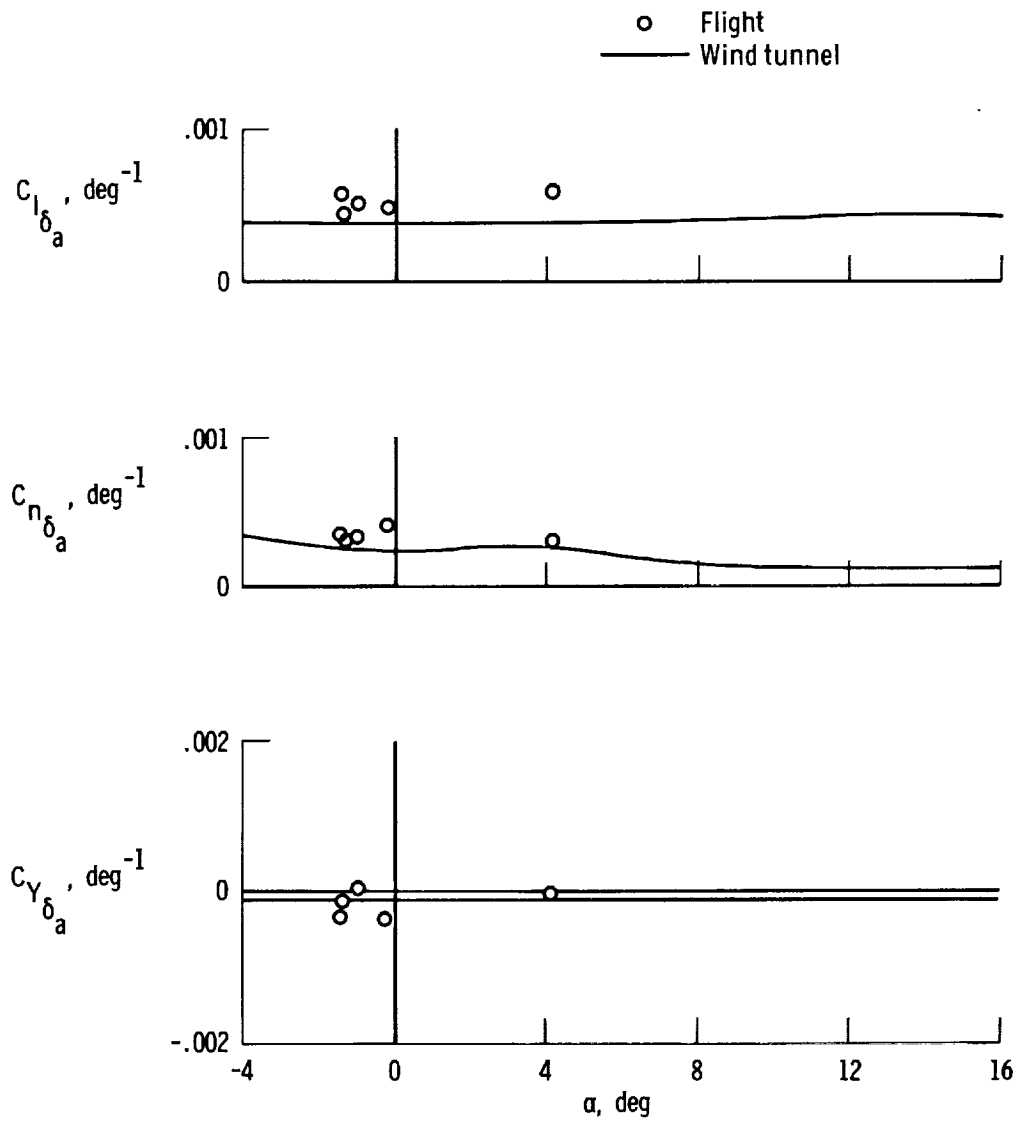
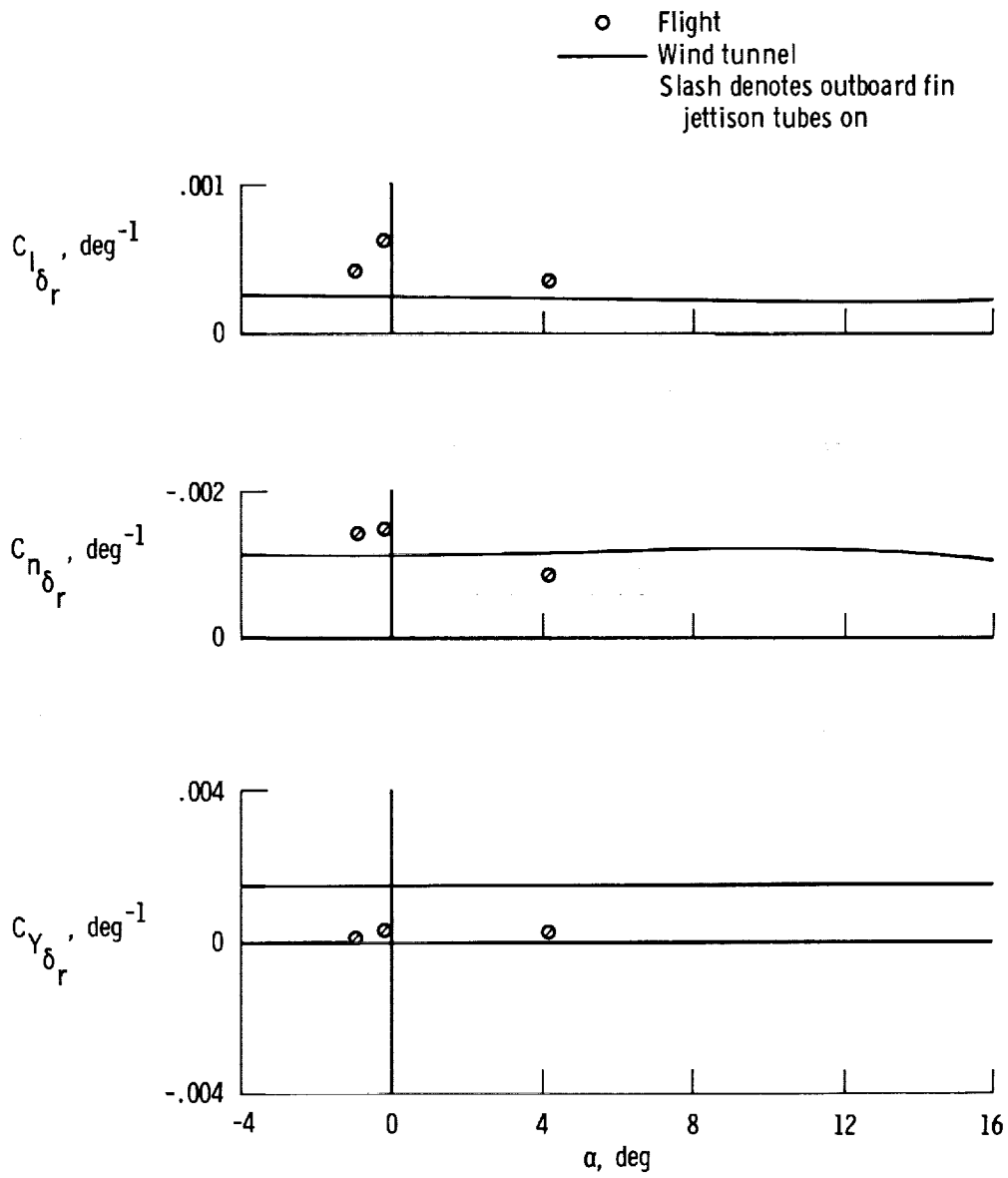


Figure 16. Comparison of lateral-directional derivatives obtained from flight data with wind-tunnel predictions for a Mach number of 1.3.



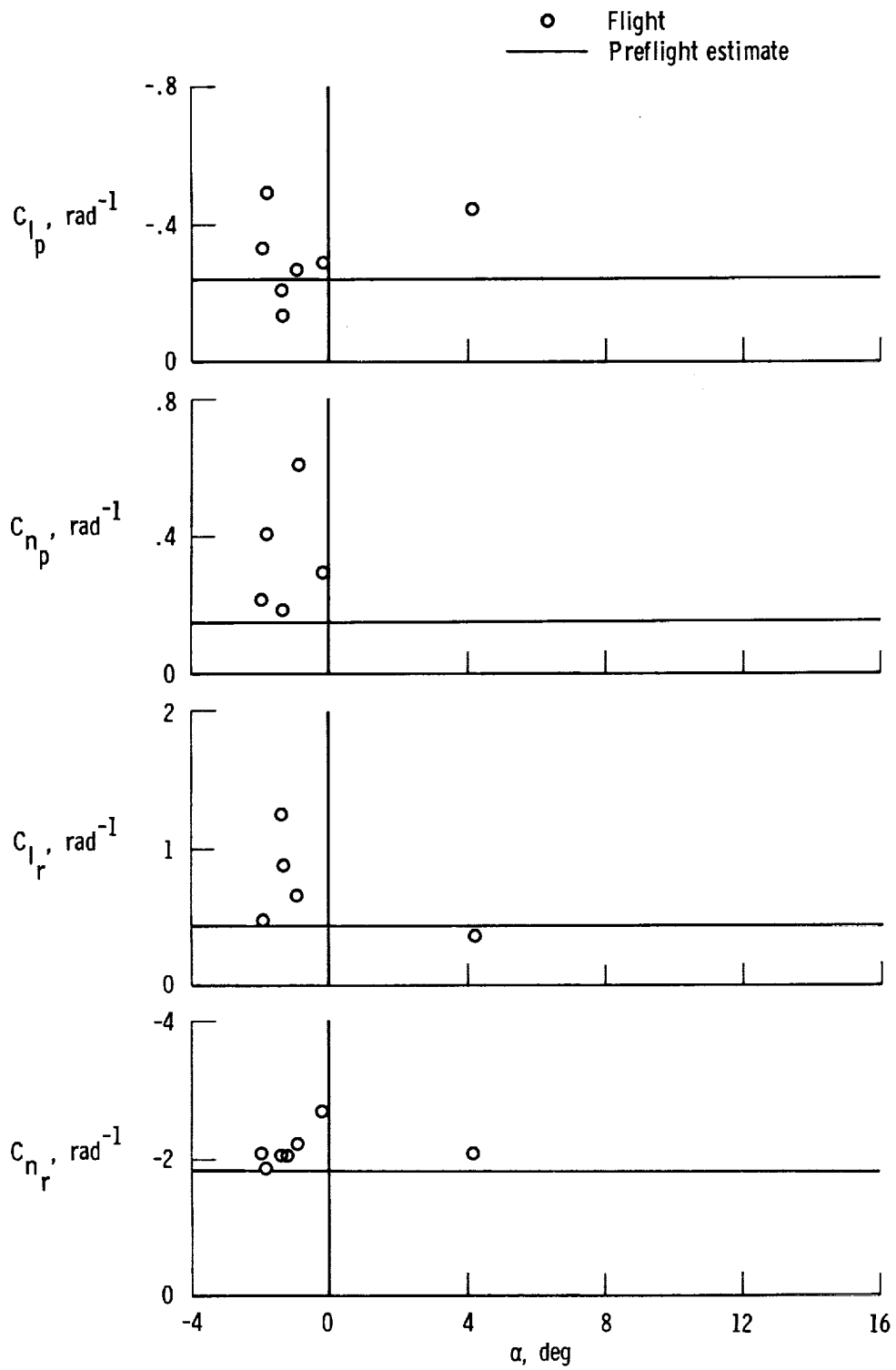
(b) $C_{l_{\delta a}}, C_{n_{\delta a}}, C_{Y_{\delta a}}$.

Figure 16. Continued.



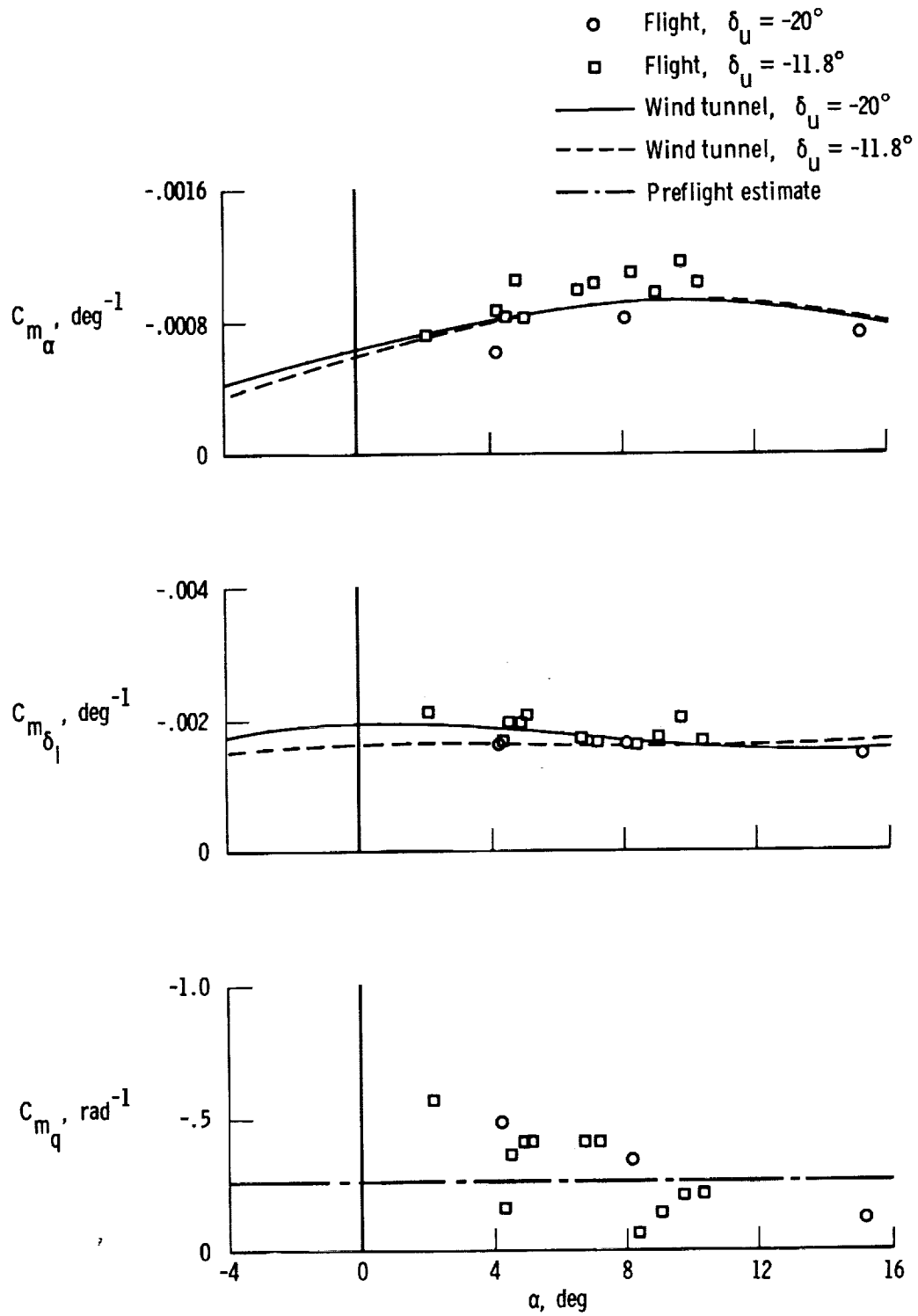
(c) $C_{l_{\delta_r}}$, $C_{n_{\delta_r}}$, $C_{Y_{\delta_r}}$.

Figure 16. Continued.



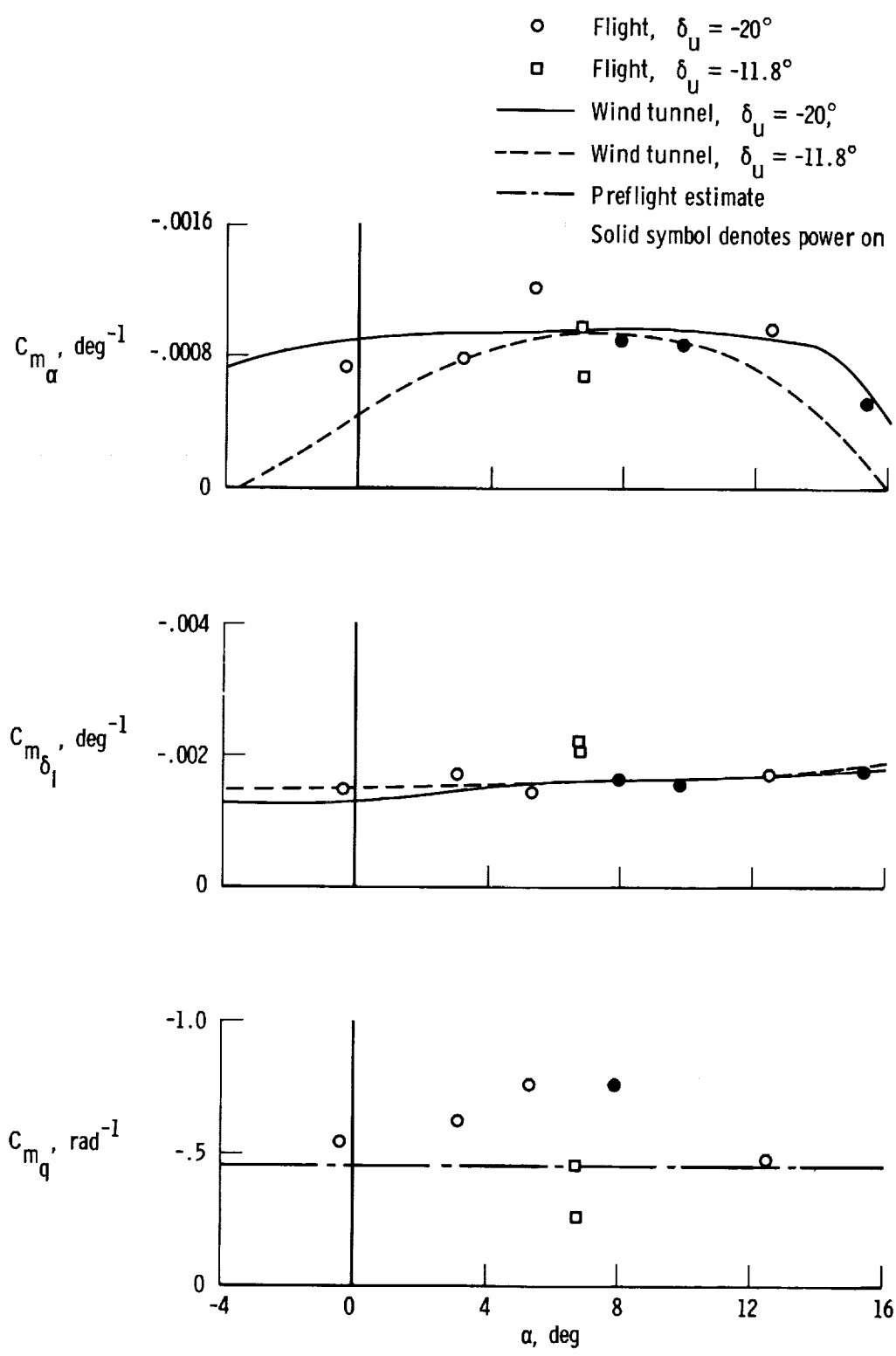
(d) C_{l_p} , C_{n_p} , C_{l_r} , C_{n_r} .

Figure 16. Concluded.



(a) $M = 0.5$.

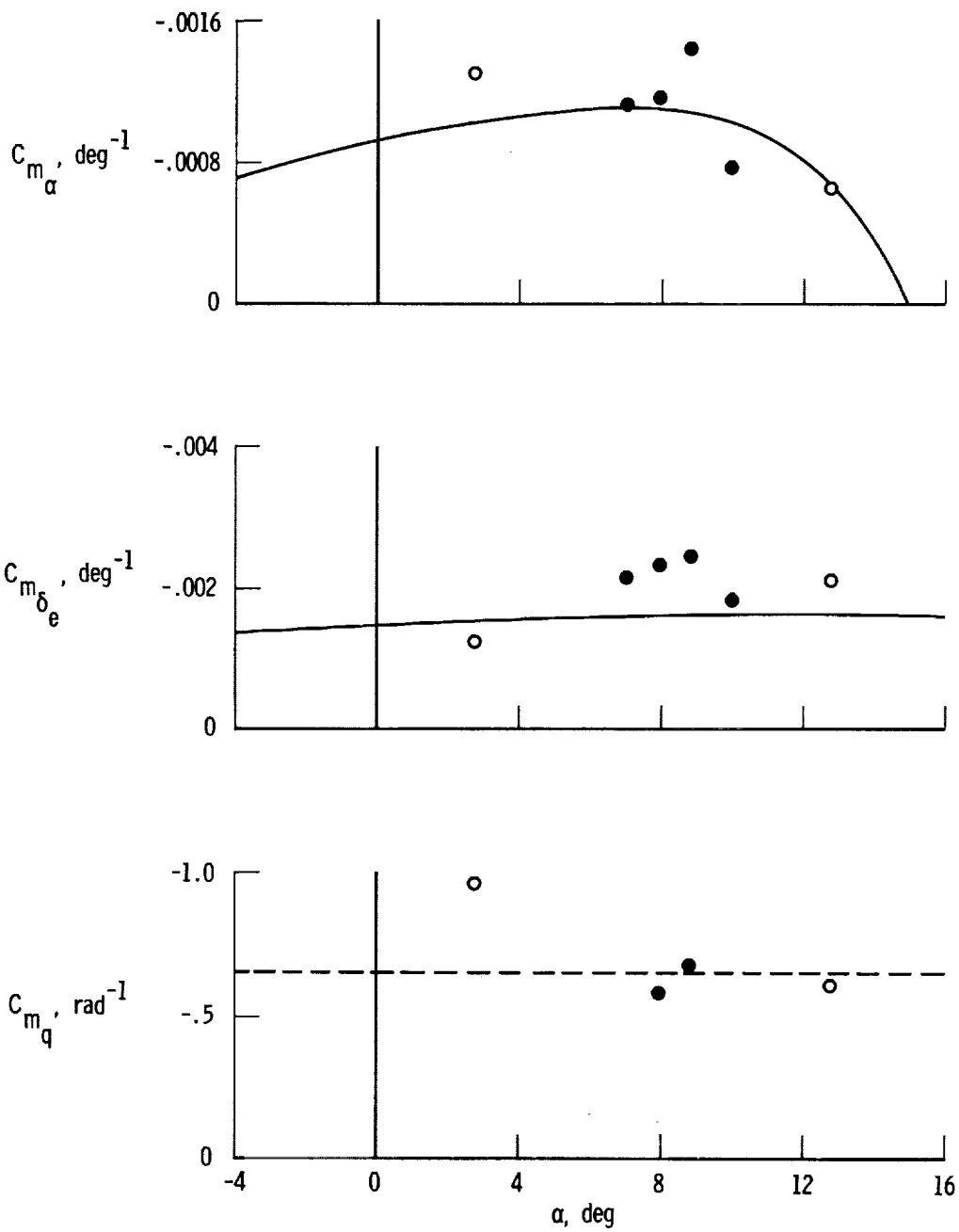
Figure 17. Comparison of longitudinal derivatives obtained from flight data with wind-tunnel predictions for Mach numbers of 0.5, 0.7, 0.8, 1.1, and 1.3.



(b) $M = 0.7$.

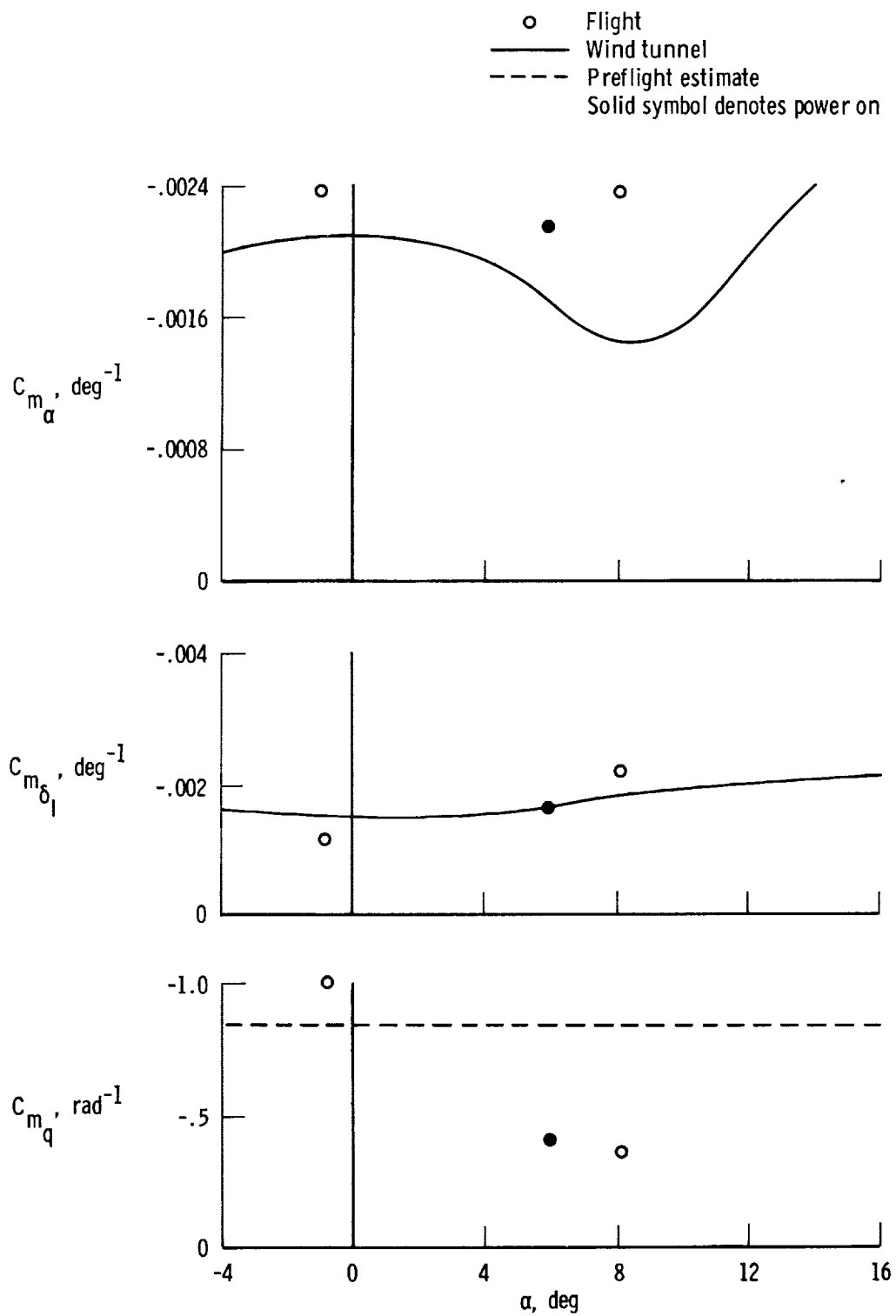
Figure 17. Continued.

○ Flight
 — Wind tunnel
 - - - Preflight estimate
 Solid symbol denotes power on



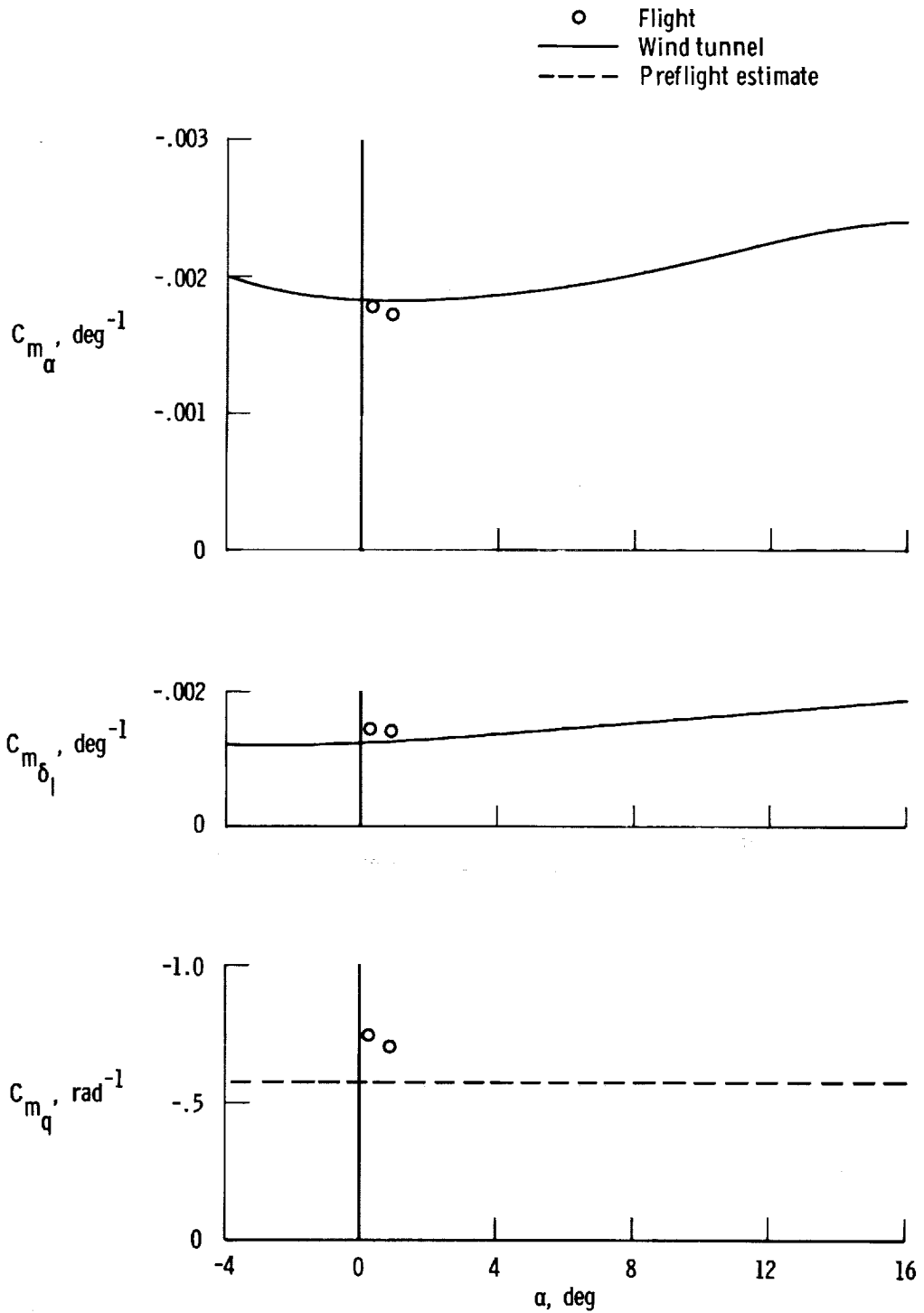
(c) $M = 0.8$.

Figure 17. Continued.



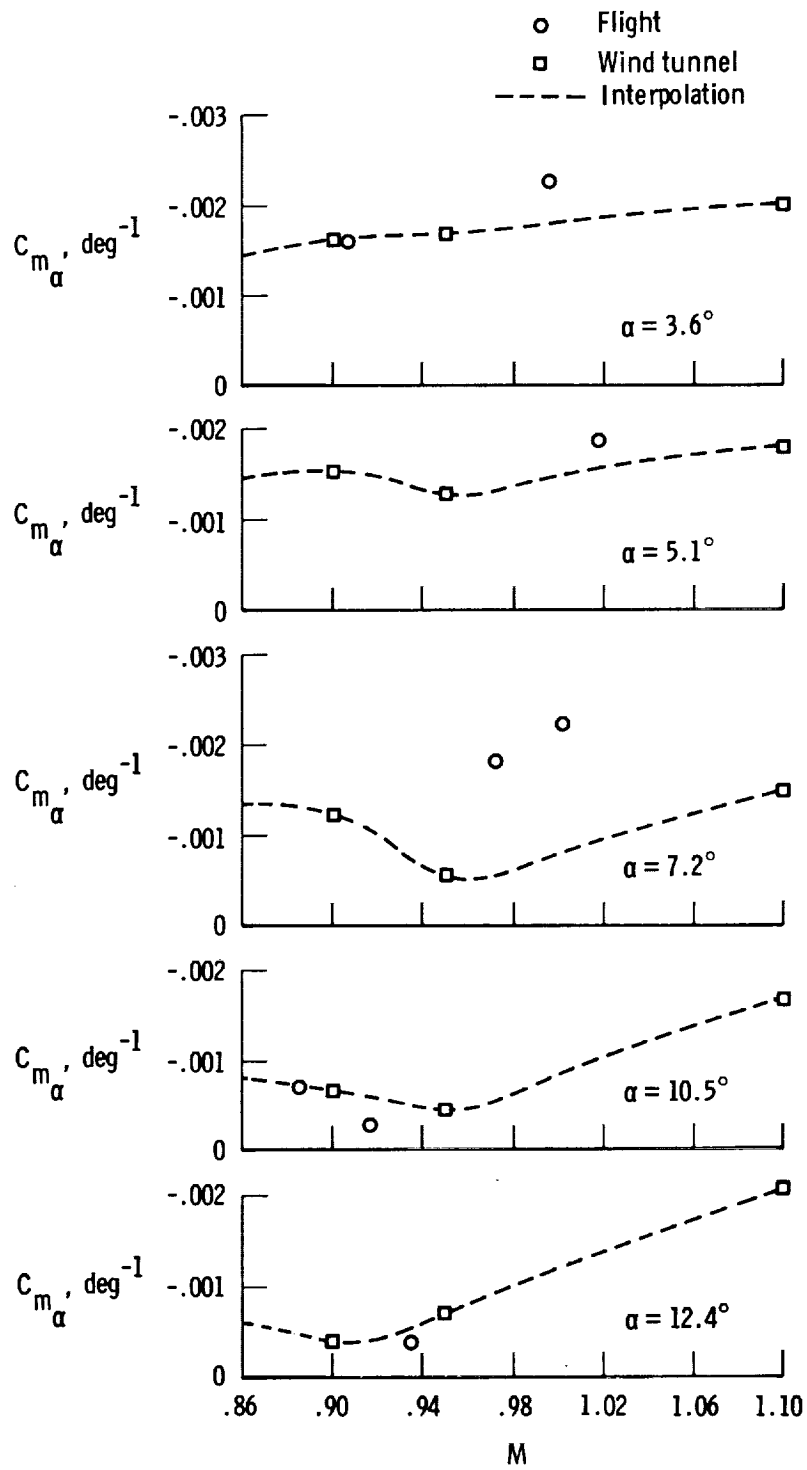
(d) $M = 1.1$.

Figure 17. Continued.



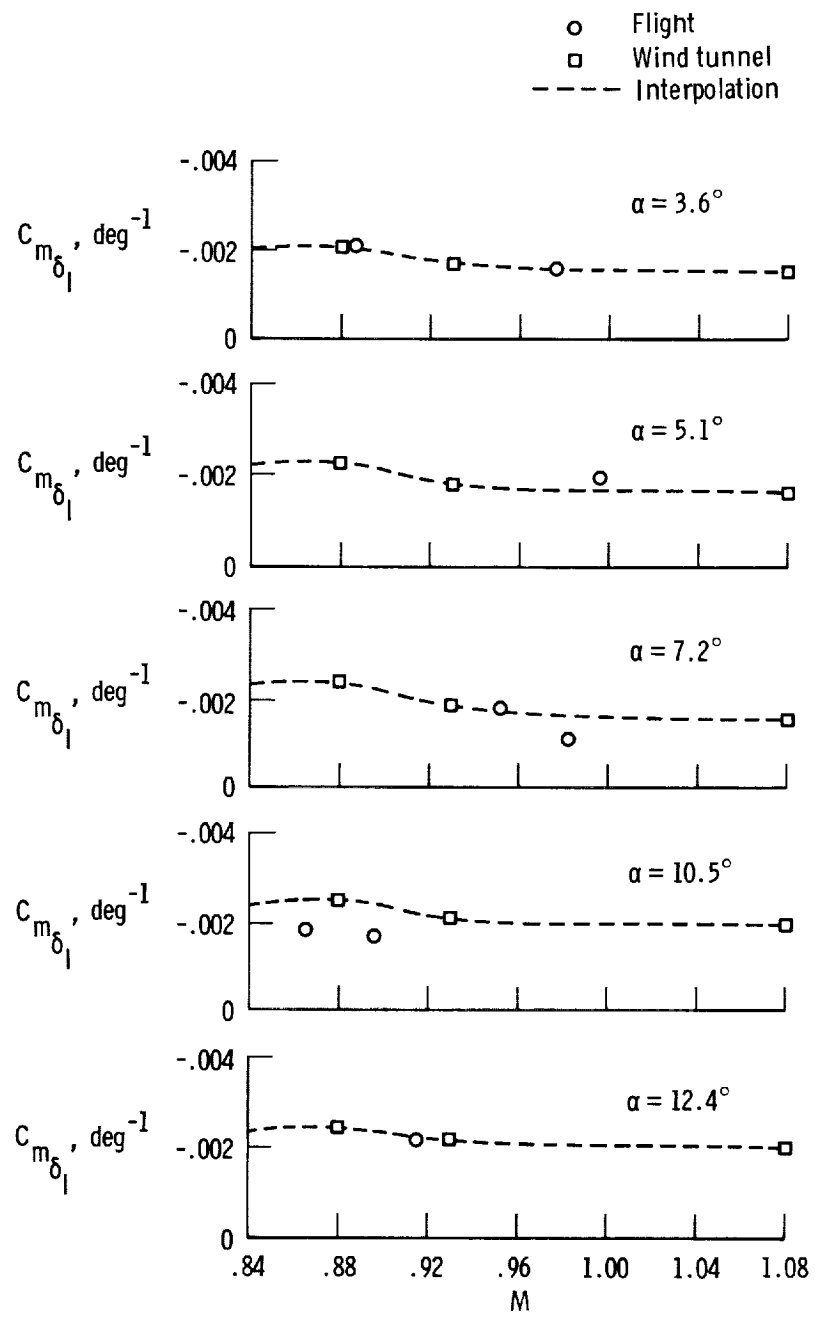
(e) $M = 1.3$.

Figure 17. Concluded.



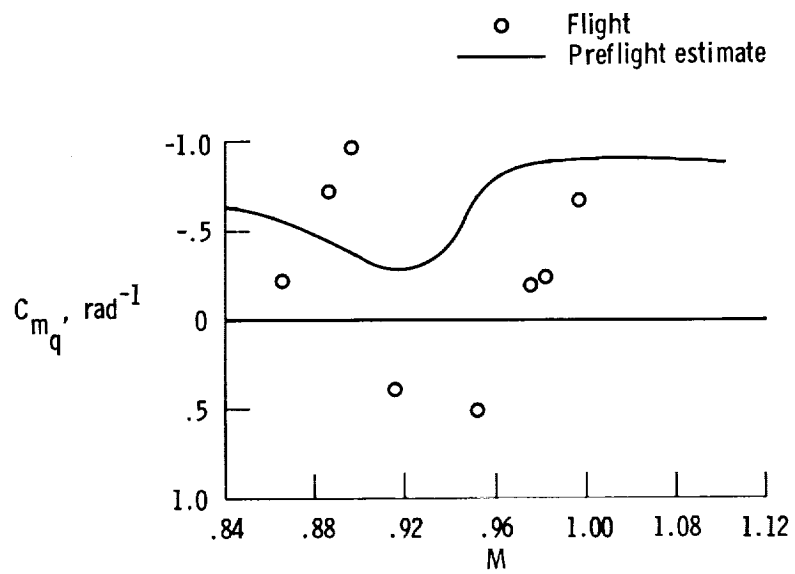
(a) C_{m_α}

Figure 18. Comparison of longitudinal derivatives obtained from flight data in the transonic speed region with wind-tunnel predictions.



(b) $C_{m_{\delta_1}}$

Figure 18. Continued.



(c) C_{m_q} .

Figure 18. Concluded.

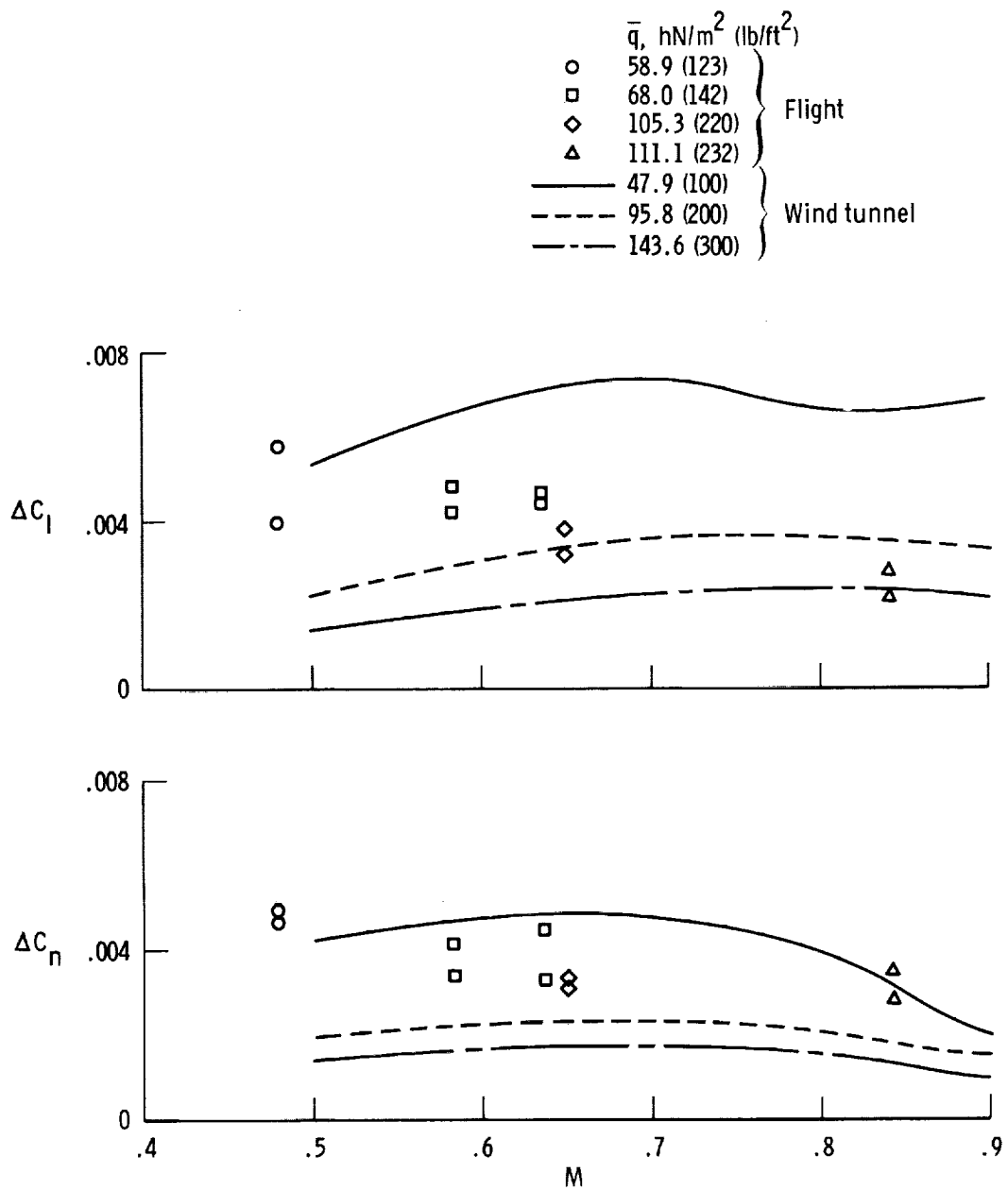
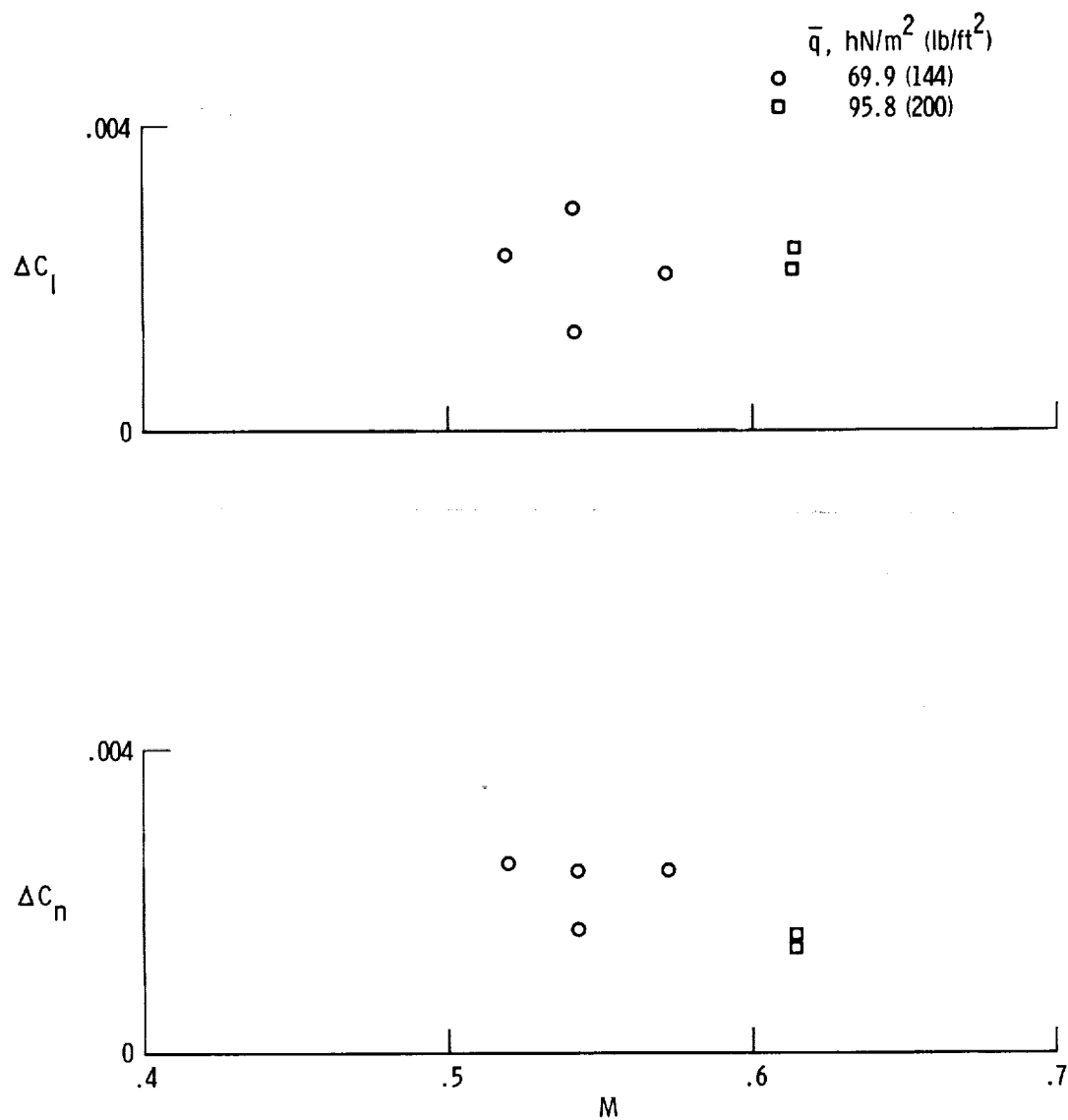
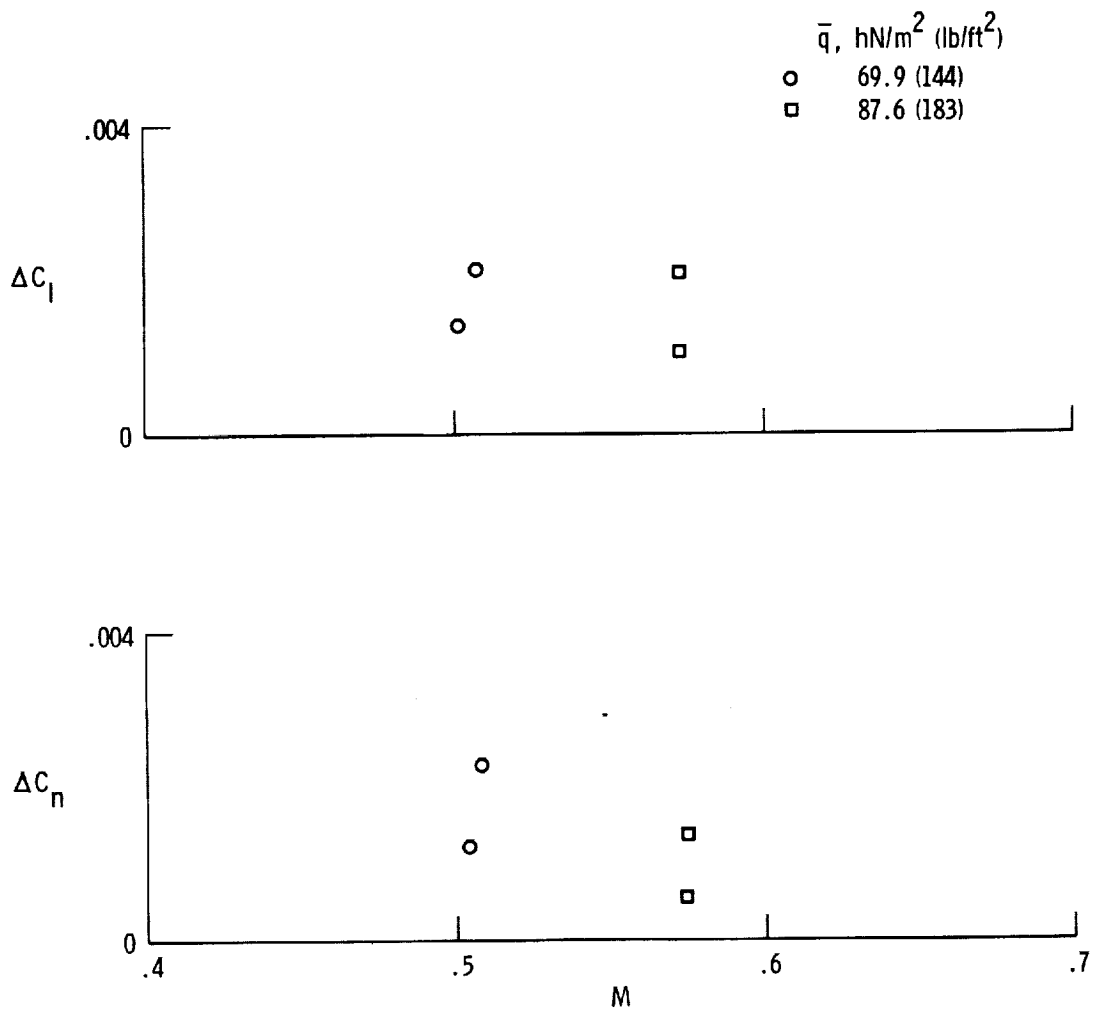


Figure 19. Comparison of flight and wind-tunnel incremental moment coefficients due to reaction control rocket operation. Outboard and opposite inboard rocket. Sign convention based on right outboard/left inboard rockets. Data normalized to two 400-N- (90-lb-) thrust rockets. Geometry 1.



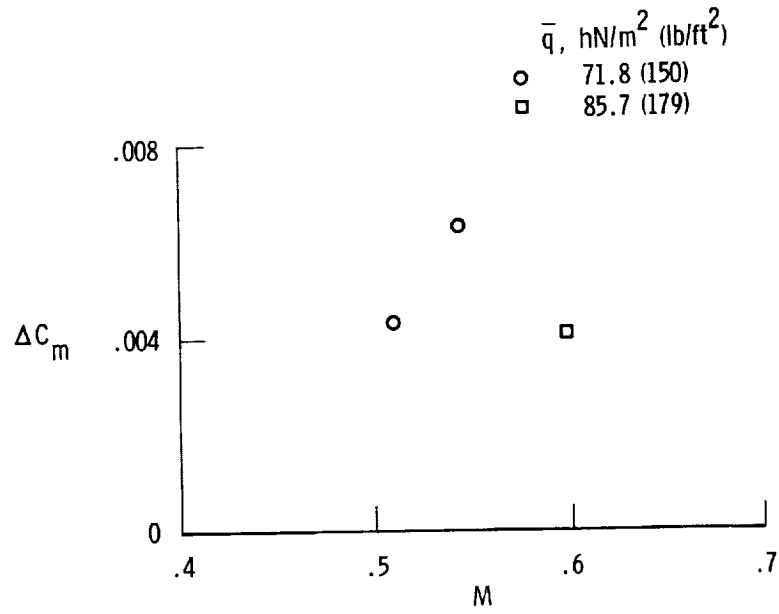
(a) Outboard rocket. Sign convention based on right outboard rocket.

Figure 20. Incremental moment coefficients due to outboard and inboard reaction control rocket operation. Data normalized to one 400-N- (90-lb-) thrust rocket. Geometry 1.

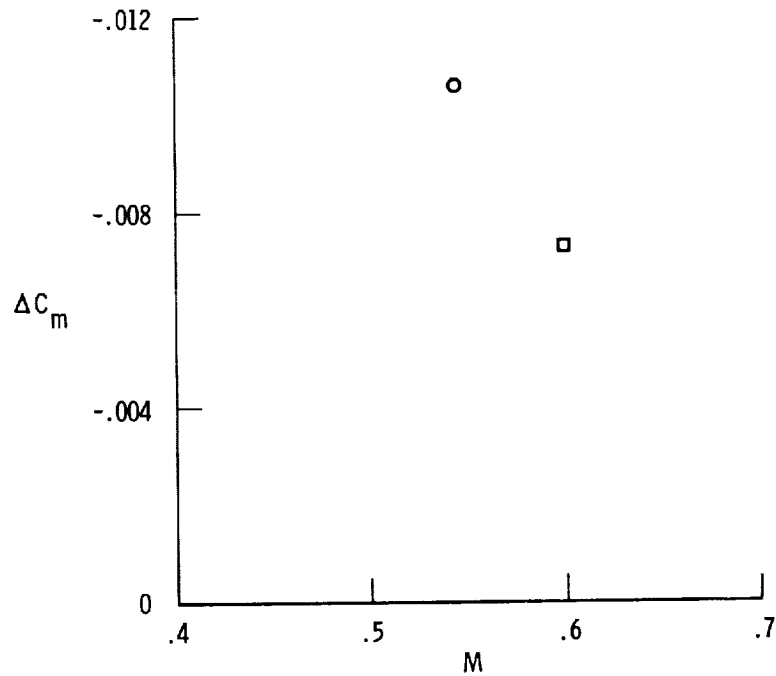


(b) Inboard rocket. Sign convention based on left inboard rocket.

Figure 20. Concluded.

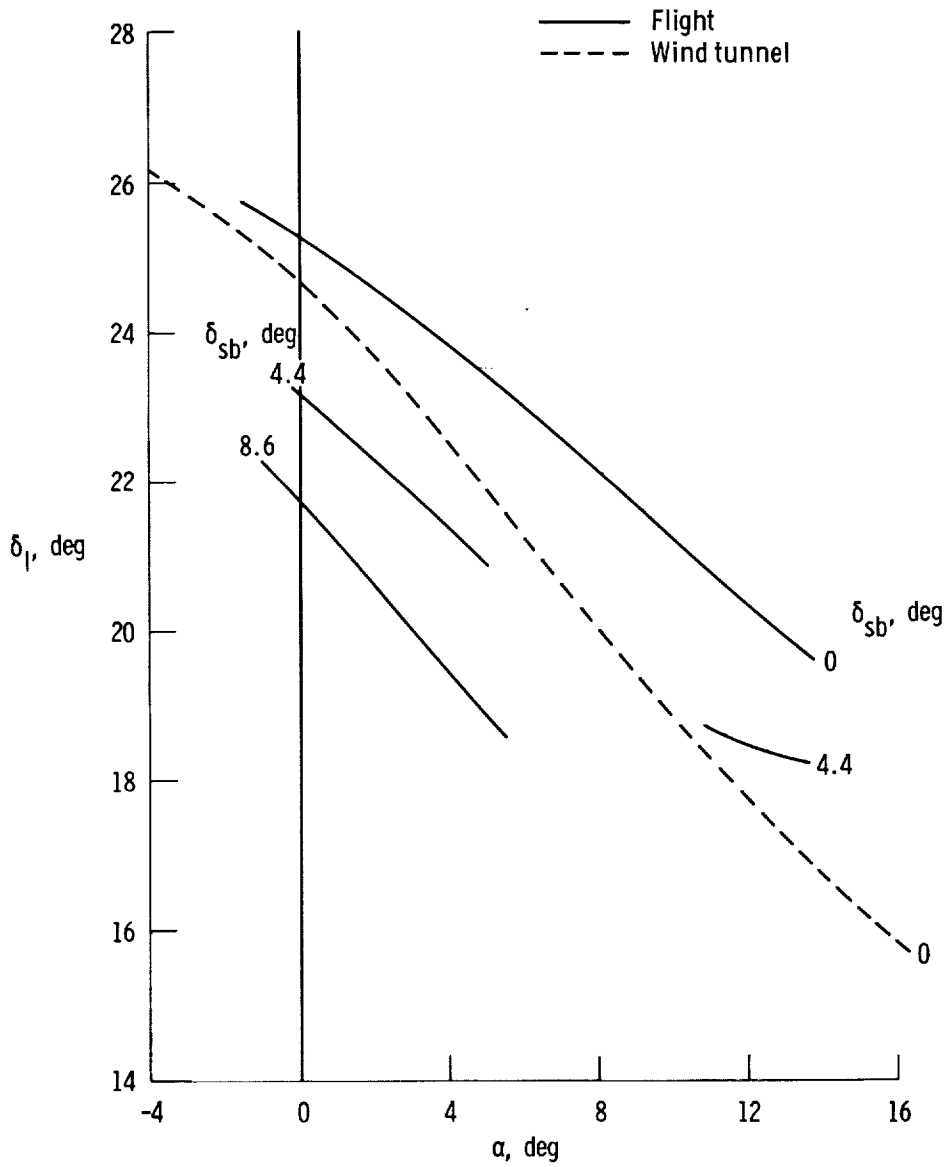


(a) Outboard rockets.



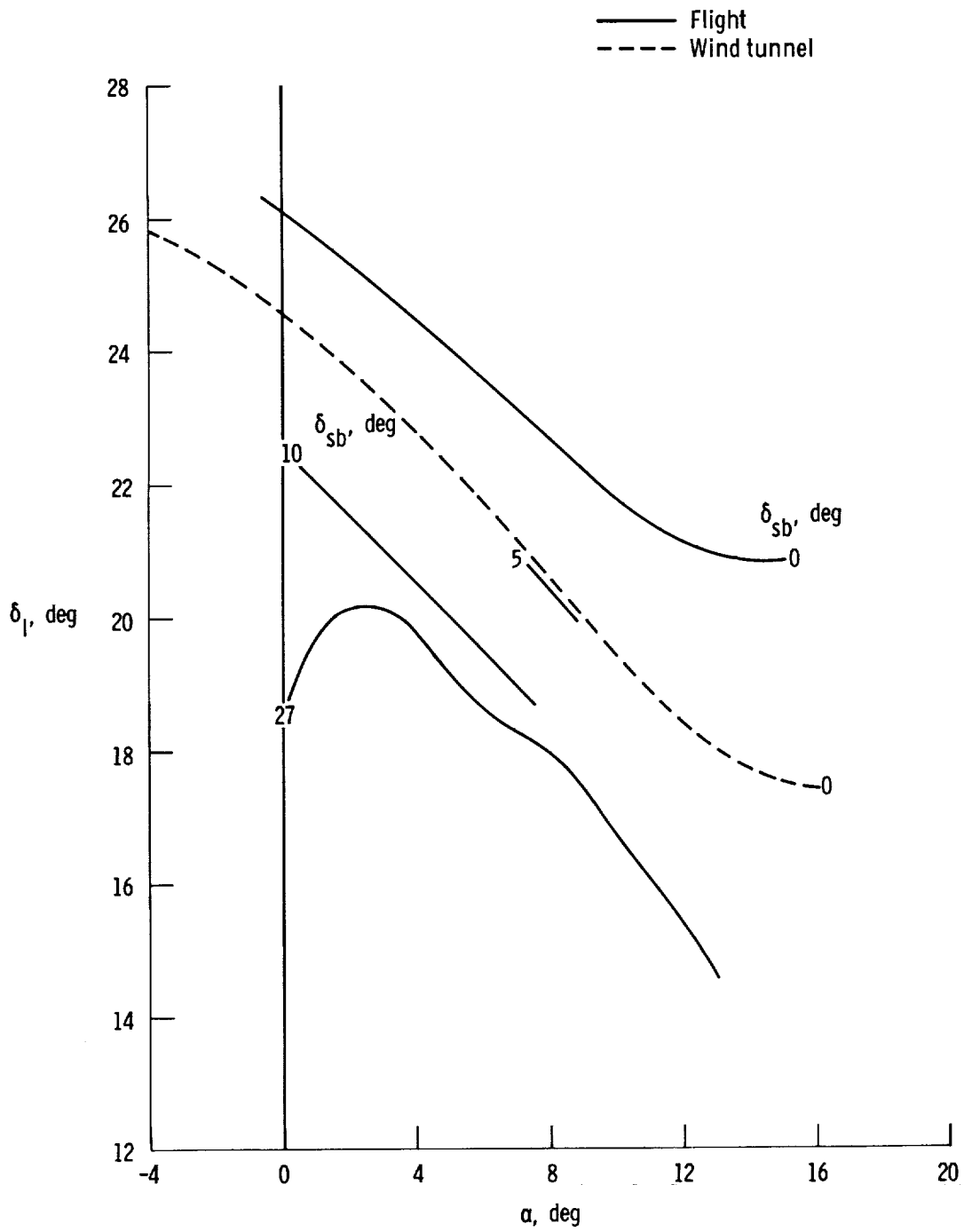
(b) Inboard rockets.

Figure 21. Incremental moment coefficient due to either both outboard or both inboard reaction control rocket operation. Data normalized to two 400-N- (90-lb-) thrust rockets. Geometry 2.



(a) $M = 0.5$.

Figure 22. Longitudinal trim as a function of angle of attack including speed-brake effects for Mach numbers of 0.5 and 0.7. $\delta_u = -11.8^\circ$.



(b) $M = 0.7$.

Figure 22. Concluded.

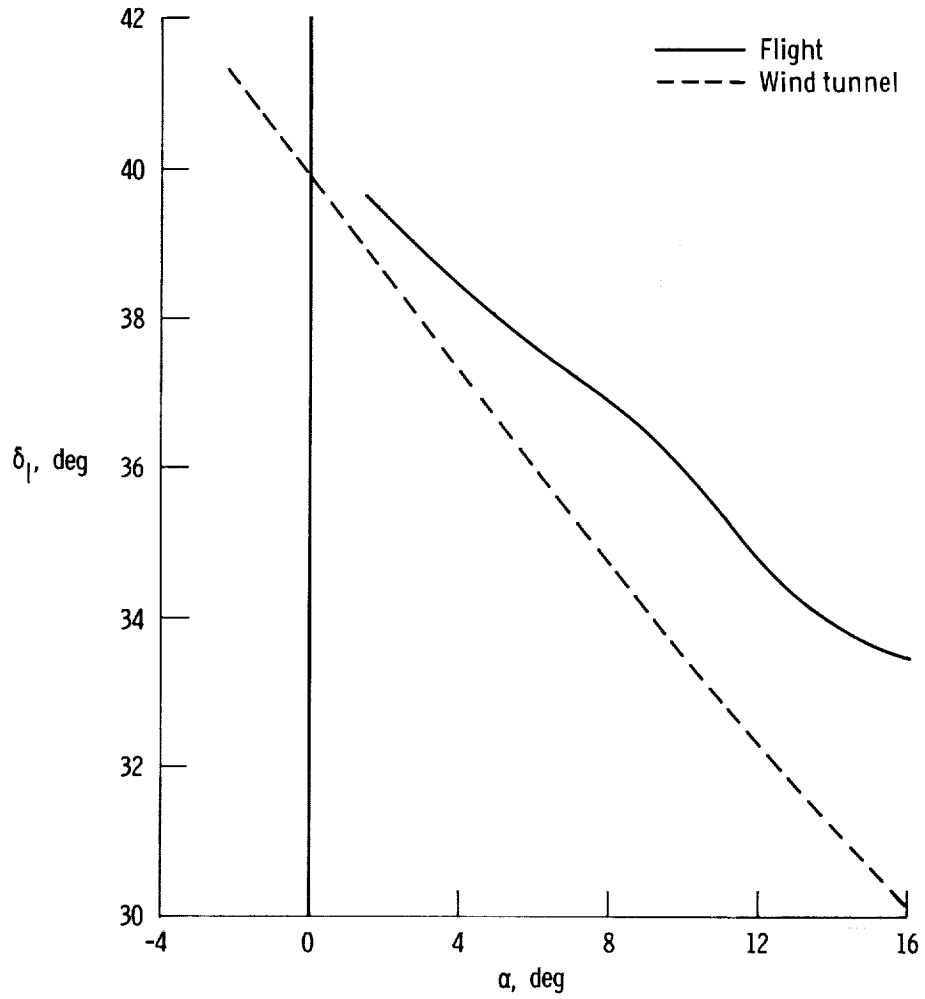
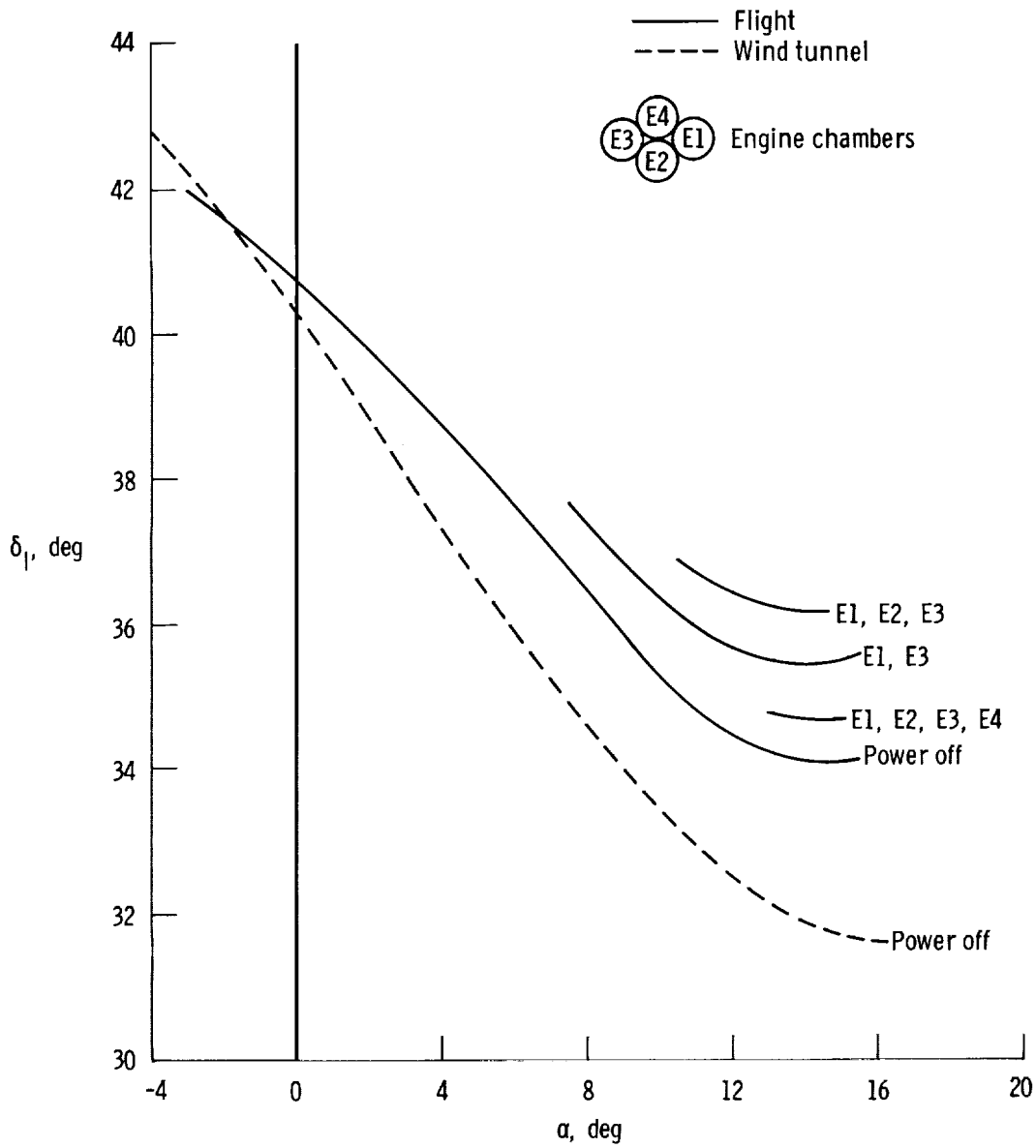
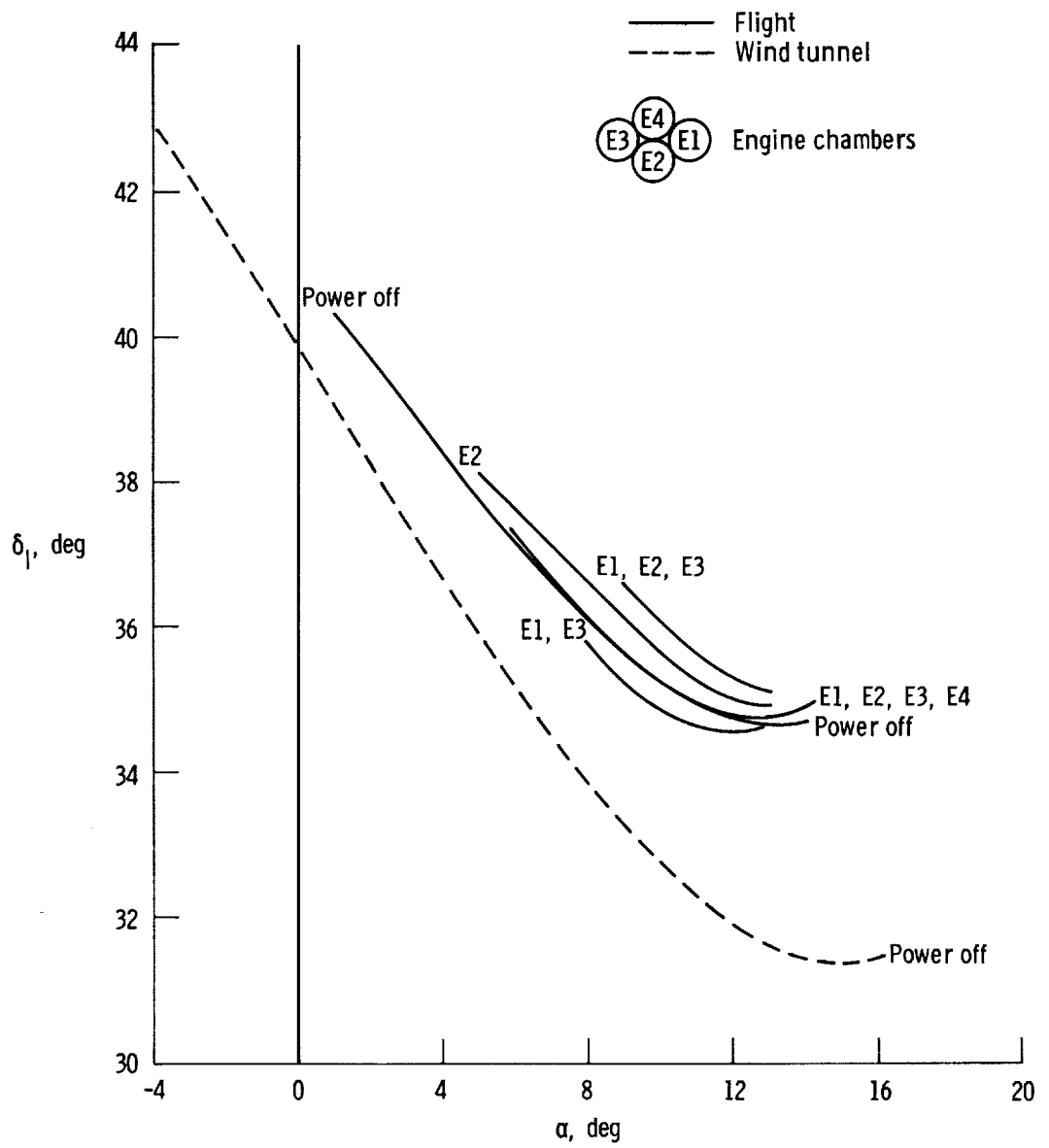


Figure 23. Longitudinal trim as a function of angle of attack with power off for a Mach number of 0.5. $\delta_u = -20^\circ$; $\delta_{sb} = 0^\circ$.



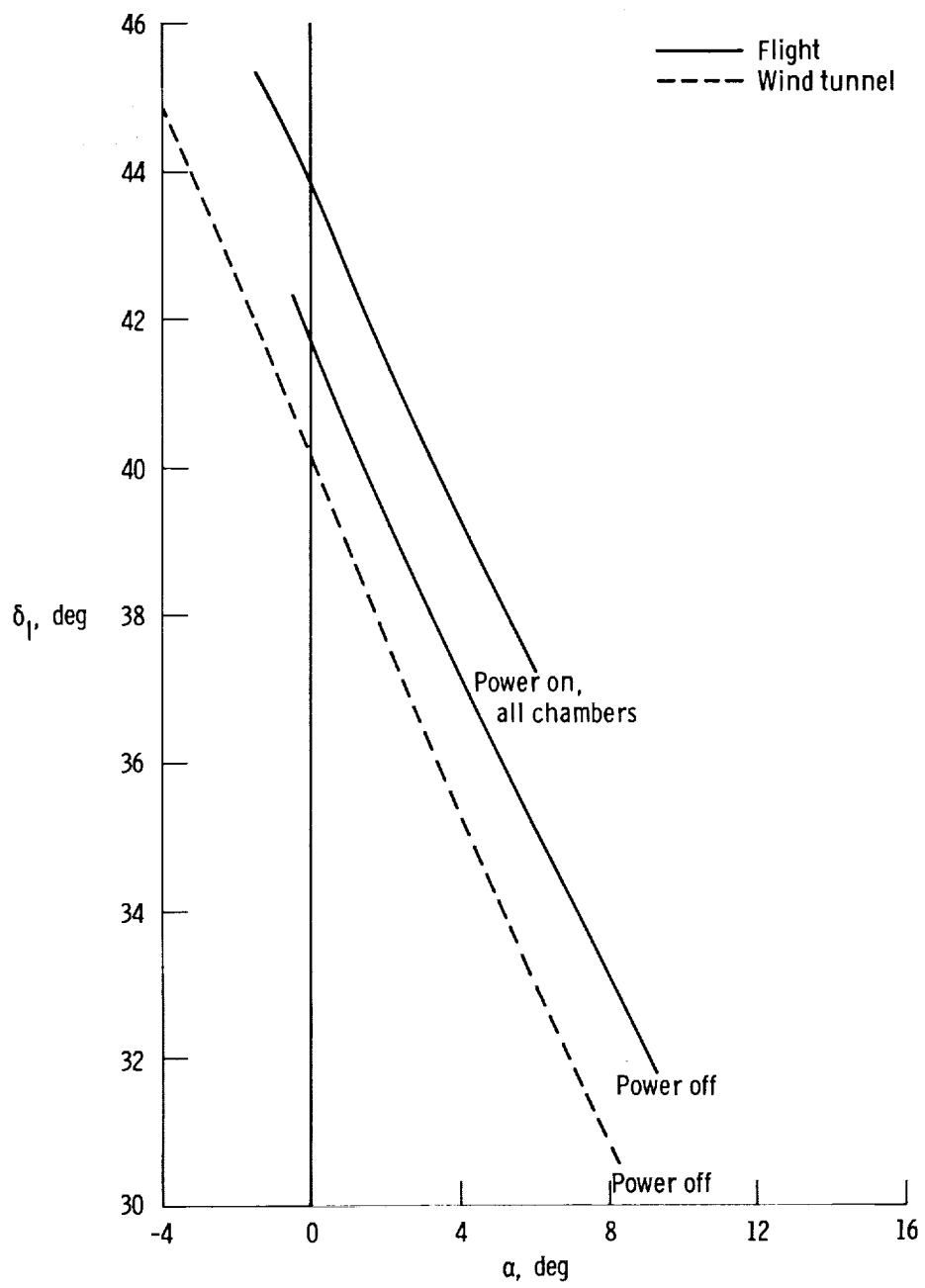
(a) $M = 0.7$.

Figure 24. Longitudinal trim as a function of angle of attack including power effects for Mach numbers of 0.7, 0.8, 1.1, and 1.3. $\delta_u = -20^\circ$.



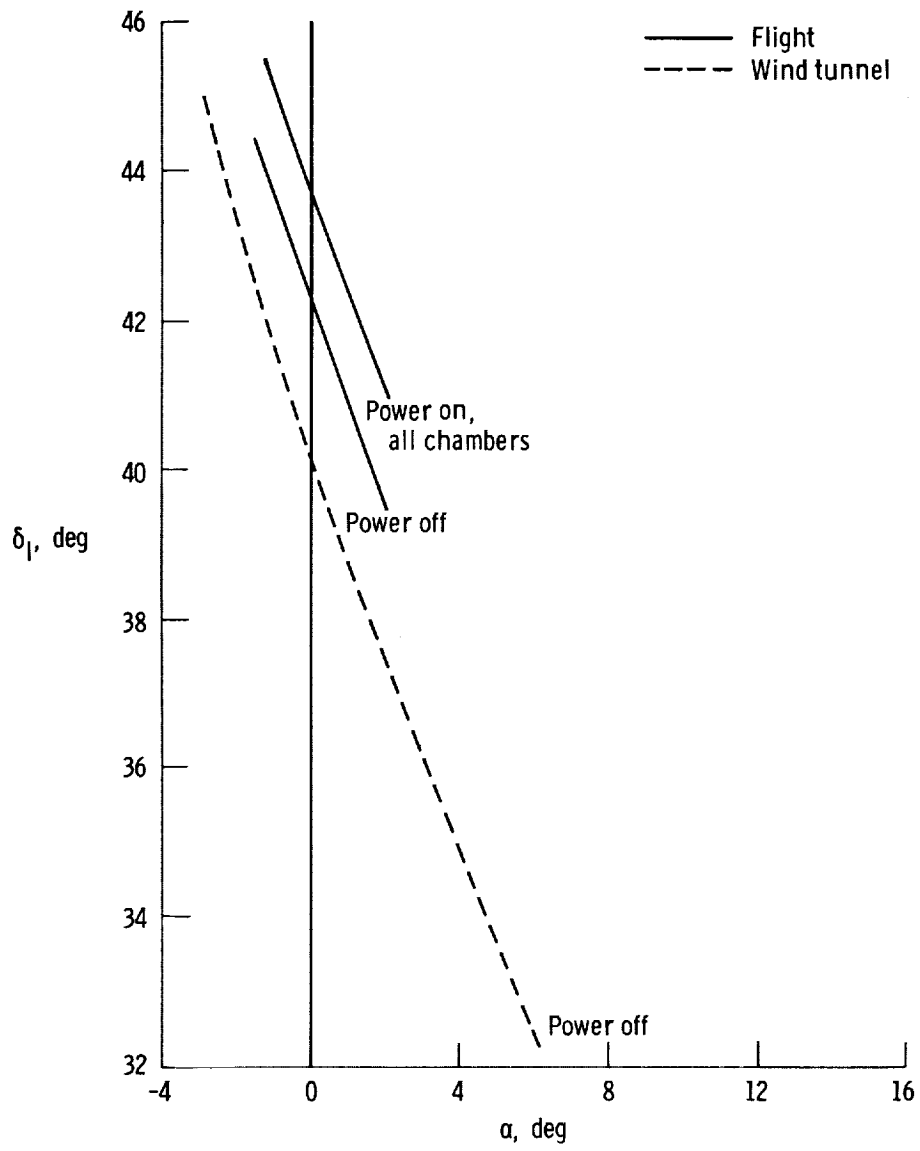
(b) $M = 0.8$.

Figure 24. Continued.



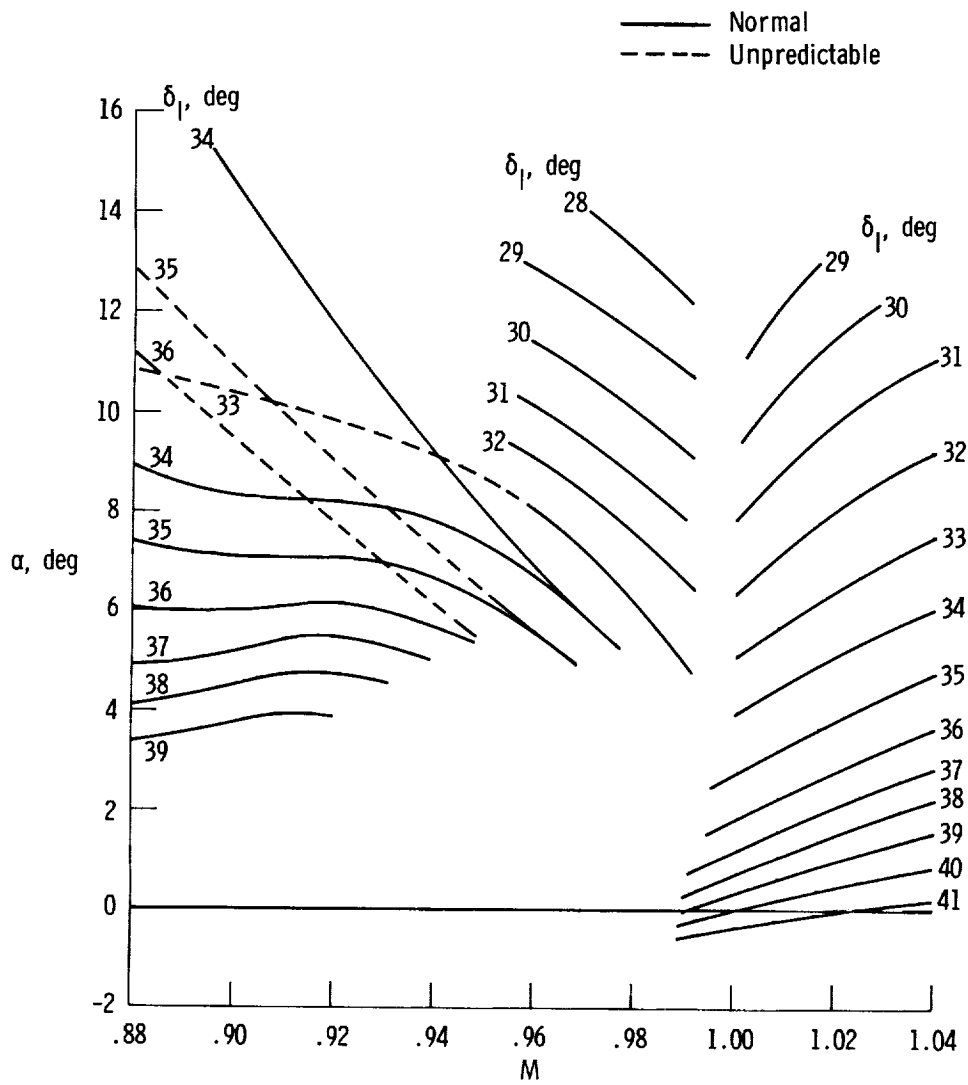
(c) $M = 1.1$.

Figure 24. Continued.



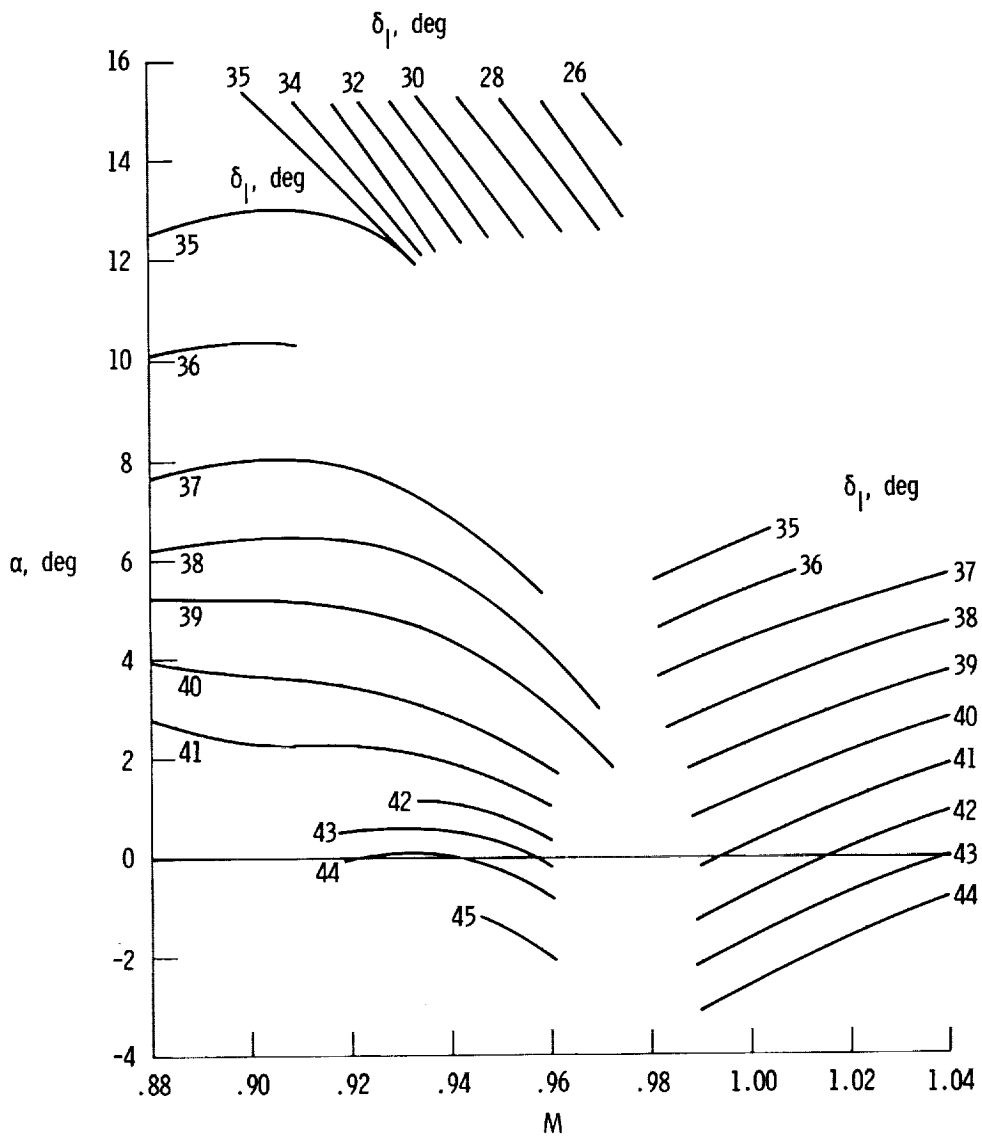
(d) $M = 1.3$.

Figure 24. Concluded.



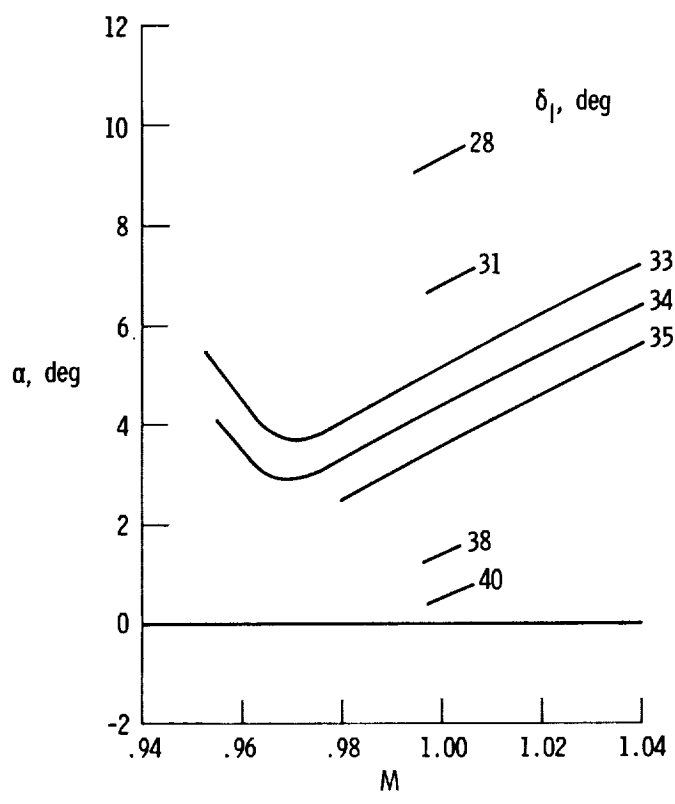
(a) Power off.

Figure 25. Flight longitudinal trim as a function of Mach number. $\delta_u = -20^\circ$.



(b) Power on, all chambers.

Figure 25. Continued.



(c) Power on, chambers 1 and 3.

Figure 25. Concluded.

